Biocompatibility of an Implantable Ophthalmic Drug Delivery Device

by

Sarah J. Cohen

B.S. Biomedical Engineering
Tulane University, 2002

SUBMITTED TO THE DEPARTMENT OF MECHANICAL ENGINEERING IN PARTIAL FULFILLMENT OF THE REQUIREMENTS FOR THE DEGREE OF MASTER OF SCIENCE IN MECHANICAL ENGINEERING
AT THE
MASSACHUSETTS INSTITUTE OF TECHNOLOGY
JUNE 2007

Signature of Author_____
Department of Mechanical Engineering
May 21, 2007

Certified by_____
Dr. Jonathan Bernstein
Charles Stark Draper Laboratory
Thesis Supervisor

Certified by_____
Professor Simona Socrate
d'Arbeloff Assistant Professor of Mechanical Engineering
Thesis Advisor

Accepted by_____
Professor Lallit Anand
Chairman, Department Committee on Graduate Students

This page intentionally left blank

Biocompatibility of an Implantable Ophthalmic Drug Delivery Device

by

Sarah J. Cohen

Submitted to the Department of Mechanical Engineering
On May 21, 2007 in Partial Fulfillment of the
Requirements for the Degree of Master of Science in
Mechanical Engineering

ABSTRACT

Diseases of the posterior eye present clinicians with a treatment challenge mainly due to the region's inaccessible location. Several drugs, including those available for the treatment of exudative age-related macular degeneration, are currently delivered by periodic injection into the eyeball. To avoid the risks and complications associated with this method, several implantable, timed release devices have been investigated to deliver these drugs directly to affected areas. Draper Laboratory and Massachusetts Eye and Ear Infirmary have proposed an implantable, fully programmable, mechanical device for long-term drug delivery to the eye wall.

To investigate the biocompatibility of this solution, test devices containing gears or a ball bearing were designed to mimic elements of its moving parts, geometry and materials. Cell culture studies identified a polytetrafluoroethylene filter with 10□m pores as a promising addition to seal devices from interaction with fibroblasts. Test devices with or without this membrane were implanted on the rabbit eye for 2 or 10 week periods. They were evaluated mechanically after implant, and surrounding tissues were inspected histologically.

Gross observation revealed a significant amount of tissue formation around the devices, especially in the conjunctiva. Devices had to be cut away from the eye surface, and there was a significant amount of tissue inside the gear devices. Notably less tissue surrounded and invaded the ball bearing devices. Histological evaluation identified the invading tissue as fibrotic at both time points, though significantly more was seen at longer implant times. Eye wall tissue was typically unharmed during implant, though an additional layer of fibrosis between the eye and the device was common. Mechanical testing of long-term gear devices after implant revealed a 1000 fold increase in torque required to turn the elements, but long-term ball bearing devices were significantly less affected (100 fold increase). Torque also increased in devices with membrane covers, due to similar fibrosis. However, in these implants, tissue was forced to enter through only the 0.002in. openings around the base of the devices. Biocompatibility for this device may best be achieved by minimizing the amount of relative micro motion allowed between the device and the eye and by sealing all openings with a porous polytetrafluoroethylene filter.

Technical Supervisor: Dr. Jonathan Bernstein
Title: Laboratory Technical Staff (Draper Laboratory)

Thesis Advisor: Professor Simona Socrate
Title: d'Arbeloff Assistant Professor of Mechanical Engineering (MIT)

This page intentionally left blank.

ACKNOWLEDGMENTS

05/21/2007

At Draper, I especially thank my thesis supervisor, Dr. Jonathan Bernstein for his advice, encouragement and continuous support of my work. Thank you also to Dr. Jeff Borenstein for his role in creating and supporting this research opportunity for me. I would also like to thank Dr. Mark Keegan for his support and his advice on all things biological and experimental, for providing testing materials and for valuable thesis comments. Thank you to Don Fyler for his assistance and direction in device design and mechanical testing. Thanks also to Ernie Kim for countless discussions at the white board and for coaching me through solid modeling and mechanical drawing. Very special thanks to John Mahoney, Ed McCormack and other members of the Draper machine shop for being patient teachers and excellent craftsmen – they have been instrumental in the production of this thesis. Thank you to Dan Traviglia for assistance with LabView and for loaning me his library. I would like to thank Betty Skinner for sharing her supplies and her experience with device cleaning. Thank you to Bob Visser for assistance with the dynamometers. Also thank you to Drs. Randy Scott and Rami Mangoubi for their suggestions about quantitative data analysis.

I thank everyone in the Bio and MEMS groups at Draper for being my mentors, colleagues and friends and for making Draper a fun place to work for the past three years! I would particularly like to thank Erin Swan for being my Course 2, Draper Fellow, drug delivery partner and my sounding board. Thank you also to Drs. Mindy Tupper, Scott Uhland, Angela Zapata, Amy Duwel and Mark Mescher for being excellent resources.

At the Massachusetts Eye and Ear Infirmary, I would like to thank Drs. Joan Miller and Evangelos Gragoudas for their advice and support. I would especially like to thank Dr. Paul Chan for lending his surgical and experimental expertise and for collaborating closely with me throughout the project. Thank you to Dr. Chris Andreolli for stepping in to perform implants as needed. I would like to thank Ed Connolly in the Laser Lab for his assistance and training throughout the project and for answering my endless questions. Thank you also to Norm Michaud for performing and arranging histology preparation.

At MIT, thank you to my thesis advisor, Professor Simona Socrate for her encouragement and suggestions. Also thank you to Professor Myron Spector for his mentorship and for sharing his biocompatibility expertise.

A very special thank you to Dr. Ben Lee at Brigham and Women's Hospital for volunteering his time and sharing his pathology knowledge.

Most importantly, I would like to thank my parents, my sister and the rest of my family, whose love, support and encouragement are central to everything that I do. Thank you also to my friends, both local and scattered, who have been some of the best cheerleaders a student could ever want.

This thesis was prepared at The Charles Stark Draper Laboratory, Inc., under Internal Company Sponsored Research Projects 20272-001, Solid Drug Delivery and 21133-001, Drug Delivery Exploratory.

Publication of this thesis does not constitute approval by Draper or the sponsoring agency of the findings or conclusions contained herein. It is published for the exchange and stimulation of ideas.

Sarah J. Cohen

This page intentionally left blank.

Table of Contents

List of Figures

List of Acronyms

AISI	American Iron and Steel Institute
AMD	Age-related macular degeneration
ASTM	American Society for Testing and Materials
BRB	Blood-retinal barrier
CMV	Cytomegalovirus
CNV	Choroidal neovascularization
CP	Commercially pure
EDM	Electrical discharge machining
ePTFE	Expanded polytetrafluoroethylene
EVA	Ethylene-vinyl acetate
FBGC	Foreign body giant cell
FDA	Food and Drug Administration
GDD	Glaucoma drainage device
GDNF	Glial cell line derived neurotrophic factor
IOP	Intraocular pressure
ISO	International Organization for Standardization
MAI	Poly(methyl acrylate-co-2-hydroxyethyl acetate)
MEEI	Massachusetts Eye and Ear Infirmary
MEMS	Microelectromechanical systems
NF	National Formulary
PBS	Phosphate buffered saline
PC	Polycarbonate
PEDF	Platelet derived growth factor
PGA	Polyglycolic acid
PLA	Polylactic acid
PLGA	Poly(lactic-co-glycolic acid)
PMMA	Polymethylmethacrylate
PTFE	Polytetrafluoroethylene
PVA	Polyvinyl alcohol
RPE	Retinal pigment epithelium
SEM	Scanning electron microscope
siRNA	Small interfering RNA
USP	United States Pharmacopeia
VEGF	Vascular endothelial growth factor
5-FU	5-Fluoroucil

Chapter 1: Introduction

Diseases of the posterior eye affect many thousands of patients, with 200,000 new cases of exudative age-related macular degeneration (AMD) alone each year [1]. There has been a recent increase in the number of therapeutics available to treat these diseases. However, a common challenge remains: what is the best method of drug delivery to the back of the eye?

Clinicians and researchers have tackled this problem in a variety of different ways. Current treatments for macular degeneration mainly require periodic injection of drug, currently either an aptamer or an antibody, into the interior of the globe. Research has also been conducted using degradable drug-loaded polymer constructs that are surgically implanted or injected via syringe into the eye for sustained release of therapeutic. Additionally, methods for passive or aided drug diffusion across the eye wall have also been investigated. These include the use of degradable polymers, but also refer to electrically driven drug diffusion known as iontophoresis.

While promising, these methods are associated with several risks. First, any injection into the eyeball has the potential to create an infection or other complications. With the newest drugs for macular degeneration, injection is required every 4 or 6 weeks, adding a renewed risk with each treatment. Every intraocular injection requires an office visit by the patient, and compliance for this time consuming, unpleasant activity presents a formidable challenge to physicians. Any intraocular implant comes with additional complications due to the surgical procedure and disruption of the intraocular materials and pressure.

While transscleral diffusion of drug has shown promise, few long-term, implantable solutions for the back of the eye have been proposed for placement outside of the eyeball. Degradable polymer devices for this application are typically used for delivery of drug on the order of days or weeks as opposed to months. Extending this lifetime requires attention to protection of the drug from degradation before its release. Simple injection of drug or drug-loaded microspheres into this space runs the risk of drug dissipation away from the localized area of interest.

With the latter problem in mind, Draper Laboratory and Massachusetts Eye and Ear Infirmary (MEEI) have proposed an implantable mechanical device designed to deliver small, timed bursts of drug directly to the external surface of the eyeball. This device would attach to

the sclera on the back of the eye and would house drug in sealed internal chambers. It would allow fluid communication and drug diffusion through a window in its base, locating the therapeutic directly to the eye surface for transscleral diffusion. In creating this pathway for the drug, the original design calls for exposing the internal device elements to the fluid, molecules and cells in the eye's external environment.

As with any implanted foreign object, the body's natural immune response will tend to attack and surround the implant with protein deposition and fibrous tissue. Because of the miniature size of machine elements such as gears and ball bearings in such a device, even a small amount of fibrous tissue infiltration could disrupt its function. A permanent, metallic device of this type also has the potential to damage surrounding ocular tissues.

This thesis investigates the biocompatibility – both the effects on the body and the effects on the device – of this type of implant. Evaluation focuses on a long-term animal model testing a set of smaller, simpler devices that contain the moving elements of the proposed drug delivery apparatus. These test devices mimic certain key elements of the Draper/MEEI device:

- Curved baseplate to mate with the eye surface
- Ports in the baseplate for drug and fluid communication
- Relative part size
- Types of moving elements inside the implant – gears and ball bearings
- Materials selected for fabrication
- Attachment of the device to the scleral surface of the animal's eye

The novel application of a porous membrane to restrict cell entry into the device interior was also considered. Material and pore size selection were chosen after cell culture studies on a set of appropriate membranes. Fibroblasts were seeded onto one side of each membrane and their ability to migrate to the non-seeded side was evaluated. The ideal filter blocks the passage of these cells, but would also be porous enough to allow drug to pass through freely. The membrane chosen from this study was applied to a subset of the implanted devices.

Torque testing of the devices before and after implant identified changes in device function while implanted. Tests utilized a small motor to apply force to the devices' rotating elements and a dynamometer beneath the devices to record applied torque. From these measurements, the mechanical effects of any protein deposition, inflammatory cells or fibrous tissue inside the device during implant were determined. The effects of the device on

surrounding tissues were also in question. Eye wall tissue from beneath the device, soft tissue covering the device and any invading tissue into the device were preserved and investigated histologically. Qualitative analysis revealed the cell and tissue types present.

In this work, the feasibility of implanting a long-term device with miniature scale, exposed metallic moving parts has been explored for attachment external to the posterior eye. The particular drug delivery system investigated in this thesis was designed with macular degeneration as its target disease and related, recently developed drugs as its target therapies. However, other posterior eye diseases present similar challenges for effective delivery of drug, and similar mechanical device designs could be proposed for placement in this location. Therefore, future drugs and device designs for any other posterior eye conditions may also benefit from the investigation presented here.

Chapter 2: Background

2.1 Eye Anatomy

2.1.1 Overview

The globe of the eye has a roughly spherical shape, measuring approximately 24mm in diameter in humans [2]. Its wall consists of three compact layers known as the outer, middle and inner coats or tunics. As shown in Figure 2.1, the sclera and cornea comprise the outer layer. The middle, or uveal, coat consists of the choroid layer of blood vessels, the ciliary body, which supports the lens, and the iris. Finally, the retina is the innermost, nervous cell-rich layer [3].

The interior space of the eye is divided into three chambers. The first, bounded by the cornea, the lens and parts of the iris, ciliary body and sclera, is the anterior chamber. This region is filled with the aqueous humor, secreted by the ciliary body into the cavity and continuously pumped out. The second chamber is the posterior, bounded by the iris and the suspensory ligaments that extend from the ciliary body to the lens. The remaining eye volume forms the vitreous chamber or posterior cavity, named for the vitreous humor, a gel-like collagen and mucopolysaccharide substance found inside [2].

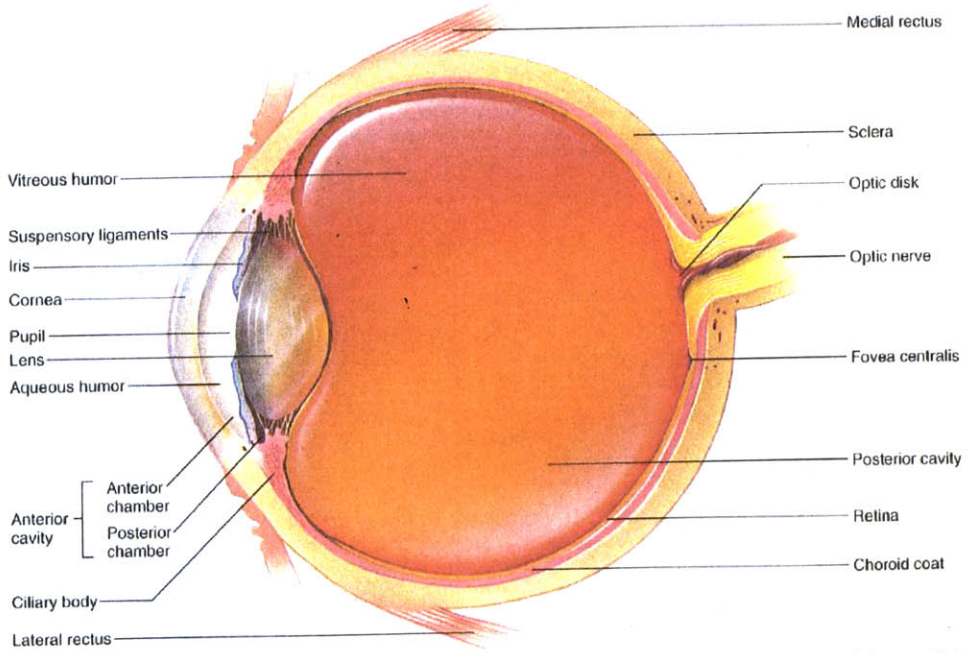

Figure 2.1 Transverse section of the eye, top view. From Hole's Human Anatomy and Physiology, 8th ed., by Shier D., Butler J, and Lewis R., WCB McGraw-Hill: 1999. Reproduced with permission from the McGraw-Hill Companies.

2.1.2 *Outer Tunic*

On the anterior side of the outer tunic, the cornea presents a transparent surface for passage and initial focusing of light. Its transparency stems from highly ordered layers of connective tissue and a sparse population of cells. Covering the remaining 5/6 of the globe's surface and serving both to protect the eye and to accommodate muscle insertion is the sclera [3]. It consists of three roughly defined layers: the episclera, the sclera proper and the lamina fusca [4]. The lamina fusca is the innermost layer and contains many pigmented cells similar to those in the choroid layer. The outermost layer is the episclera, a loose membrane containing many blood vessels [5]. It also serves as the insertion site for the six extrinsic muscles, which allow for motion of the globe. As shown in Figure 2.2, these are the superior, inferior, medial and lateral rectus muscles and the superior and inferior oblique muscles [3].

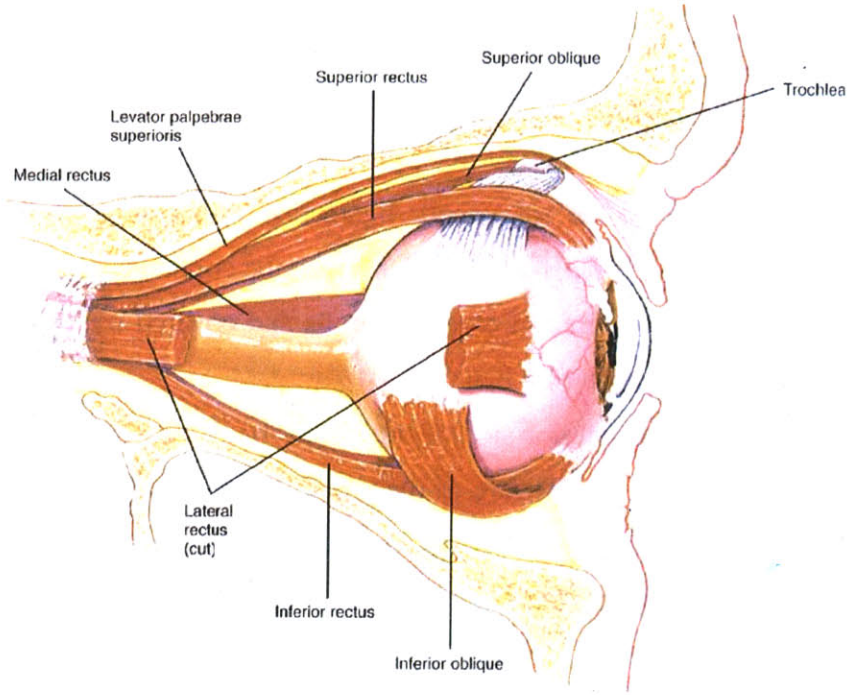

Figure 2.2 Lateral view of the eye in its orbit. From Hole's Human Anatomy and Physiology, 8th ed., by Shier D., Butler J, and Lewis R., WCB McGraw-Hill: 1999. Reproduced with permission from the McGraw-Hill Companies.

Between these two layers, tightly woven collagen fibers continuous with those of the cornea form the sclera proper. Near the cornea, these fibers run anterior to posterior; at the equator, they run circumferentially; in the posterior portion of the eye, they run at right angles to each other. In humans, this tissue ranges in thickness from about 0.7mm near the cornea to 0.5mm near the equator to 1.0mm in the posterior. The sclera proper has a low degree of

vascularization [2]. Both fibrous and pigmented cells are found throughout the sclera, and a layer of squamous cells line its outer surface [5].

At the junction between the sclera and the cornea is a concave region called the limbus (or corneoscleral junction). Within this region, a network of porous structures directs fluid pumped from the anterior chamber to the Canal of Schlemm, immediately posterior to the limubs. Also called the scleral venous sinus [3], this canal leads fluid to the venous system via several channels [4].

2.1.3 Middle Tunic

The majority of the uveal layer is made up of the choroid coat, a dark layer of blood vessels that supplies the adjacent retina [2]. Veins in the outer region of the layer split into capillaries near the retina. The choroid coat is tightly bound to the sclera in only five locations: near the optic nerve where the arteries enter the eye, and at the exit sites of each of the four major veins [4].

At the front of the eye, the choroid layer continues forward to become the ciliary body. The former extends muscles to the suspensory ligaments, which are in turn responsible for controlling the curvature of the lens. The lens, along with the cornea, controls the shape of light as it enters the globe. It is composed of elongated cells and covered by the lens capsule, both allowing for transparency to the entering light [2].

The iris connects to the anterior side of the ciliary body. Its circumferential and radial muscles [3] allow it to regulate the aperture of the pupil, thereby blocking or allowing differing amounts of light to pass into the eye. Due to its location and geometry, it also regulates the amount of fluid flow between the anterior and posterior chambers of the globe [2].

2.1.4 Inner Tunic

After light passes through the pupil and is refracted by the lens, it travels to the photoreceptor cells of the retina, which lies directly inside the choroid layer. The outermost layer of the retina is Bruch's membrane, which separates the retina from the choroid layer. Attached to this membrane is the retinal pigment epithelium (RPE), a layer of hexagonal cells held together by tight junctions. This epithelium is therefore responsible for maintaining the blood-retinal barrier (BRB) [6]. The RPE in turn connects to the rods and cones – black and white or color photoreceptors, respectively. Continuing towards the inside of the eye, the rods

and cones connect to a mesh of nerve cells and fibers, then to a layer of only fibers. The latter carry nerve signals to the optic nerve and on to the brain for processing [2]. Figure 2.3 shows a cross section through eye wall tissue.

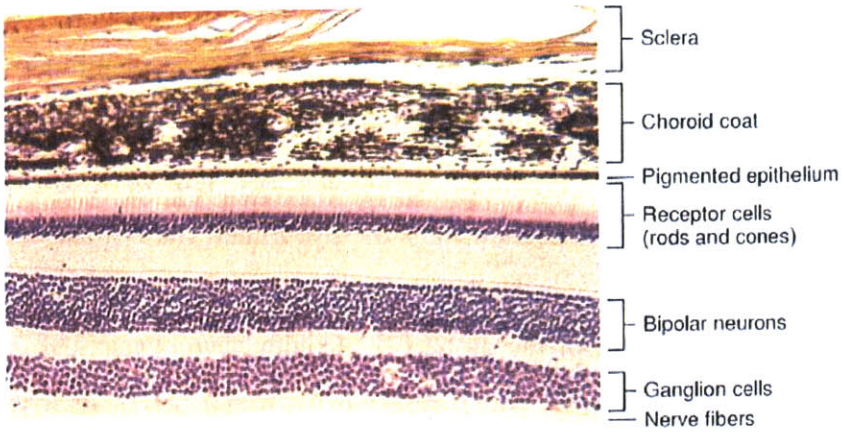

Figure 2.3 Histological section of the tissues in the eye wall. From Hole's Human Anatomy and Physiology, 8th ed., by Shier D., Butler J, and Lewis R., WCB McGraw-Hill: 1999. Reproduced with permission from the McGraw-Hill Companies.

In primates, an approximately 5-6mm region in the posterior of the retina is known as the macula, at the center of which is the fovea. This area is responsible for the central 15-20 degrees of vision [6]. The cells in this area are long, slender and tightly packed. In the fovea, the photoreceptors are almost entirely cones [2]. The entire macular area can be broken into several concentric rings. Starting from the center, they are the umbo (center point of the fovea and the thinnest area), the foveola, the outer margins of the fovea, the parafovea (thickest area) and the perifovea [6].

2.1.5 External Structures

The globes are situated in two bony orbits of the skull. In humans, these orbits are approximately pyramid shaped and are each angled about 45 degrees laterally from center, with the medial walls roughly parallel to each other. The optic nerve and ophthalmic artery exit through the optic foramen in the back of each orbit [7].

Each eye is shrouded by connective tissue called Tenon's capsule, from which emerges a medial and a lateral check ligament spanning from the eye to the periosteum covering the orbital bones. This set of three tissues comprises the suspensory ligament and is largely responsible for supporting the eye. Other similar ligaments run above and below the eye, though they are less

consistent between individuals. All space between connective tissue in the orbit is filled with fatty tissue, serving to cushion and support the eye and helping maintain its position in the orbit. A layer of connective tissue covers all structures, including this fatty cushion [7].

At the front of each globe is a set of eyelids (Figure 2.4), called palperbrae, each consisting of four layers: skin, striated muscle, connective tissue and conjunctiva. The muscles serve to open and close the eyes, and the connective tissue contains glands that secrete lubricating oil. The conjunctiva is a mucous membrane that folds between the eyelid and the globe [3]; the palpebral conjunctiva section lines the eyelid and the blulbar conjunctiva section rests on the globe. These regions are connected by a loose area of conjunctiva, which forms conjunctival sacs near the equator of the globe [2]. Conjunctiva consists of an epithelial layer that contains mucous producing cells, which rests on a stromal or connective tissue layer that attaches to the eyelid or rests on the eyeball [8].

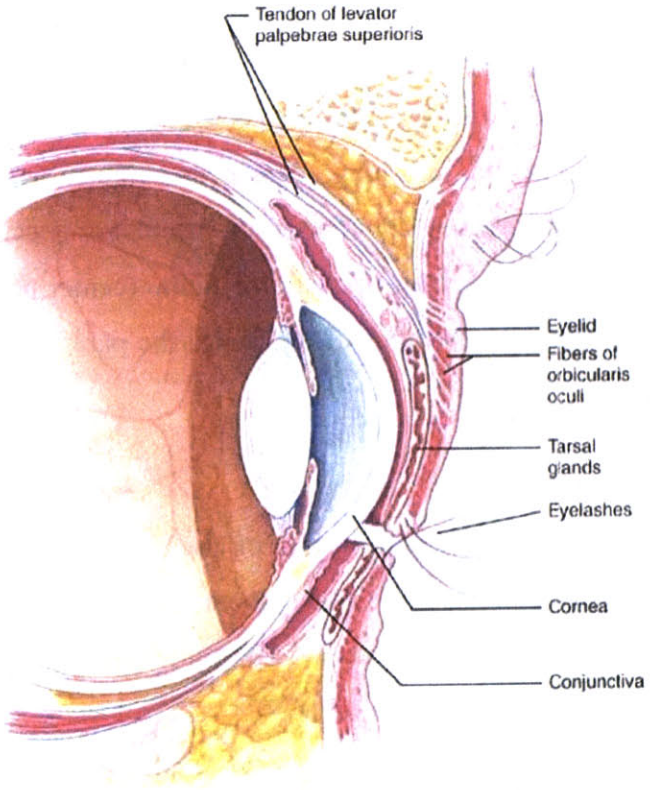

Figure 2.4 Sagittal section of the closed eyelids and anterior portion of the eye. From Hole's Human Anatomy and Physiology, 8th ed., by Shier D., Butler J, and Lewis R., WCB McGraw-Hill: 1999. Reproduced with permission from the McGraw-Hill Companies.

2.2 Eye Pathology

2.2.1 Disease Overview

Many diseases that affect the tissues of the eye present potential challenges for drug delivery and may benefit from implantable solutions. A variety of bacterial, viral and fungal infections can affect most structures of the eye, originating from either external or blood borne sources. These have been treated with pharmaceuticals, which have varying degrees of success [9]. Other than infections, common diseases that can be treated from the front of the eye are glaucoma and cataracts. In the posterior eye, conditions often present treatment challenges complicated by the inaccessible location and the need for long-term treatment. These diseases mainly affect the retina, the RPE and the choroid coat.

Glaucoma is defined by an increase in intraocular pressure (IOP) due to several possible causes for increased resistance to aqueous humor outflow. A chronic increase in IOP can lead to damage of surrounding tissues, including corneal edema, necrosis of the iris and most devastatingly, damage to the optic nerve [10]. Treatments for this disease therefore focus on reduction of the IOP, namely in the anterior chamber. Initially, a variety of drugs in drop form may be used to control production of aqueous humor or facilitate its removal from the anterior chamber. In cases when drug treatments or surgery are insufficient, a glaucoma drainage device may be implanted. Typically, these devices consist of a tube inserted into the anterior chamber to direct fluid out to a plate sutured onto the sclera in the subconjunctival space. Variations include addition of a pressure valve inside the tube, drainage of fluid to the limbus area and fluid drainage directly to the canal of Schlemm [11].

Cataracts affect the transparency of the lens. While many causes and types do exist, cataracts are generally areas of opacity in the lens and often grow with time [12]. Despite the severity, it is the most common treatable cause of blindness in the world. It is most frequently treated by surgical removal of the damaged natural lens and insertion of a prosthetic lens in its place. This new lens may be inserted in one of three locations: between the cornea and iris, in the pupil or behind the iris. Intra ocular lenses are usually constructed of polymethylmethacrylate (PMMA) and are designed with a central transparent "lens" portion with support extensions on either side [13].

In the posterior eye, macular dystrophies are genetic conditions causing loss of vision, often by change in the RPE or choroid layers. Stargardt disease, for example, shows yellow deposits in the macula, with RPE atrophy in later stages. Potentially affecting both retina and choroid, retinitis pigmentosa is defined as a progressive loss in rod and then cone function, especially diminishing peripheral vision [14]. Some of these diseases are also complicated by choroidal neovascularization (CNV), or new blood vessel formation in the choroid layer, causing vision loss in diseases such as Sorsby fundus dystrophy and Best vitelliform macular dystrophy [15].

Macular edemas are characterized by a breakdown of the BRB, allowing fluid accumulation posterior to the retina. Diabetic macular edema, for example, begins with a change in the permeability of the barrier, and fluid leakage can take place at one or many foci. Central and branch retinal vein occlusion is often associated with cystoid macular edema whereby the barrier breaks down near the retinal veins [15].

One severe, acute complication of macular edema is retinal detachment, a lifting or pulling of the retina from its underlying layers. Most commonly the cause, a tear in the retina allows fluid to enter the subretinal space, separating the retina from the underlying tissues. In other cases, either an internal fibrous membrane pulls away the retina or a fluid pocket builds behind the retina to push it away [16]. While silicone oil has been used inside the vitreous cavity to push the retina against the globe, retinal detachments are often repaired by implanting a scleral buckle onto the outside of the posterior of the eye. This typically flexible block of material serves to indent the vitreous cavity to meet the new location of the retina. The technique of suturing a buckle to the sclera dates back to the 1930s, and success is reported in about 90% of cases [13, 17].

Associated with retinal detachment is proliferative vitreoretinopathy, a condition whereby a variety of benign cells proliferate in the vitreous cavity and line the detached retina on both sides. A variety of drugs have been used to treat this condition, mostly aimed at the prevention of one of the disease stages. Steroids and other anti-inflammatory drugs encourage the integrity of the blood-retinal barrier, while drugs like 5-Fluorouracil (5-FU) discourage cell proliferation. Because half-lives of these drugs are relatively short after intravitreal injection, other delivery methods have been investigated such as slow release polymeric delivery vehicles [9].

2.2.2 *Age-Related Macular Degeneration*

Of the macular edemas, exudative AMD is very common and is the leading cause of blindness in people over 55 in the United States [18]. Characterized by a loss of central vision, the cases of all AMD fall into two subgroups: atrophic (dry), which may lead to exudative (wet). The former is known for its degenerated RPE and progressive damage to photoreceptors, while the latter is much more severe due to CNV [1, 19]. In fact, the wet form accounts for only 10% of AMD patients, yet it is responsible for 90% of all severe vision loss cases [20].

The earliest dysfunction in AMD is the age-related degeneration of the RPE in the macular region. Damage to this cell layer leads to improper maintenance of the blood-retinal barrier, poor chemical processing during the visual cycle, and incomplete uptake of photoreceptor cell waste. This cascade is driven by the insufficiency of new RPE cells, which allows for the accumulation of lipofuscin granules that contain cytotoxic molecules. Common to all AMD cases is the deposition of drusen, yellow material consisting of RPE remnants and a variety of proteins. These deposits form between the RPE and Bruch's membrane. It is both the resulting mechanical displacement of tissue and the associated inflammatory response that then cause damage to the overlying photoreceptors [1].

As an AMD case progresses to the wet form, new blood vessels stem from the choroid layer with a tendency to leak through the BRB and form scars, leading to severe vision loss. Many theories have been investigated as to the instigating factor for CNV formation, including thickening of Bruch's membrane by drusen, inflammatory degeneration of Bruch's membrane and reduction of retinal blood flow due to scleral stiffening [19].

All of these conditions may lead to an increase in the relative amount of vascular endothelial growth factor (VEGF), which has been implicated in a wide variety of diseases showing neovascularization. VEGF is a necessary factor for new vessel formation, as it encourages endothelial cell reproduction and increases vascular permeability for new branching [19]. In the healthy choroid, VEGF is balanced by the anti-angiogenic pigment epithelium derived factor (PEDF). In wet AMD, however, VEGF is produced in relatively higher concentration, which eventually leads to fluid accumulation in the retina and vision loss [1].

There is no current treatment for dry AMD, but several treatment methods have been used or proposed for wet AMD. Some involve the chemical or thermal disruption of new vessel formation – photodynamic therapy, transpupillary thermotherapy, thermal laser photocoagulation

and low dose radiation therapy. Surgical methods of removing CNV, translating the retina away from damaged areas and transplanting healthy RPE have also been used [1, 21, 22]. Additionally, pharmacologic agents such a steroids, small interfering RNA (siRNA) and PEDF are being developed [1, 19].

Recently, the most promising treatments are the anti-VEGF agents pegabtanib, bevacizumab and ranibizumab. Pegabtanib sodium (Macugen®) is a short pegylated, modified RNA oligonucleotide that binds to only the major VEGF isoform responsible for CNV. With 0.3mg intra-ocular injections every 6 weeks, trials showed stabilized vision in 70% of patients [23]. On the market to treat metastatic colorectal cancer, bevacizumab (Avastin®) is a full-length monoclonal antibody to VEGF and has been proposed for off label use to treat CNV. A shorter, 48kDa antibody fragment, ranibizumab (Lucentis®), has more recently shown the greatest promise to treat this disease. By design, this drug binds to and neutralizes all forms of VEGF [24]. Several clinical trials with this drug have shown approximately 95% of patients experience a minimal loss of vision, with approximately 75% maintaining or increasing visual acuity. Trials were conducted with 0.3 or 0.5mg doses injected intravitreally once every four weeks for 1-2 years [1, 19, 25]. This drug received FDA approval in July 2006 for monthly dosing of 0.5mg [26].

2.3 Biocompatibility

2.3.1 General Considerations

With any implanted device, the interface between the foreign object and the body tissues must be examined and considered. The body has a natural healing process for its wounded tissues, which are typically unavoidable in an implant surgery. The body will also mount an attack on any material that it considers non-self, which may change the function or properties of a device. Further, the chemical and mechanical nature of device materials in the body environment may contribute to irritation of surrounding tissues. It is both device effects on the body's health and body effects on the device function that define biocompatibility as used in this thesis. As stated by Dee, Puleo and Bizios: "Biocompatibility, therefore, must account for the interactions between tissues and biomaterials. The use of the prefix 'inter' implies that not only can biomaterials affect biological responses, but also the milieu of the body can affect materials [27]."

Immediately after being placed in the body, an implant is likely to adsorb the proteins abundant in all tissues and body fluids. Proteins may further unfold upon adsorption due to the changes in their chemical environment, often adding to their bonding strength. Less stable proteins are more likely to unfold in this case. Any adsorbed protein may in turn attract antibodies, other proteins or leukocytes [27].

Biomaterials can influence certain protein adsorption by their surface properties. Rough topography provides increased surface area for protein attachment. Chemical composition of the material will also determine the types of interactions possible with local proteins. For example, hydrophobic surfaces are more likely to bind protein than hydrophilic ones. Surface potential can encourage adsorption of charged molecules and will affect the distribution of ions in the surrounding solution. As the first proteins bind to a material, they may do so in a similar manner due to the availability of surface area on the material. As more bind, however, space limitations force proteins to change conformations. Any protein unfolding or shielding of active sites will likely alter the molecule's function [27].

Implantation usually causes a wound in the patient, to a varying degree. The body will then naturally try to heal that wound, but will likely be unable to remove the offending foreign object. Natural wound healing consists of coagulation, inflammation, repair and remodeling. The coagulation cascade can be initiated by the intrinsic pathway – platelet contact with non-healthy vasculature or foreign substance, or by the extrinsic pathway – release of tissue thromboplastin after tissue trauma. Both cascades lead to the formation of a fibrin clot around the damaged area or foreign material. Even an implant that does not contact blood can encourage this series of events if it allows adsorption and activation of a protein called factor XII [27].

Subsequent dilation of the capillaries brings greater blood flow to the area, accompanied by an increase in capillary permeability. Redness and swelling in the area results [28]. Inflammatory leukocytes are then encouraged to move towards the damaged site with the duty of destroying any invading irritation by releasing chemicals such as lysosymes. These cells include tissue macrophages, circulating monocytes, and circulating neutrophils [27]. The dead space alone, inevitably created by placement of an implant, will encourage migration of macrophages to the body-device interface [29].

In the natural case, mitosis of inflammatory cells forms a granulation tissue in the area, which is later replaced by collagen molecules and other necessary elements for new, healthy tissue. In the situation of an implant, however, the inflammatory cells do not have the capability to destroy the foreign object chemically or by phagocytosis, leading to a situation known as frustrated phagocytosis. Macrophages in this case will replicate and fuse together into "foreign body giant cells" (FBGC's) around the material, isolating it from the body. Rather than remodeled tissue, new fibroblasts are recruited to form a fibrous capsule around the material, creating a more permanent wall between the foreign object and the body [27]. This process generally progresses for 1-2 weeks after implant and then enters a chronic phase. Later stages tend to show a fibrous tissue capsule with relatively few, spindle shaped fibroblasts. Materials that leach particles or ions may be toxic to cells or surrounding tissues and will typically be surrounded by an increased number of inflammatory cells during chronic phases [28].

A variety of conditions as well as material and implant properties may affect the extent to which the foreign body response will occur. These include the site of implantation, the availability of blood supply in the area, any mechanical forces the device creates, chemical release from the materials and pre-existing pathologies or infections. One report recently showed that solely a dead space or low pressure area in connective tissue as small as 60□m encourages fibrous tissue formation locally around a material [30]. Thinner capsules will form around implants that are round, static, chemically stable, and that have straight sections and textured surfaces [27]. Capsule thickness generally increases when there is relative motion between the device and the surrounding tissue. Extreme cases may lead to a fluid-filled sac around the entire implant, or around sharper edges [28].

2.3.2 Biocompatible Materials

Despite these challenges to implantation, a variety of materials have historically been used for long term residence in the body. These include metals, ceramics and polymers, and they fall into one of four categories with respect to their properties in vivo: inert, interactive, viable or replant [28].

The first recorded use of a metal implant was by Petronius in 1565, who used a gold plate to repair a cleft palate. Use of gold, iron, bronze and brass materials continued to be developed through the 1860s at which time sterile surgical techniques were developed. With this change, it

became apparent that different materials (e.g., platinum, gold, silver, lead, zinc, aluminum, copper, magnesium) produced different effects in the body. Through the early 1900s, the need for corrosion resistant materials was identified as important for future implants [31].

More recently, this list of needs has expanded beyond corrosion to address any adverse effects caused by a device in the body. While a material's biocompatibility does depend on the situation in which the device is implanted, a material that for example is toxic to surrounding cells is typically rejected for use. The Food and Drug Administration (FDA) requires that devices be subjected to testing for all potential adverse effects on the body by its constituent materials. Tests should be selected from the battery developed by the International Organization for Standardization (ISO), listed under ISO 10993. The selection process should take into consideration the material properties as well as the nature of the material's contact with the body. The ISO 10993 tests include "acute, sub-chronic and chronic toxicity; irritation to skin, eyes and mucosal surfaces; sensitization; hemocompatibility; genotoxicity; carcinogenicity; and, effects on reproduction including developmental effects." Additional tests may be necessary to gain FDA approval depending on the situation [32].

In addition to these requirements, materials in implants are chosen for their other properties such as mechanical strength, or ability to react in a particular way with surrounding tissues. Metals have been used extensively in implants and are most useful for their mechanical properties [31]. The four most common metals used in implantable devices are stainless steel (American Iron and Steel Institute (AISI) 316L, or American Society for Testing and Materials (ASTM) F138,139), cobalt-chromium-molybdenum alloy (ASTM F799), titanium (commercially pure (CP) grade 4), and titanium-aluminum-vanadium alloy (Ti6Al4V) [27].

Type 316L stainless steel (18Cr14Ni2.5Mo) is a vacuum-melted low carbon variation on the standard 316 material. It has a maximized pitting corrosion resistance due to its chemistry, and the vacuum process adds to its cleanliness. This stainless steel has been used in applications such as bone screws and pins, bone plates, joint replacements, wires and meshes for orthopedic applications and casings for laryngeal prosthesis and pacemakers [31].

Titanium gains its corrosion resistance from the oxide layer that forms on its surface, which leads to lower corrosion compared to stainless steel or cobalt-chromium alloys. It has been shown to have minimal fibrous tissue response as compared to these other metals. Titanium is manufactured as CP or in alloy form. CP grades are dependent on the carbon and

iron content, where the higher purity has lower strength and hardness but higher corrosion resistance. Alloys used for medical applications are made with aluminum and vanadium or niobium. Ti6Al4V has generally higher strength and fatigue limit than the commercially pure metal. On titanium, however, if the oxide layer on the surface is worn away, any metal-metal contact leads to high friction and wear rates. Titanium and alloys have been used for implants such as pacemaker cases, pump housings, dental implants, craniofacial implants, hip and knee joint replacements and screws and staples for spinal surgery [27, 31].

A wide variety of polymers have also been used in implantable devices. These range from biodegradable to chemically inert materials. Of the latter, polytetrafluoroethylene (PTFE, Teflon®) has been used extensively in the body, especially for vascular grafts [31]. PTFE was created in 1938 at DuPont and consists of a carbon backbone bonded to fluorine atoms. Its compact structure and minimal molecular branching contribute to its high density, low modulus and low coefficient of friction. The material is preferable for in vivo applications due to its extreme resistance to chemical reactions. As a bulk material in vivo, a minimal amount of tissue reaction occurs, though the particulate or powder forms of PTFE are highly reactive. PTFE can also be expanded (ePTFE) to form a microporous structure, which is advantageous for some applications [33].

Ceramic materials have also been used for a variety of applications. One of these is zirconia. Most often stabilized with yittrium oxide (Y_2O_3), it has relatively high strength and fracture toughness and can be polished to a very smooth surface. This material has been largely used for femoral heads in hip replacements and has been shown to produce far less wear debris in those implants as compared to metal heads. Degradation of this material in body fluids has been of concern, and newer zirconia/alumina composites are being developed to solve this problem [34].

2.3.3 Device Biocompatibility

In order to be considered biocompatible, an implanted device must perform as is suitable for the function and environment. Because of this vague notion, it is necessary to consider the biocompatibility of every implant separately in its intended environment [35]. Recent studies have investigated biocompatibility of permanent sensor or drug delivery implants made using microelectromechanical systems (MEMS) technology in silicon. Important factors for these

applications include the potential toxicity or inflammatory response due to the less used silicon as a biomaterial. Also, fibrous tissue occlusion of the sensor or of the delivery ports may disrupt the function of the device. Yang et al. investigated the biocompatibility of a silicon-based pressure sensor by implanting several percutaneously along rabbit lumbar muscles for 1, 4 or 12 weeks. Results showed that granulation tissue formed around the devices, slowly replaced by fibrous tissue. With time, capsule thickness and density of inflammatory cells decreased, while fibroblast density increased. Despite this reaction, the authors concluded that the device was "biocompatible" for their application [36].

Similarly, Voskerician et al. have studied the biocompatibility of their drug delivery device created with gold, silicon, silicon dioxide, silicon nitride and SU-8 photoresist. Testing materials separately, coupons of each inside an AISI 310 stainless steel cage were implanted subcutaneously in a rat. After 4, 7, 14, and 21 days, the number and types of cells present around the materials were identified. All materials were associated with an acute inflammatory period, though the number of macrophages and FBGC's decreased over time. FBGC's were found to cover the drug wells in a fabricated mock device, though it was unclear whether the wells were intact or opened in these cases. In a similar experiment, this group tested the local effects of gold salts produced after electrical activation of each well. Analysis indicated that there was an increase in the inflammatory response after the voltage was applied, though the cell density cleared by 21 days [37, 38]. These studies focused on only the short-term effects of implanting this device.

2.3.4 Scleral Materials and Devices

As discussed in Section 2.2.1, two devices have been used regularly on the sclera: the scleral buckle and the glaucoma drainage device. Their biocompatibility varies in nature depending on the materials used and their design. Both devices are intended to reside on the sclera for periods of years.

Scleral buckles are solid, flexible bands that are sutured to the sclera in order to indent the globe towards a detached retina [17]. Absorbable materials for this device include autogenous tendon, absorbable gut and pigskin gelatin [13]. More typically, however, non-degradable silicones and hydrogels are used in the form of porous sponges, smooth blocks or encircling bands [17]. They are designed with soft, flexible properties so as to cause minimal

erosion to the sclera during long-term attachment. Silicones encourage formation of a surrounding fibrous capsule, which has the advantages in this case of securing the device and strengthening the sclera [13]. This tissue mass may, however, also prevent eye motility. Hydrogel buckles were introduced in the 1980s and were most commonly based on poly(methyl acrylate-co-2-hydroxyethyl acrylate) (MAI and MIRAgel). This material, however, has been associated with buckle failure due to excessive swelling and subsequent material fragmentation [17]. These effects may be due directly to FBGC granuloma on the periphery of the device. Comparing excised silicone and MIRAgel buckles, the silicone buckles were more often associated with bacterial infection and the solid forms more associated with scleral erosion as compared to the sponge forms [39].

Glaucoma drainage devices (GDD's) have been used to relieve fluid pressure in the anterior chamber. Several versions exist, though most consist of a tube that resides in the chamber on one end and leads to a plate sutured to the sclera on the other end. The plate anchors the implant and allows for fluid to be drawn out from the tube into a bleb, to then dissipate in the subconjunctival space. Tube materials have historically been made from silicone rubber or nylon; plate materials typically include PMMA, polyethylene and silicone rubber [40].

While silicone rubber has been shown to be effective as a scleral buckle, for GDD's inflammation and fibrous encapsulation around the plate directly affect the drainage function of the device. With all GDD's, this effect is the leading cause of failure [11]. Additional complications include erosion in tissue around the system [40], infection and decreased intraocular motility [41]. While it may be the aqueous humor that stimulates fibrous tissue formation [11], both the micro motion of the plates on the eye surface and choice of material have been suggested as the cause of most complications [13]. The more rigid materials may exhibit more micro motion against the tissues, which may in turn increase the inflammatory response. Adding windows for tissue ingrowth to these materials may anchor the device, reducing the motion and decreasing the eventual fibrous capsule thickness [11]. Implantation of solely the plate results in a layer of avascular fibrous tissue around the material that remains consistently after 4 weeks of implantation. Ayyala et al. showed that polypropylene encourages much greater fibrous tissue formation than silicone rubber plates [42]. Boswell et al. showed that a novel ePTFE plate with different geometry encouraged a thinner, less dense fibrous capsule as compared to the silicone [43].

2.4 Local, Implantable Drug Delivery

2.4.1 Drug Delivery Challenges

Systemic delivery, whether by ingestion or injection, is a routine method of transporting medication to affected areas in the body. This method proves to be challenging or dangerous for many current or newly developed therapeutics. Ingesting a drug requires that it be protected against digestive actions in the stomach, that it be capable of crossing the intestinal wall and that it pass through the liver without losing its activity before entering systemic circulation. Injected drugs do bypass the digestive tract, but needle use is impractical for many applications [44, 45].

In response to these hurdles, alternative methods of systemic drug delivery have been developed or proposed. These include methods of drug inhalation. They also include transdermal delivery, which may allow for either systemic delivery or for local delivery to tissues near the skin surface. Transdermal delivery has been investigated by diffusion from a patch, by adding a current to drive drug through the skin, by using ultrasonic waves to disrupt the outer layer of skin, allowing drug to pass through [44, 45] or by first piercing the top layer of skin with microneedles [46, 47]. Additionally, wearable devices are also on the market for continuous, controlled, systemic drug delivery. One such device is an insulin pump made by Medtronic, consisting of a small, wearable control box and drug reservoir. This cartridge connects to a small tube, inserted on one end under the skin [48].

Regardless of these newer methods, however, systemic delivery for many treatments still requires a much larger amount of drug delivered to the entire body in order for a therapeutic amount to arrive at the intended location. Care must be taken to strike the optimal balance between toxicity to body tissues and inefficiency. In all systemic delivery, side effects to non-diseased tissue are of particular concern. [44, 49]. For example, because VEGF is a ubiquitous agent for controlling new blood vessel formation, the therapeutics for AMD (Section 2.2.2) could have a devastating effect on healthy vessels in the body if delivered systemically.

Furthermore, many new drugs are larger molecules such as proteins (commonly antibodies) and DNA which often have short half-lives in body fluids. These drugs can be designed with chemical side chains or embedded as part of a liposome to increase the time to degradation [9, 44]. However, a bolus injection of drug, even directly to the concerned area, will be cleared by the body and by diffusion. Depending on the treatment, all of these shortcomings

of current drug delivery require repeated dosing, which also encounters the unpredictable challenge of patient compliance.

2.4.2 New Local and Implantable Solutions

To counter these issues and to improve drug efficacy, a wide variety of drug delivery methods that are both local and implantable have been investigated and some brought to clinical practice. Simply stated by Moses, et al., with reference to chemotherapy drugs, "The drug itself becomes more effective when placed next to, and delivered directly to, its targeted tissue, and much higher local drug concentrations can be achieved compared to traditional approaches [49]." These new methods fall into two major categories: those using passively controlled polymer technology and those using programmable, actively controlled technology.

Early materials for the former were non-degradable polymer networks into which drug could be embedded for slow outward diffusion. This drug-carrier complex could then be implanted at the site of disease for localized treatment over a period of time governed by drug diffusion. Embedding drug in later materials like degradable lactic-glycolic acid copolymers (polylactic acid – PLA; polyglycolic acid – PGA; poly(lactic-co-glycolic acid) – PLGA) allowed for release by diffusion through the pores as well as by bulk degradation of the carrier itself [49]. These materials can be formed into a variety of shapes for insertion into specialized sites [50]. For example in a different material, chemotherapy agents have successfully been introduced into tumors in the brain via porous polyanhydride pads, allowing the drug to be delivered over three weeks [49].

Drug delivery from the commonly used bulk eroding polymers typically occurs in three phases. First is an initial burst of drug, second is a slow period of diffusion from the device and third is a final drug burst when the device is broken apart. While phase two is well regulated, the initial and final bursts are much less controlled. A newer device made of two polymers with differing degradation time constants has been shown to release ganciclovir to treat cytomegalovirus (CMV) over 200 days without the uncontrolled drug bursts [50].

In the category of actively controlled implantable drug delivery, MEMS technology has been used to create such devices. These implants consist generally of a series of sealed reservoirs, each containing a single dose of drug. To deliver, the seal on each reservoir is individually opened, using thermal and electrical means. Drug then diffuses into surrounding

fluid, landing first on the nearest tissues before having the potential to be cleared or dispersed through the systemic blood flow [51]. Recent in vivo work has shown relatively consistent delivery of lyophilized leuprolide acetate in a polyethylene glycol matrix using this system [52]. Though that application intended systemic delivery, this type of implantable device may also be very useful for localized delivery.

2.4.3 Ocular Drug Delivery Challenges

Drug delivery to the eye presents a distinctive set of challenges. Historically, only diseases external to the eye or in the anterior of the globe could be treated. Though treatments with drops or ointments are generally successful, even drug delivery to these highly accessible regions proves less than straightforward. A drug administered topically encounters many hurdles before having the opportunity to penetrate the cornea [4]. The anterior side of each globe is bathed in a constant flow of tear film consisting of lipid, aqueous and mucous layers [2]. Typical tear turnover is 16% per minute, most of which is cleared through the tear duct system. Due to this continuous wash, drugs applied to the tear film are generally only allowed to reach the aqueous humor 1% of the time [53]. Aside from tear removal, proteins in the tear film may bind to drug molecules, prohibiting their diffusion through the cornea. Drug may also be metabolized here [4].

Once traversing the tear film, a drug must still be able to pass through the corneal epithelial layer in order to diffuse to the rest of the anterior chamber [4]. Topically applied drug may also diffuse through the conjunctiva and sclera to the internal tissues. This path is inefficient for most drugs, because it often diffuses first into the local capillaries, which then disperse it systemically. Drug that does diffuse through the anterior eye structures only proceeds to the posterior tissues in minimal doses [53].

Systemically delivered drugs for the posterior eye encounter the blood-ocular barrier, which allows only lipophilic molecules to pass [9]. Hydrophilic drugs will only diffuse from the blood stream when the BRB is disturbed, typically indicating that the related disease has reached its end stage and a drug therapy approach is less helpful [54]. Additionally, for some classes of molecules, such as organic acids, the RPE actively pumps drugs out of the ocular cavities and into the blood stream. Lipophilic molecules can easily diffuse back across the BRB once

delivered to the vitreous or retina [53]. Maintenance of appropriate drug concentrations in the posterior eye is therefore a unique challenge.

2.4.4 Posterior Eye Drug Delivery Approaches

2.4.4.1 Intravitreal Delivery

To avoid hurdles of topical and systemic drug delivery to the posterior eye, intravitreal injection has been used widely. It is the most direct method of delivering drug to the vitreous and retina, though it is also associated with a considerable number of risks. Reports have shown a significant elevation in IOP up to 9 months after one injection of the steroid triamcinolone acetonide. Cataract progression has been reported in 6.2-6.6% of similar injections [55, 56]. Reports of endophthalmitis after anti-VEGF agent injections range from 0.7-1.6%, though another study suggested that most injection related infection cases were caused by departures from protocol [57]. Other side effects to this method include hemorrhage and retinal detachment. Since the newer macular degeneration drugs depend on periodic intravitreal injection, risk of side effects is increased over the lifetime of treatment. [53].

Dispersion of drug injected into the vitreous depends on diffusion through this viscous, non-stirred medium. Hydrostatic pressure, osmotic pressure and to a lesser extent, convective flow and active transport also influence the drug's path. After intravitreal injection, lipophilic molecules typically move from anterior to posterior and are eliminated through the retina. Hydrophilic molecules and those with poor permeability to the retina tend to diffuse towards the anterior eye, exiting through the anterior chamber [53].

Drug half-life in the vitreous is also influenced by the position and volume of injection. Increasing injection volume may increase clearance. Additionally, adding volumes of greater than 20μl generally requires removal of vitreous to balance the internal pressure. Half-lives of intravitreally injected drugs can range from less than one hour [9] to almost three days [53]. Though not as extreme as systemic delivery, this method still requires a larger bolus dose to allow for the appropriate bioavailability to treat the affected areas.

To address the repeated risk of side effects and the need for longer half-lives between injections, several groups have investigated use of polymers as intravitreal drug delivery vehicles. On the market currently is a reservoir type device (Vitrasert®) designed to reside across the thickness of the eye wall. It is coated with a degradable membrane for controlled

release of the drug glanciclovir to treat intraocular infections [58, 59]. Beeley, et al. made similar devices of Nitonol, PMMA or chromic gut with a drug eluting polymer coating for intravitreal delivery of triamcinolone acetonide over 4 weeks [60]. These devices all require large incisions in the globe for placement and must be removed after drug delivery is complete.

Implants have been created for similar trans-globe implant, but with fully biodegradable materials PLA, PGA or PLGA. They have been used to deliver a variety of drugs at therapeutic levels including antiviral, antifungal, antimetabolic, immunosuppressive agents and steroids. These show a reduced risk of retinal detachment compared to the non-degradable implant, and no inflammatory response was seen [50]. Alikacem et al. used similar PLGA rods to deliver VEGF to study its effects on the blood-retinal barrier. Release was governed by diffusion and continued over 3 weeks [61].

Other devices with degradable elements have been designed for full implantation inside the vitreous. Beeley et al. implanted a sub-retinal polycaprolactone rod to deliver triamcinolone acetonide over 4 weeks. Drug was localized to the posterior eye segment, with higher concentrations in the vitreous than in the retina or choroid. No fibrosis or hemorrhage of subretinal fluid was detected [62]. In a much longer term in vitro study, poly(propylene fumarate) rods were investigated for their ability to deliver another steroid, fluocinolone acetonide. All formulations of the material released drug over 400 days, though variations determined the timing of initial and final bursts of drug [63]. Poly(ortho esters) have also been considered for intravitreal delivery of 5-FU [64].

Degradable microspheres containing drug have been considered for intravitreal use. These small particles circumvent the need for a surgical implant, since they can be delivered by injection instead. Moritera et al. were the first to use this technique, injecting PLA microspheres that cleared from the vitreous after 48 days [59]. More recently, Andrieu-Soler et al. injected PLGA microspheres containing glial cell line derived neurotrophic factor (GDNF), a protein to slow photoreceptor death. In a 20-day study, there was a significant increase in the amount of healthy photoreceptors in eyes with these drug loaded microspheres [65]. In addition to the risks associated with intravitreal injections, a temporary decrease in vitreous transparency may also occur [59].

Despite these successes, it has been argued that nanospheres, even with a lower drug encapsulation efficiency, may in fact make better delivery vehicles because cells can incorporate

them by endocytosis. One group introduced PLGA nanoparticles containing dye intravitreally in a rat model. After 24 hours, a significant concentration of dye was seen in RPE cytoplasm, and this level remained elevated over a 4-week period [54].

2.4.4.2 Transscleral Delivery

The route of transscleral drug delivery to the posterior segment has also been investigated. If effective for the application, this method is less invasive than the intravitreal approach, showing reduced risks of side effects such as infection and ocular damage during delivery. The sclera has been shown to be permeable to a large range of molecular weight molecules. Ambati et al. showed in vitro that the sclera is permeable to biological molecules as large as IgG (150kDa molecular weight) [66]. In an in vivo study, slow release of fluorescently labeled IgG from a scleral pocket was shown to accumulate in the choroid and retina, without significant buildup systemically or in the vitreous [67]. Further, chemical modification of the sclera by molecules such as prostaglandins increases the tissue's permeability, as shown with various molecular weight rhodamine labeled dextran molecules [68].

Using this concept, periocular injection of drug, either beneath the conjunctiva or between Tenon's capsule and the sclera, has also been in use. Subconjunctival injection improves bioavailability to the vitreous 10 times over systemic delivery. It has been shown that drug first saturates the sclera before diffusing inward. Injecting below Tenon's capsule places the drug in closer proximity to the sclera and generally allows only localized diffusion. Either of these routes of injection leads to similar levels of drug in the retina and vitreous, though closer placement of drug allows for longer delivery times [53].

As with the intravitreal route, polymer vehicles have also been used to deliver drugs transsclerally. Polymer discs have been investigated for either episcleral or intra-scleral attachment. For example, a polyvinyl alcohol/ethylene-vinyl acetate (PVA/EVA) polymer has been implanted intra-sclerally and used to deliver the steroid betamethasone at therapeutic levels over 4 weeks. A similar study using a PLA vehicle was shown to suppress inflammation in the eye for 8 weeks. Throughout this period, there was a consistently higher drug concentration in the retina and choroid than in the vitreous [69].

Microspheres injected periocularly have had success in delivering drug to the retina and choroid. Carrasquillo et al. have delivered Macugen® in PLGA microspheres in an in vitro study of transscleral permeability. They showed a low burst release, and an average delivery of

2μg/day across the entire thickness of the eye wall [70]. Others have delivered PKC412, a kinase inhibitor known to block VEGF receptors, in microspheres to slow CNV formation in animals. There was a significant amount of drug in the choroid 10 days after injection, with an increase over the next 10 days in the retina and vitreous [54]. Kimura et al. used PLA microspheres to prevent fibrosis after glaucoma filtration surgery. In this case, drug was released for 20 days without a significant burst effect [59]. Researchers have also considered nanoparticles for subconjunctival delivery as well. In this environment, nanoparticles tend to show a faster rise and steeper decline in bioavailability compared to 2 week delivery from microspheres [54]. Though polymer drug delivery to the posterior eye may be effective over the short term, long-term, steady delivery of biological molecules has not been shown.

To enhance diffusion of molecules across the sclera, an electrical method known as iontophoresis has been used in both animal and human experiments with charged drug molecules. Briefly, a power source drives drug molecules from a reservoir into the tissue via electrode; another location on the animal's body holds a second electrode to complete the electrical circuit. For transscleral applications, the iontophoresis apparatus consists of a narrow tube carrying the drug to an eyecup electrode attached to the conjunctiva via suction [53]. A wide variety of drug types including antibiotics, steroids and antiviral agents have been delivered across the sclera by iontophoresis [71]. Studies have also shown that oligonucleotides will travel across scleral tissue under the influence of an electric field [72]. This method of delivery is relatively effective. In one study using the anti-viral drug foscarnet, low clearance was shown, thus maintaining therapeutic drug levels in the vitreous for 60 hours. Differing distributions of drug were observed dependent on the type of drug delivered [71].

As a non-invasive, well-tolerated method, iontophoresis has the potential to replace systemic drug delivery and delivery by repeated intravitreal injections for posterior eye diseases. Due to the direct link between amount of current and delivery time to the drug levels, this method is also controllable. Despite risk of side effects for iontophoresis including the potential for burns, edema and inflammation, numerous safety studies have shown low risk of these effects [71, 73]. Iontophoresis, however, has not to date been applied to implantable, sustained, local drug delivery.

2.5 Summary

The eye is a delicate and intricate sensory organ that is prone to several diseases of both its anterior and posterior segment. Pharmaceutical, surgical and device approaches are commonly employed to treat many of these conditions. Recent drugs have become available specifically for some diseases of the posterior segment, but delivery to this region presents many challenges including its physical inaccessibility and the protective blood-ocular barrier. For these applications, localized, long-term drug delivery has been emphasized for success of these treatments.

For any new implantable device, biocompatibility must be investigated. Two devices have already been implanted for long-term residence on the scleral surface: the scleral buckle and the glaucoma drainage device. While these devices do encourage a significant amount of fibrous tissue encapsulation by the body, they are often biocompatible enough to serve their function. Materials such as titanium and stainless steel have been used extensively in other implants with a lesser degree of reaction from the body. However, they have not typically been used for scleral implants.

A variety of implantable, passively or actively controlled implants have been investigated for introduction of drug either intravitreally or transsclerally. Passive polymer implants are often useful for short-term delivery, though they also do not allow for complex control over dosing regimens. Active implants are to date relatively intricate and have not been designed for local implantation near the retina. Intravitreal introduction of drug solution is the current method of delivery, though any delivery to this space risks damage to the internal structures or disturbance of the vitreal transparency or pressure. Transscleral drug delivery has shown promise experimentally in terms of safety and efficacy. However, while there has been much research in this area, few long-term devices for scleral attachment have been created.

Chapter 3: Device and Testing Apparatus Design

3.1 Introduction to Device Concept

In collaboration with MEEI, Draper Laboratory has proposed an implantable solution to the posterior eye drug delivery challenge. This particular design takes advantage of the ability for transscleral drug diffusion and would be sutured directly on the scleral surface, with no part of the device penetrating the globe. The entire device is enclosed in a metal case whose base is rounded to match the curvature of the globe. A window in the base allows for passage of drug to the sclera and requires interstitial fluid to reside inside the device. Design specifications call for all wetted parts to be made from materials well known to be biocompatible [74, 75].

Central to the design is a drum containing an array of microwells in its wall, each measuring approximately 1.2mm x 0.5mm x 0.13mm. In this proposed device, a portion of lyophilized drug is sealed in each well by a flexible metalized parylene coating. Adjacent to this drug drum is a second cylinder with a series of blades protruding from its wall (pin drum). As shown in Figure 3.1, the base of each drum is a gear, and the gears from the drums are spaced to articulate against each other [74, 75]. A ball bearing (Figure 3.2) supports the drug drum and allows for smooth rotation.

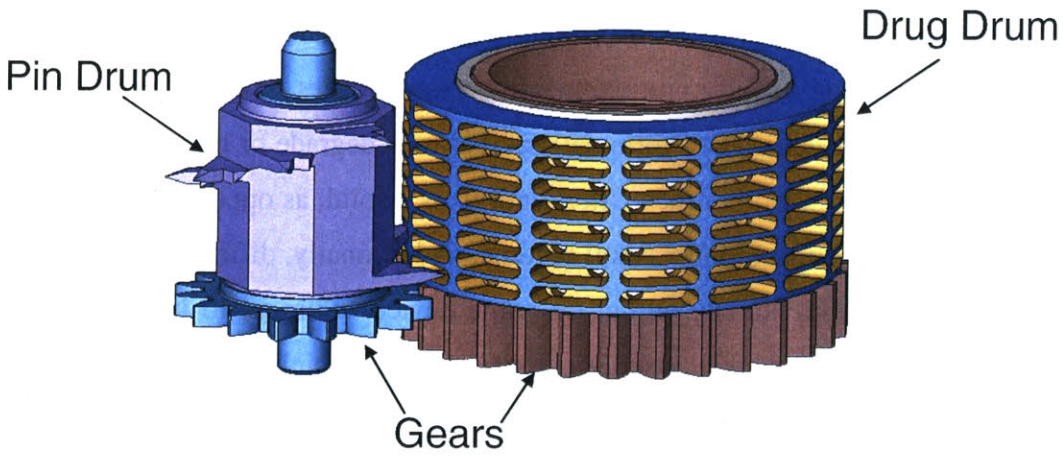

Figure 3.1 Drug and pin drums in the proposed Draper/MEEI ophthalmic drug delivery device.

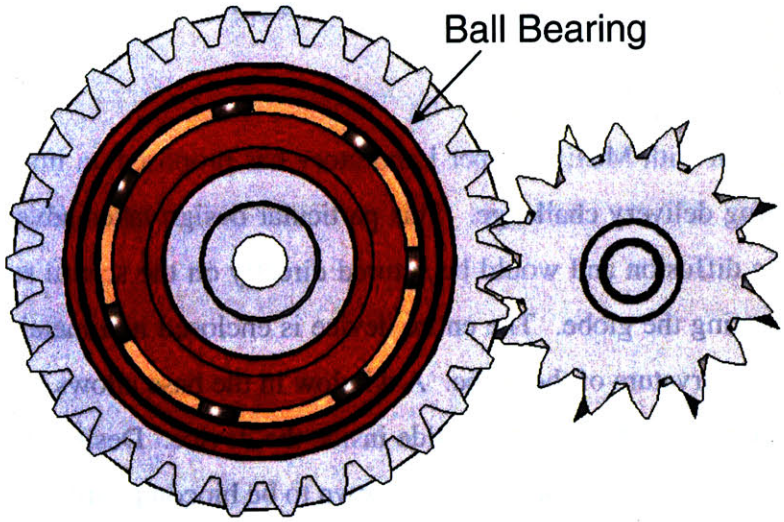

Figure 3.2 Bottom view of the two drums on the Draper/MEEI device, showing the ball bearing location.

To operate the device, an internal battery powers an oscillator circuit, which, through a series of gears inside the drug drum, causes the two drums to turn against each other. As this action occurs, the blades on the pin drum sequentially break open each well of the drug drum. Opening a well in this manner exposes the drug to fluid inside the device. Drug diffuses out of its chamber and to the scleral surface, where it can then diffuse through the eye wall. This device could accommodate dosing protocols from hours to days, and the intended device life in the body is on the order of months to years [74, 75].

Such a device is advantageous over other transscleral methods in its ability to release a controlled amount of drug in fully programmable dosage profiles. Drug storage in sealed, dry compartments allows for delivery of formulations that may degrade or become inactive in fluid, especially after long implantation times. Storing drug as a solid, as opposed to a liquid solution, allows for more drug to be stored in a small volume. Additionally, different types of drug could be stored and released individually within the same device. Surgery to implant this device is similar to that for scleral buckle insertion, thus requiring minimal surgeon training. The procedure is relatively non-invasive, allowing for short surgery and relatively easy recovery for the patient. This device allows for the patient to have a passive role in the application of drug, nearly removing patient compliance as a complication.

Despite these advantages, it is unclear the extent to which first, this device will affect the area of implantation and second, the body will respond to such an implant. Scleral buckles and GDD's are implanted in similar locations on the sclera, though they are made of different

materials, contain many fewer parts, and serve a much different function. Materials such as titanium and stainless steel are considered to produce a low level of fibrous encapsulation in other applications, but have not typically been implanted on the sclera. With the novel use of miniature moving metallic parts exposed to the exterior eye environment, it is unknown what effect any protein adsorption and foreign body response may have on the function of the device. Power requirements are particularly affected by the amount of added friction (or lubrication) a biological response may contribute. Size and shape requirements may be affected by the amount of fibrous tissue formation around the device. Additionally, the amount of scleral erosion may influence the method of attachment and materials used on the base of the device.

In vitro modeling of this system would give an incomplete picture of the biocompatibility of this device. It may be possible to simulate the protein solution in the interstitial fluid surrounding the eye. However, cell reaction to the foreign body and any mechanical effects of the device on surrounding tissues could not sufficiently be investigated in vitro. In addition, due to the lack of knowledge about exactly how the system may operate in this case, analytical models would be highly complex and require a large number of assumptions and simplifications. It is therefore necessary to investigate the biocompatibility of this device in an animal model. The rabbit was chosen for this study due to its common use in ophthalmic models of human conditions. Its eyes are also large enough to hold an implant with parts comparable in size to those for a human, yet the animal is small enough to house several at a time.

3.2 Design Goals and Parameters

Space available behind the rabbit eye is more limited than the human eye. Measurements taken on an example rabbit eye revealed the following approximate values:

- Eye outer diameter (medial-lateral direction): 18.5mm
- Circumferential space between superior and lateral muscles: 10mm
- Allowable height between globe and orbit: 3-3.5mm
- Allowable depth behind limbus: 4-7mm

The full prototype drug delivery device would not fit in this space. It was therefore necessary to create a test device to investigate biocompatibility. Since gears and ball bearings are the major articulating elements, devices were designed to contain each. These devices would allow for both mechanical and histological evaluation. It was proposed that mechanical testing

involve the change in torque required to turn the moving elements after implant. As such, the test device should allow for a controlled method of torque application and measurement. Because the proposed drug delivery device turns its gears so slowly (approximately 15° of rotation per day for the pin drum if dosing every three days), it was proposed that a non-powered, static test device would effectively model the system. Assuming that any device motion would disrupt tissue formation in vivo, this device model would therefore represent a worst-case scenario for biological response.

Two devices were designed, one investigating gears and the other ball bearings. Models can be viewed in Figure 3.3, Figure 3.4, Figure 3.5, and Figure 3.6. Mechanical drawings are available in the Appendix. Both devices have generally rectangular baseplates, each curved on one face to a spherical radius that matches the curvature of the rabbit eye. Both also have a generally rectangular cover that conceals the internal machine elements plus tabs extending from their ends to hold sutures. Maximum dimensions on the gear device measure 9.43mm x 4.47mm x 3.05mm (0.371in. x 0.176in. x 0.120in.). Maximum dimensions on the ball bearing device measure 8.22mm x 4.57mm x 2.90mm (0.324in. x 0.180in. x 0.114in.).

Through the thickness of the baseplate in the gear device are two slots that run much of the length of the part. They allow for communication to the sclera and are similar to the drug port in the delivery device in placement and dimension. Additionally, through the thickness of the baseplate are two small holes to accommodate the bottom shafts (0.381mm, 0.015in. diameter) of two gears. This gear pair forms a small gear train with ratio 1:1.5, where the larger gear is similar in size to that on the pin drum in the prototype device. Each gear is supported on the baseplate face by a 0.762mm (0.030in.) diameter shoulder in the shaft.

The baseplate supports four integral posts rising from each corner of the top face. On top of the posts in the baseplate, a flat plate gearbox cover is bonded, which allows for the gears' top shafts to protrude through by 0.015in. This assembly of the baseplate with the two gears and flat cover comprise the gearbox that is used for mechanical testing before and after implant. Some gearboxes were machined with slightly oversized holes (about 0.001in. larger). These devices were tracked and evenly distributed among experimental groups.

Surrounding five sides of the gearbox is the test device's cover. The cover is mostly a rectangular prism in shape but is also curved on the bottom to fit the eye surface. The top shafts of the gears fit through holes in the cover such that their tops rest flush with its outer surface. On

each end of the cover at the eye surface are tabs with two round suture holes each. By suturing it to the sclera, the cover then contains and holds the gearbox in place without physically attaching to it. This design allows for simple removal of the cover post-implant for microscope evaluation. Approximately 0.051mm (0.002in.) of space exists between the gearbox and the inside of the cover on all sides.

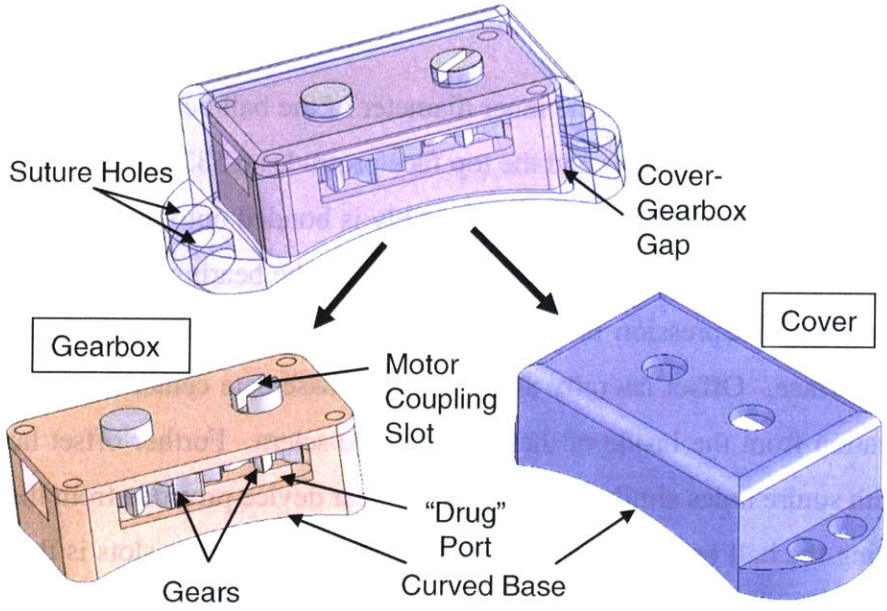

Figure 3.3 Overview of gear device.

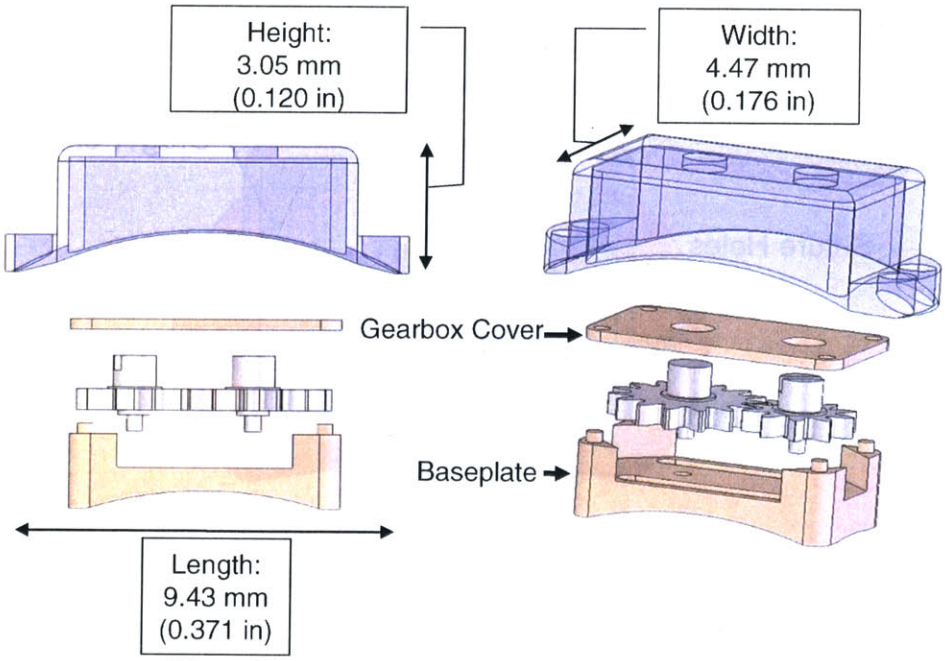

Figure 3.4 Dimensions of gear device, exploded view.

The ball bearing device was designed for mechanical testing only and does not therefore have an easily removable cover. The ball bearing itself measures 1mm inner diameter and 4mm outer diameter. Races on the bearing are made from titanium (Ti6Al4V) and the balls are formed from zirconia (ZrO_2 + HfO_2: 94.75%, Y_2O_3: 5%, Al_2O_3: 0.25%). This ball bearing is currently used in an implanted device, though is not exposed to body tissues in that configuration.*

A small shaft is bonded into the inner diameter of the ball bearing so that the bottom face is flush with the bottom of the races and the top face protrudes 0.533mm (0.021in.) above the top of the races. The outer race of this bearing assembly is bonded onto the center of the baseplate. Four protrusions from the top face of the baseplate locate the bearing by its outer circumference. Beneath the bearing, a depression in the baseplate allows the inner race to turn freely without contacting the surface. Offset laterally away from the baseplate center are two slots that allow for communication from the inside of the device to the sclera. Further offset laterally from the center, tabs with suture holes similar to those on the gear device protrude from the baseplate.

Enclosing the ball bearing with its supports and the baseplate slots is the device's cover. It is generally rectangular in shape and bonded to the surface of the baseplate. It is located by the protrusions from the baseplate in one direction and by an internal shelf that mates with the top of the outer race in the other direction.

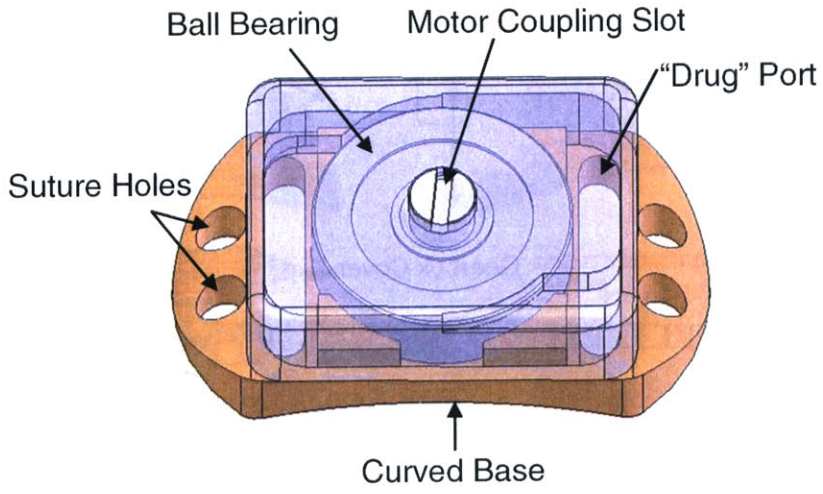

Figure 3.5 Overview of ball bearing device.

* Weibel, J., MPS Micro Precision Systems, electronic mail, Aug. 2006.

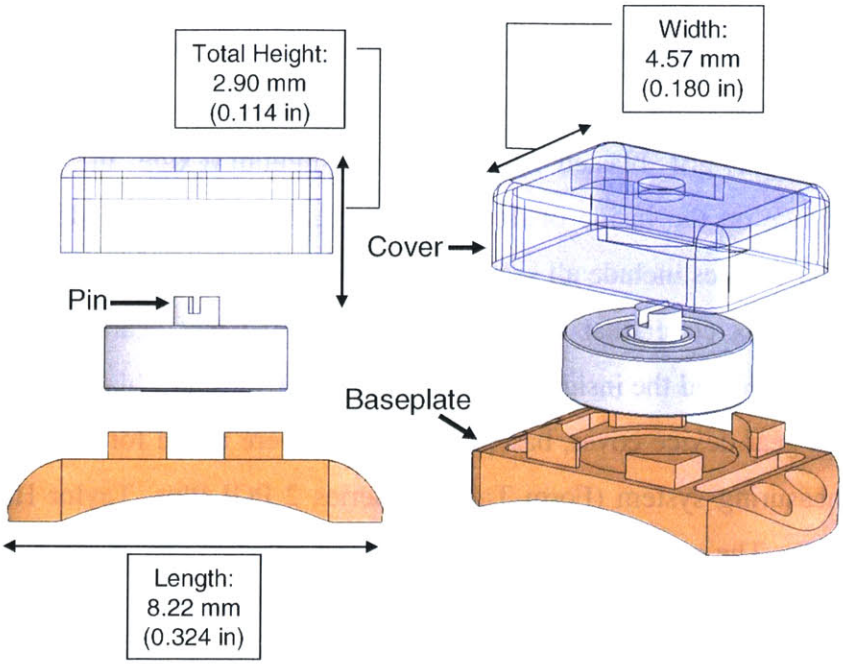

Figure 3.6 Dimensions of the ball bearing device, exploded view.

3.3 Fabrication and Surface Properties

For the exposed parts of the Draper/MEEI drug delivery device, materials were specified from the list of metals typically used for implants and known to be chemically safe in the body. In order to focus on immune effects on the moving parts, novel materials were not considered for the test device. Instead, only titanium (Ti6Al4V) and stainless steel (316L) were used. In order to control for effects of each material, any one test device was fabricated entirely of one material. The gear devices were constructed from either Ti6Al4V or from 316L stainless steel. The ball bearing housings were constructed of Ti6Al4V only. Since the balls of the bearings are made from zirconia, the bearing devices contained two different materials in each test device.

The ball bearing was purchased from MPS Micro Precision Systems (Faulhaber Group, Bienne, Switzerland). For the gear devices, pinion stock was purchased in the necessary gear sizes. Stainless steel (316L) stock was purchased from WM Berg (East Rockaway, NJ), and titanium (Ti6Al4V) stock was custom made by Rush Gears (Fort Washington, PA).

All other parts and modifications were made by the Draper Laboratory machine shop. Wire electrical discharge machining (EDM) was used to remove bulk material from the gear stock. Slots in the tops of the driving gear shaft and in the ball bearing pin were also carved out by wire EDM. All other parts were made by traditional machining.

For both devices, the curved surface of the baseplate that contacts the scleral surface and all outer surfaces of the cover were polished in order to be less attractive for cell attachment. Internal surfaces were grit blasted with 27μm aluminum oxide in order to achieve a homogeneous surface on the inside of devices and to allow for epoxy adhesion. Grit blasted surfaces of the gear devices include all sections of the baseplate that do not contact the globe and the side of the gearbox cover that faces the gears. On the ball bearing device, the internal sections of the baseplate and the inside surfaces of the cover were grit blasted.

An example gear device cover, baseplate and gear were tested for surface roughness (R_A) using a finish measuring system (Form Talysurf Series 2 PGI Plus, Taylor Hobson Precision, Leicester, England). The outside of the cover was hand polished and showed some inconsistent sections of surface roughness. Values varied from 5.69 to 11.32μin. Grit blasted sections of the baseplate measured 26.00μin., and the highly polished spherical surface measured 1.661μin. Similarly, the gear face measured 1.376μin. surface roughness.

3.4 Mechanical testing apparatus

To perform torque testing, a 2.71W, 12V DC motor with an encoder counting 224 cycles per shaft revolution (Faulhaber Group, MicroMo Electronics, Clearwater, FL) was interchangeably coupled to each device. Torque necessary to turn the devices' moving elements was recorded by a precision dynamometer, and the output was routed to a computer. A LabView (National Instruments, Austin, TX) interface was created to plot and record real time data. Torque data and information about motor position were recorded in 20ms intervals into data files for future analysis.

The dynamometer (Dynamics Research Corporation, Andover, MA) consists of a circular metal plate supported horizontally on an air bearing and connected to a set of electronics. A steady stream of clean instrument air flows through the instrument at all times to create the bearing. The entire precision unit is housed in a rectangular box resting on legs with adjustable height. As a torque is applied to the circular plate at the top of the box, the instrument detects the rotation and attempts to correct the plate's position. The resulting torque necessary to realign the plate is equal in magnitude to the input torque. This effort by the dynamometer is then output as a voltage, which can be scaled by the instrument console.

Two dynamometers were used during the course of this work, differing in maximum torque capacity: (1) 1400 dyne-cm and (2) 10,000 dyne-cm. The input plate on dynamometer (1) is allowed to turn 360°, while on dynamometer (2) a hard stop restricts rotation to less than a few degrees. The two are otherwise indistinguishable. Before use, both were aligned to vertical and calibrated using the recommended application of known weights at known distances with various instrument tilt. Each reported torque to within 3% accuracy of the output value.

To test the gear and ball bearing devices on this equipment, it was necessary first to mount each device onto the dynamometer input plate. Figure 3.7 shows a model of the mechanical testing setup, and mechanical drawings for all adaptor parts can be found in Appendix A. Because of the differing footprints between the two devices, one holder was created for each. Holders were designed to rest on the input plate, in effect acting as simple cylindrical extensions of this plate with a recess at the top to support a device. This device pocket was situated such that the driving element (slotted shaft) of the device was centered on the input plate. Pockets were designed to be 0.254mm (0.010in.) larger in both length and width than each device and deep enough to hold a majority of the device height – 1.78mm (0.070in.) for the gear device, 2.03mm (0.080in.) for the ball bearing device. A threaded hole was placed collinear to the diagonal of the rectangular pocket. A #0-80 set screw in this hole could then push the device into the corner of the recess, reproducibly aligning it with respect to the dynamometer. These holders were fabricated from stainless steel. Their weight created enough friction against the input plate to prevent slippage and to translate the input forces to the dynamometer.

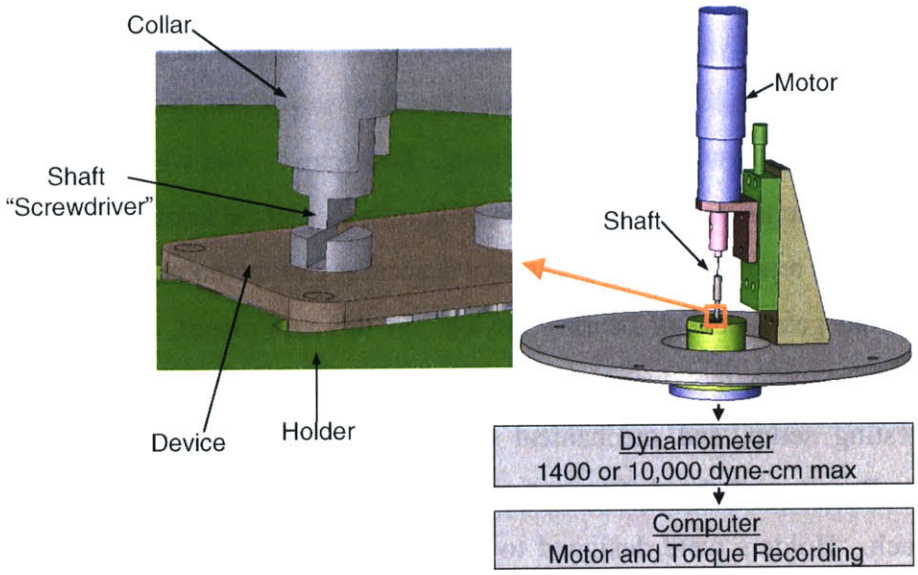

Figure 3.7 Mechanical testing apparatus.

After mounting a device to the instrument, the motor then needed to be attached with its shaft reliably close to the center of the input plate and with three degrees of freedom to adjust for error and to lower the motor to the device. The free turning motor shaft added a fourth degree of rotational freedom. A donut shaped aluminum plate was designed to be screwed to the top frame of the dynamometer and to allow attachment of the motor. Since the top frame is adjustable in both horizontal directions, only vertical adjustment was then needed. The motor was attached to this plate via a previously fabricated stand including a vertical lead screw, lending the third degree of freedom to the motor.

Finally, mating of the motor shaft to the device-driving shaft was necessary. A flexible adaptor was designed of three separate sections. The top section slip fit over the motor shaft and was secured with a set screw. The bottom section consisted of a two-tiered cylindrical rod with a flat section at the far end from the motor. This flat was designed to mate with the slot in the device-driving shafts much like a flat-head screwdriver fits into a screw. Connecting the top and bottom adaptor sections was a thin steel wire, attached inside each by a cyanoacrylate adhesive (Henkel Loctite, Düsseldorf, Germany). The degree of freedom created by this flexible design allowed for small misalignments during turning and for ease of mating the shaft with the device.

In order to allow for the appropriate amount of flexibility in this shaft, an optimization evaluation was used to choose the diameter and exposed length of steel music wire. It was estimated that 0.020in. of lateral displacement was necessary at the tip of the shaft. In order to transmit torque consistently, twisting of the wire should be limited to less than 2°. Using the

following equations, a wire diameter and length was chosen that required a minimal amount of force to deflect the wire, with a minimal amount of twisting allowed (Figure 3.8).

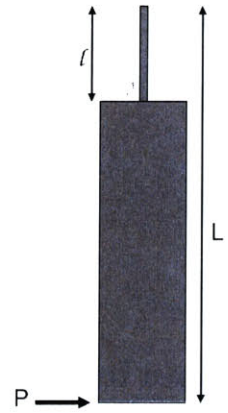

Figure 3.8 Geometry for calculation of appropriate wire length on the motor shaft adaptor. P – lateral force, L – total shaft length, *l* – wire length.

For this arrangement, it was noted that the deflection at the base of the shaft is dependent on a force and a moment acting at the junction between the wire and the stiff shaft, plus the deflection of the stiff shaft due to the angles created by the force application.

$$d = \frac{Pl^3}{3EI} + \frac{P(L-l)l^2}{2EI} + \left(\frac{Pl^2}{2EI} + \frac{P(L-l)l}{EI}\right)(L-l)$$

Equation 3.1 Shaft deflection.

where P is the laterally applied force at the shaft tip, E is the Young's modulus, I is the bending moment of inertia for the cylindrical wire, L is the total shaft length and *l* is the wire length. Simplifying and solving for P,

$$P = \frac{3dEI}{l^3 - 3Ll^2 + 3L^2l}$$

Equation 3.2 Force to move shaft tip a distance d away from vertical.

It was also noted that the twisting angle of the wire is

$$\theta_t = \frac{Tl}{GJ}$$

Equation 3.3 Angle of wire rotation.

where θ_t is the twisting angle, T is the expected applied torque, G is the shear modulus and J is the torsional moment of inertia for the cylindrical wire. The following values were estimated for the part and material:

$L = 0.815in$

$T = 1400dynecm \approx 0.00124lbfin$

$E = 3.0x10^7\ psi$

$G = 1.15x10^7\ psi$

$d = 0.02in$

Diameters of available wire included 0.008, 0.010, 0.011 and 0.0135 inches. Wire lengths considered were 0.010, 0.100, 0.250, 0.500, 0.750 and 1.00 inches. P and θ_t were calculated for each wire diameter and length. Values allowing for P near 0.0022lbf (about 1 gram force) and θ_t below 2° were found. From this list, the 0.010 inch diameter wire, with a 0.250 inch length was chosen for the shaft, where P = 0.0024lbf and θ_t = 1.57°.

A collar was designed to slip fit around the bottom section of the shaft adaptor for use with the gear devices. Once the shaft tip was properly mated with the gear shaft, the collar was lowered so that its inner diameter mated with the gear shaft's outer diameter. This restraint locked the motor shaft into place on the gear, preventing any lateral motion. Due to the recessed design of the shaft on the ball bearing device, this collar was not necessary during its testing.

In the event that neither dynamometer withstood sufficient torque to allow the gears to turn, a secondary testing setup was created using a manual torque watch (Waters Manufacturing, Inc.) as the measuring tool. A torque watch consists of two concentric cylinders that are allowed to twist with respect to each other with a stiffness maintained by an internal spring. The amount of torque necessary to rotate one against the other has been pre-calibrated and is reported by dial indicator on the top of the instrument. To interface with the devices, another shaft was created like the bottom of that on the motor. One end of it was secured into the torque watch chuck, leaving it free to mate with the device's shaft on its other end. This torque watch-shaft assembly was mounted vertically on a ring stand by the top cylinder. Beneath it was placed the device holder with the device in position. Using the ring stand, the instrument was carefully lowered to the device and locked into place. Keeping the assembly intact, the holder was rotated beneath the instrument until it generated enough torque to turn the gears. An approximate maximum

torque value was recorded. As holder rotation continued, the approximate steady state torque value was also recorded.

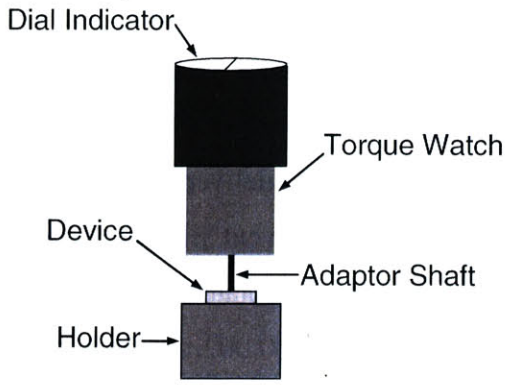

Figure 3.9 Secondary torque testing apparatus schematic.

Chapter 4: Membrane Material Selection

4.1 Introduction

Because the drug ports on each device present an opportunity for cell and tissue infiltration, sealing these openings with a porous membrane was investigated in a subset of implants. To be useful for the Draper/MEEI delivery device, such a membrane would need to allow drug diffusion readily. In order to prevent fibrous tissue infiltration, it must also block passage of fibroblasts. To be tested on the baseplates of the gear devices described in Chapter 3:, these filters should be approximately 50μm (0.002in.) thick, within the clearance between the gearbox and cover. The material should also have enough compliance to mate with a curved surface.

It was estimated that a membrane with a minimum pore size of 1μm would be permeable to most drugs to be delivered. Many drugs are orders of magnitude smaller; even a relatively large antibody such as IgG is less than 50nm in diameter [76]. It was assumed that no chemical reactions or electrical interactions occur between the drug and membrane material, and that drug delivery takes place over a long time period (hours to days). A drug dose should then easily pass through a material with holes at least one order of magnitude larger than the molecule. Larger pores and higher porosity would further increase the ability of drugs to diffuse to the sclera.

Since it was estimated that a typical fibrous cell is 10μm in diameter, pore size for the membrane should be in the range between 1-10μm. A thorough search of commercially available filter membranes yielded a limited selection of appropriate products. Materials included PTFE and polycarbonate (PC). Thicknesses ranged from 7μm to 85μm, and porosity ranged from about 10 to 80%.

A literature review of cell migration studies did not clearly identify an appropriate pore size or material to fit this need from among the available options. Classic fibroblast migration studies have investigated 2-D movement of cells on flat surfaces [77]. For example, Lallier et al. studied mobility of fibroblasts and pre-osteoblasts on the horizontal and angled surfaces of a tissue culture flask [78]. Additionally, Thampaity and Wang studied 1-D fibroblast migration on specially grooved silicone plates [79]. Three-dimensional migration is important to study for applications such as cancer cells, and Zaman et al. investigated their migration through gel matrices of varying properties [80]. Similarly, Chen et al. used a tissue culture well insert to

investigate fibroblast movement through a gel-coated polycarbonate membrane [81]. However, a study of the minimal pore size through which a fibroblast might travel has not been reported.

4.2 Experimental Methods

For application to this drug delivery device, an in vitro study comparable to that by Chen et al. was performed to determine the optimal material and pore size for preventing cell migration through a membrane. Four membranes were selected and seeded with NIH/3T3 fibroblasts (ATCC #CRL-1658, pass 48) to investigate the cells' ability to penetrate through the material. Isopore™ track-etched polycarbonate membranes with 1.2, 5 and 10μm pores and Omnipore™ PTFE membranes with 10μm pores were selected as listed in Table 4.1 (Millipore, Billerica, MA).

Material	Pore Size (μm)	Thickness (μm)	Porosity (%)
PC	1.2	11	23
PC	5	10	8
PC	10	10	8
PTFE	10	85	80

Table 4.1 Materials for in vitro selection test.

Scanning electron microscope (SEM) images of the membranes revealed differing finishes on either side of the PC membranes (Figure 4.1). Communication with the vendor revealed no difference in chemical treatment on either side, but instead a difference in drying during manufacture. The membranes dry on a belt surface; the side facing the belt has a rougher finish than the side facing the air. Due to a difference in fabrication methods, the PTFE membrane did not display this dual finish. The vendor claims that both materials are hydrophilic in nature. Because PTFE is naturally hydrophobic, hydroxyl groups have been attached to the surface during manufacturing to change the polarity.

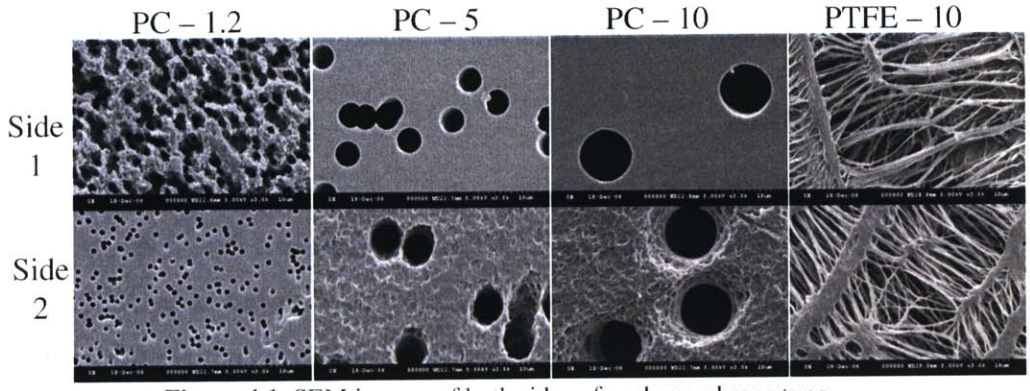

Figure 4.1 SEM images of both sides of each membrane type.

To prepare the membranes for cell seeding, six circles of each material were cut with a 12mm tissue punch. From 24 cell culture inserts (Millipore), the provided membranes were removed. Each new membrane was attached to the bottom of an insert and sealed around the edges with a silicone coating (3140RTV, Dow Corning, Midland, MI). PC membranes were all attached with the rougher surface towards the inside of the insert. Glue was allowed to dry overnight at room temperature. Cell culture inserts with new membranes were sterilized in 70% ethanol for one hour and were allowed to air dry. Each was then placed in one well of a 12-well tissue culture plate, thus creating two chambers in each well: one inside the insert and one surrounding it in the plate (Figure 4.2). The system was shaped such that the bottom of the membrane was a wall of the outer chamber and the top of the membrane was a wall of the inner chamber.

One milliliter of cell culture medium was placed in the outer chamber of each well. Medium consisted of Dulbecco's Modified Eagle Medium with L-glutamine (ATCC, Manassas, VA), 10% fetal calf serum (ATCC) and 1% penicillin (100U/ml)/streptomycin (100µg/ml)/amphotericin B (0.25µg/ml) solution (Invitrogen, Carlsbad, CA). Into the inner chamber, a suspension of 10^5 cells in 0.5ml of media was seeded (Figure 4.2). With this assembly, fluid communication was allowed through only the membrane. Cells were cultured for 3 days at 37°C in a 5% CO_2 environment.

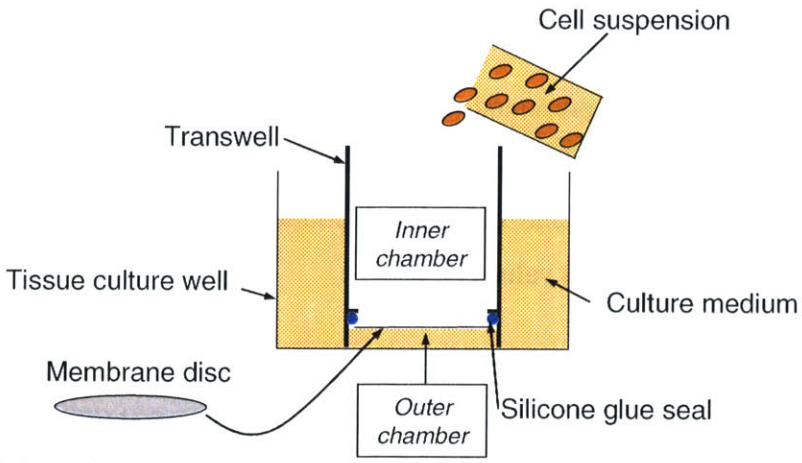

Figure 4.2 Schematic of cell culture apparatus for investigating cell migration through a membrane.

Each insert apparatus was then removed from the culture plates without mixing the contents of the two chambers. While still intact with the insert, membranes were rinsed once in phosphate buffered saline (PBS, Invitrogen) before being soaked in a 4% paraformaldehyde solution for 15-20 minutes. After cells were fixed, membranes were rinsed twice in PBS. Filters were then carefully peeled off of the inserts, ensuring that tweezers touched only the edges, and stored in PBS at 4°C until being processed for microscopy. To stain cells, membranes were incubated at room temperature in 1μM DAPI stain (Invitrogen) for at least 3 minutes before being returned to PBS. Membranes were mounted in glycerol between two cover slips for imaging (Axiovert 200, Carl Zeiss, Thornwood, NY) with a standard DAPI filter cube, in epifluorescence mode.

On each side of each membrane, one fluorescent picture was taken over a $0.145mm^2$ area in each quadrant using the following steps:

1. Start with the objective at the top, center of the membrane
2. Move down 3mm, left 2mm for picture 1
3. Move right 4mm for picture 2
4. Move down 4mm for picture 3
5. Move left 4mm for picture 4

Cells in each view were tallied and averaged over each side of each membrane. Tallies were divided by the area in the field of view to obtain counts in terms of cells per square millimeter. Two-tailed Student's t-tests were performed to determine statistical significance between groups (t-test: Two Sample Assuming Unequal Variances).

4.3 Results and Discussion

Results for this study are presented in Figure 4.3 and Figure 4.4 in terms of the cells per square millimeter of membrane surface area. Generally, due to sparse and irregularly spaced cell populations on the PC membranes, and varying cell counts on the PTFE membranes, each group displayed a wide range of cell count values.

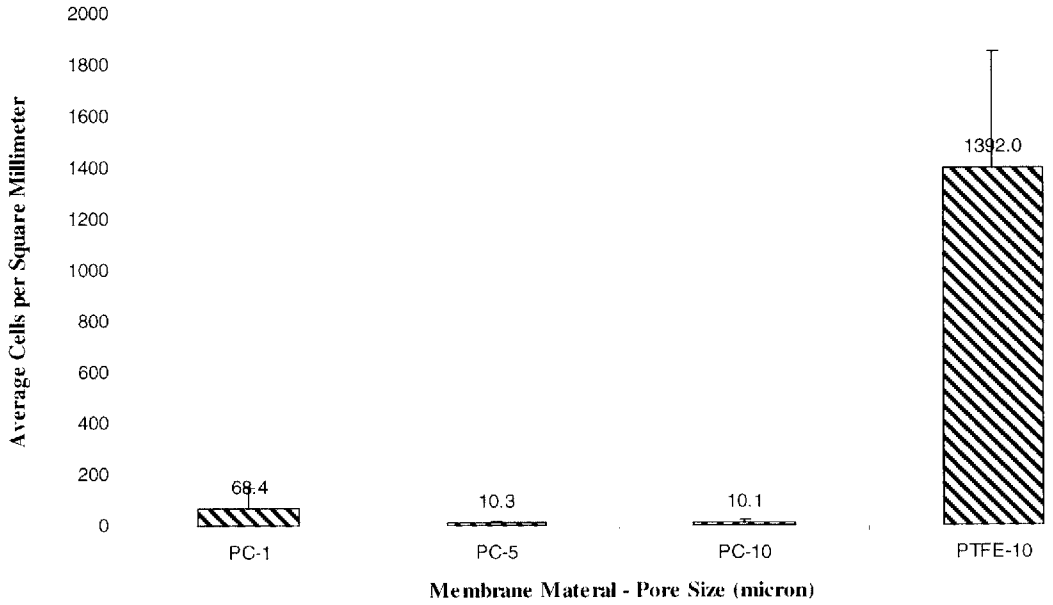

Figure 4.3 Average number of cells per square millimeter on the seeded side of each membrane.

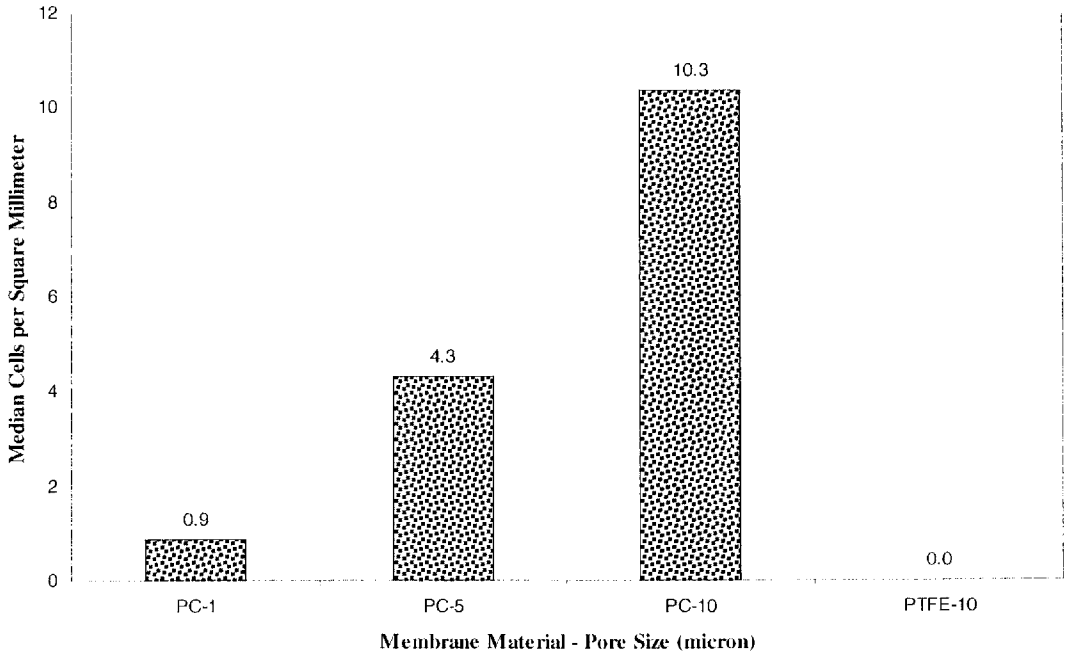

Figure 4.4 Median number of cells per square millimeter on the non-seeded side of each membrane.

Overall, the PC membranes supported many fewer cells on the seeded sides as compared to the PTFE membranes. By inspection, areas of the PTFE membranes showed confluent regions of cells on the seeded side. Conversely, simple inspection of the PC membrane top sides revealed relatively few cells, though rare locations did show confluent patches. The PTFE membranes had a statistically significant amount of cells adherent to the top sides compared to each of the PC membranes ($p<0.001$ in all cases).

Within the PC group of membranes, more cells were observed on the 1.2μm pore filter than on the 5 or 10μm filters. Referencing the SEM images of the rougher membrane sides, the surface of the 1.2μm membranes is more uneven than that of the other two PC membranes. Further, the PTFE membrane retained a far larger number of cells on the top side than the 1.2μm filter. Relating the cells per square millimeter on the seeded side of the membrane to the membrane porosity, an increasing trend indicates that the rougher the surface, the more cells remain attached. While a surface unattractive to cells would make a device more inert in the body, for this application it may be more advantageous for cells to grow onto the device and prevent it from causing disruptive micro-motion. In the case of the latter hypothesis, the PTFE membrane is preferable.

Inspection of the data shows a clear pore size dependence in the PC membranes on the likelihood that cells will pass through the filer. Considering the median, average and range information, more cells passed through the 10μm pores than through the 5 or 1.2μm pores. Similarly, more cells passed through the 5μm pores than the 1.2μm pores. However, comparing to the 10μm pore PTFE, many fewer cells passed through the PTFE than through any of the PC membranes. Observations of the media consumption in the outer chamber of each tissue culture well correlates with the results from imaging.

These results suggest that cells much more readily migrate through the track etched, uniform holes in the PC membranes as compared to the irregular meshwork of the PTFE filter. Based on the data from the top sides, they may also suggest that cells on the PTFE adhere well to the top side and are therefore not encouraged to migrate to find footing. Similarly, cells that do not adhere well to the top surface of the PC membranes may be more encouraged to migrate.

In terms of preventing fibrous tissue infiltration into an ophthalmic device, the PTFE membrane was judged to have the largest potential for success among those tested. It allows for abundant cell attachment on the side of cell seeding. This characteristic may encourage tissue to

attach to the base of the device and anchor it in place, likely reducing any further inflammatory response. This membrane also allows very few cells to pass through, likely restricting the amount of tissue that will impair the device function. Finally, this PTFE material is highly flexible, allowing for relatively simple assembly onto the device's spherically curved base plate. Therefore, the Omnipore^{TM} 10μm pore membranes were chosen for use on devices.

Chapter 5: In Vivo Experiment

5.1 Experimental Design

The proposed drug delivery device would remain in the body on the order of 1 year before either refilling the drug or replacing the entire device. As such, the most important biocompatibility information for a test device would come from long time points. It was proposed to study effects on the animal and on the device at 10 weeks to represent the long term and 2 weeks to represent the short term effects.

Additionally, since the device design calls for fabrication with known biocompatible materials, testing identified differences in biological response or affect on the eye between these materials. Effects of adding a porous membrane to these devices was also investigated, as discussed in Chapter 4:. As mentioned in Section 3.2, the fourth variable in this study was the type of moving element used in the device. Since the major articulating parts in the Draper/MEEI device are gears and ball bearings, each represented a separate group to be tested. Long term experimental groups were titanium gear (Ti-l), stainless steel gear (SS-l), stainless steel gear with membrane (SSM-l) and titanium ball bearing (BB-l). Short term groups were stainless steel gear (SS-s) and stainless steel gear with membrane (SSM-s) (Table 5.1).

Group Name	Device Type	Material	Implant time 10 wks	Implant time 2 wks
Ti-l	Gear	Titanium	4	
SS-l	Gear	Stainless Steel	4	
SS-s	Gear	Stainless Steel		2[†]
SSM-l	Gear	Stainless Steel + PTFE	4	
SSM-s	Gear	Stainless Steel + PTFE		3[†]
BB-l	Ball Bearing	Titanium	3[‡]	

Table 5.1 Number of devices in each experimental group.

[†] One device from each of these groups was removed from an animal that survived only 10 days post-implant (See Section 5.6).
[‡] One device from this group was displaced from the implant location during week 10.

5.2 Cleaning and Assembly

After fabrication and purchase of parts, all were cleaned to remove any residual grease, oil and adhesive. Parts were sonicated for 3-5 minutes in each of n-heptane, methanol and acetone and were dried between baths. Parts were stored in clean, covered glass dishes until assembly.

Epotek 730 two-part epoxy (Epoxy Technology, Billerica, MA) was chosen for assembly of all devices. This material is certified as biocompatible according to United States Pharmacopeia (USP) and National Formulary (NF) standards [82]. It was also chosen for its high viscosity (80,000 – 120,000 cPs) to prevent migration of epoxy during assembly. As per manufacturer instructions, epoxy was cured for at least 2 hours in an oven at 80°C. Assemblies were allowed to cool in the oven before removing them.

To assemble the gear devices, both gears were set into place on the baseplate and checked to ensure they moved freely. A watchmaker's oiler was used to place small amounts of epoxy on the tops of each baseplate post, taking care not to touch the gears with the adhesive. The gearbox cover was set into place, ensuring that the posts and gear shafts mated correctly with the cover. After a short application of pressure at each post, excess epoxy was removed with lens paper, and devices were allowed to cure.

Membranes were added to the SSM groups after this cure step (Figure 5.1). The gear box was inverted in its torque testing holder and held in place via set screw. Using a small oiler, a bead of epoxy was applied around the outer edges of the curved base. A rectangular section of the membrane was cut and laid on the device. A hollow plastic cylinder was attached vertically to the top of the holder such that it surrounded the device. A Dacron™ rod, custom made with the inverse baseplate curve at its end, slid through the plastic holder and rested on the membrane and device. Even pressure was therefore applied around the membrane to seal it to the baseplate. An additional 200g weight was placed on top of the rod for extra pressure. This assembly was allowed to sit at room temperature for approximately 1 hour before being removed to the oven for complete cure at 80°C. Membranes were then trimmed around the baseplate using scissors and a blade.

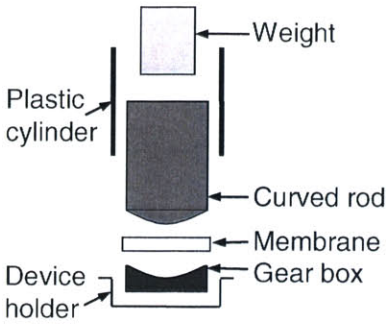

Figure 5.1 Membrane assembly apparatus schematic.

To assemble the ball bearing devices, the pin-ball bearing unit was created first (Figure 3.6). The pin was dipped into epoxy and cleaned of excess. With the ball bearing on a flat surface, the pin was slipped inside its inner race and pushed down to meet the flat surface. Epoxy was allowed to cure before excess was scraped away from the pin with a blade. Next, epoxy was added to the inside of the protrusions from the baseplate, and the ball bearing-pin unit was set inside such that the outer race was attached to the baseplate. Additional epoxy was added around the outer race as necessary. Epoxy was added to the outer, long edges of the baseplate face, outside of the protrusions. The device cover was placed over the baseplate, ensuring that the cover centered over the pin and was firmly attached at the baseplate. Devices were cured as described.

All devices were then cleaned briefly with bursts of compressed air and documented with microscope pictures before mechanical testing. (See Figure 5.2, Figure 5.3 and Figure 5.4 for examples.)

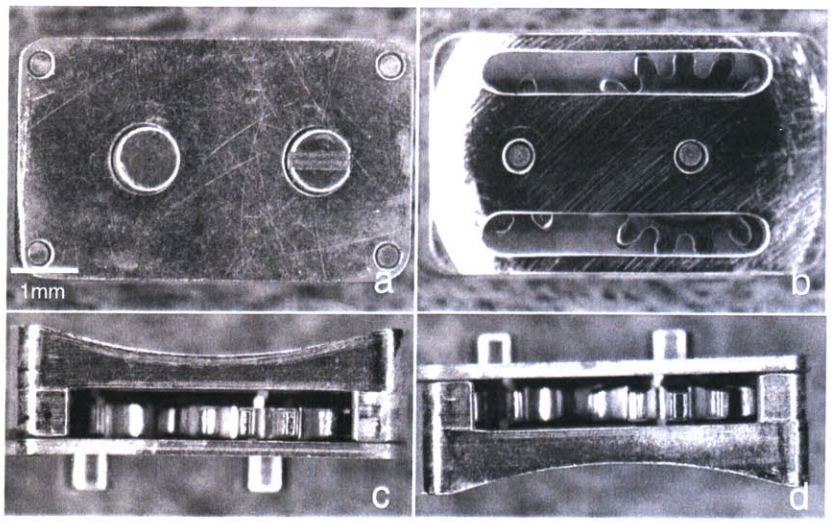

Figure 5.2 Pre-implantation photographs of a typical gearbox: (a) top, (b) bottom, (c,d) sides.

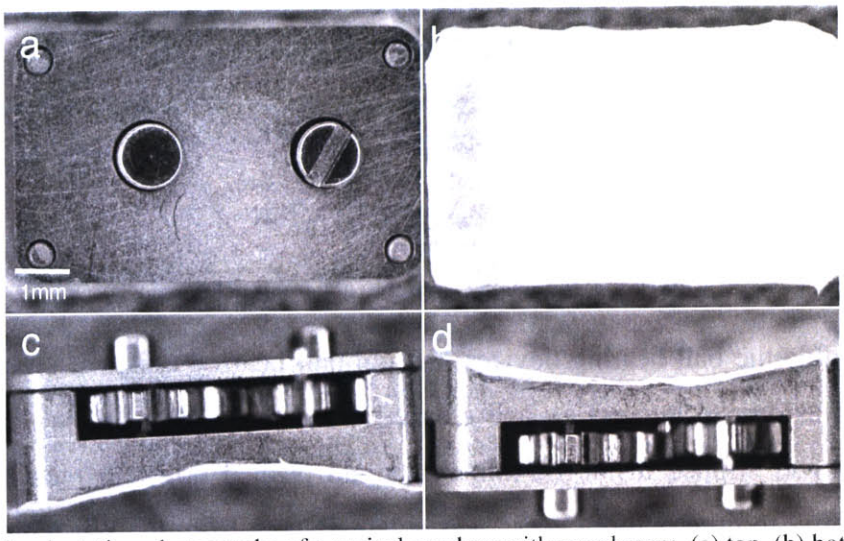

Figure 5.3 Pre-implantation photographs of a typical gearbox with membrane: (a) top, (b) bottom, (c,d) sides.

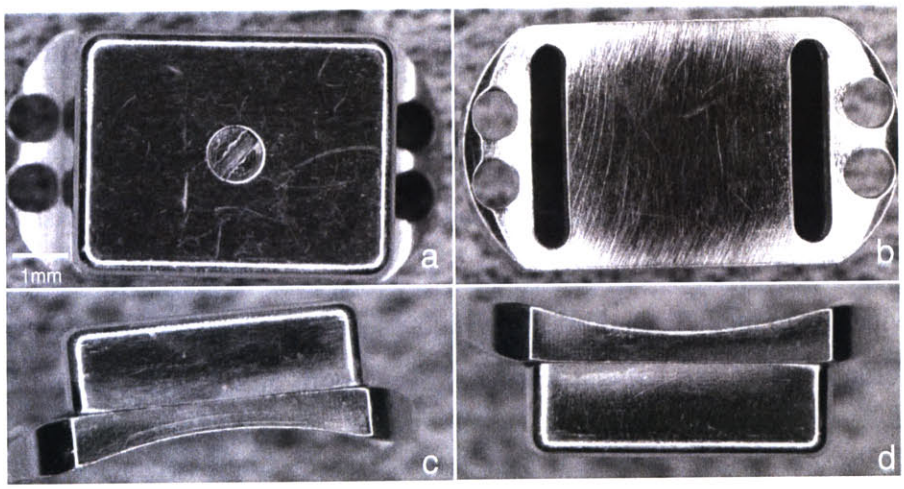

Figure 5.4 Pre-implantation photographs of a typical ball bearing device: (a) top, (b) bottom, (c,d) sides.

5.3 Mechanical Testing-Pre Implantation

Each device acted as its own control in this experimental design. In order to establish a baseline torque value, devices were tested on the dynamometer apparatus, as described in Section 3.4, before implantation. Briefly, devices were placed in the proper holder and screwed into place. The holder was set on the dynamometer, followed by the motor on its stand. The motor shaft was carefully shifted using the x-y plane controls to align it with the device shaft. It was also manually spun on its axis to align the flat "screwdriver" end of the shaft with the slotted "screw head" of the device shaft. The motor shaft was then lowered to mate with the device shaft, taking care that the motor shaft did not apply downward pressure on the device. For the

gear devices, the collar was lowered partway over the gear shaft to hold it in position. For the ball bearing devices, no collar was used.

Torque measurements from the dynamometer were recorded at three different motor speeds, in the following order: 4.01rpm (218mV), 7.20rpm (275mV) and 13.4rpm (400mV). The motor was turned off between speeds, but the device remained in place throughout all three sets of recordings. It was assumed that slower speeds would allow for more thorough evaluation of the torque. The lowest speed was experimentally determined to be the slowest reliable speed by the motor, and the other two were chosen as incremental increases from that point.

After testing, devices were sterilized in a bath of 70% ethanol solution for 2 hours. In a sterile hood, they were then sealed into pre-sterilized bags for transport to MEEI.

5.4 Implantation

Only one implant was attached per eye, and several animals received two total implants. Procedures were performed at MEEI by one of two surgeons. The MEEI Animal Care Committee approved this protocol. Due to several constraints, rabbits with the titanium devices and short-term stainless steel devices were 12-18 months old at implant, while the remainder of devices went into 5 month old rabbits

Animals were anesthetized with 1-1.5 mL of a mixture of 50mg/ml ketamine (Phoenix Pharmaceutical, St. Joseph, MO) and 20mg/ml xylazine (Phoenix Pharmaceutical) by intramuscular injection. For each eye receiving an implant, the lids were separated and held open by a speculum (Figure 5.5a). Betadine drops on the eye cleared the area of bacteria, and drops of proparacaine (Alcon, Fort Worth, TX) numbed the eye. The conjunctiva and Tenon's capsule were carefully separated from the globe in the area between the superior and lateral rectus muscles (Figure 5.5b). Two stitches were thrown through the sclera with 7-0 nylon suture (Ethicon, Somerville, NJ) and threaded through the suture holes on the device. Sutures secured the device on the globe with a 1-1-1 knot on either side. For the gear device, sutures were placed approximately 4.5mm posterior to the limbus, with 9mm between the two. For the ball bearing device, sutures were placed approximately 6mm from the limbus, with 7mm between the two (Figure 5.5c) This configuration allowed at least 2mm between the limbus and the device edge. The conjunctiva was pulled back over the device and secured with a 2-1-1 knot of 7-0 Biosorb sutures (Alcon, Fort Worth, TX) (Figure 5.5d, Figure 5.5e, Figure 5.5f). Antibiotic drops and

ointment were applied, and the speculum was removed to allow the lids to re-close. Animals were monitored daily for the first week post surgery, and antibiotic ointment was applied daily as needed. Animals in the long-term study were monitored once a week thereafter.

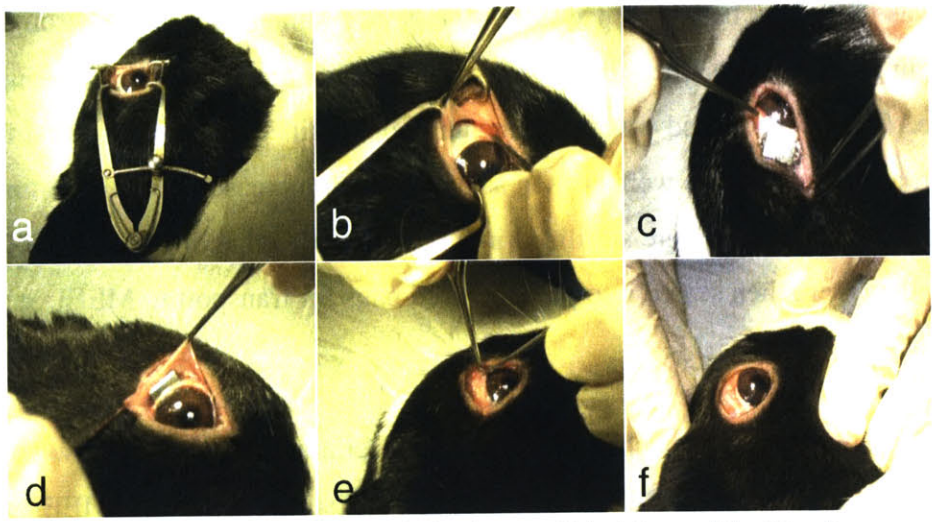

Figure 5.5 Surgical procedure for implanting test device into a rabbit: (a) open lids, (b) pull away conjunctiva and Tenon's tissue to expose sclera, (c) place device on sclera, (d) after suturing, cover device with tissues, (e) close conjunctiva with sutures, (f) final implant state before re-closing lids.

5.5 Device Removal and Testing

On the day of device removal, the animals were anesthetized with 1-1.5mL of a mixture of 50mg/ml ketamine (Phoenix Pharmaceutical) and 20mg/ml xylazine (Phoenix Pharmaceutical) by intramuscular injection. They were euthanized by an intraperintoneal or intracardial overdose of pentobarbital sodium (Vortech Pharmaceutical, Dearborn, MI). Each eye was enucleated, taking care to leave any tissue surrounding the device intact. Without removing this tissue, devices were cut away from the scleral surface as needed to disengage the device from the eye. Tissue surrounding the device was removed and fixed for histology in either 10% formalin (Electron Microscopy Sciences, Fort Washington, PA) or in Karnovsky's fixative (Electron Microscopy Sciences). On the gear devices, the outer device cover was removed and also fixed for histology. The globe was marked with cuts or a tissue marking dye (Thermo Fisher Scientific, Waltham, MA) as to the location of the device, and it too was fixed for histology.

Parts of the devices for mechanical testing included the gearbox of the gear device and the entire ball bearing device. Each was immediately placed into a small tube packed with a thin, saline-soaked wipe. Tubes were stored on ice or in a 4°C refrigerator until testing. This moist,

chilled environment was intended to preserve the tissue in its in vivo form around the device for the most accurate mechanical testing.

Tubes with devices were transported from MEEI to Draper. Microscope pictures were taken of the gross tissue on the devices, taking care not to disturb the tissue and to replace them quickly to their moist, cool environment. Mechanical torque testing was then performed on each device in the same manner as during pre-testing (Section 5.3). In the event that the dynamometer apparatus was insufficient, the manual system was used as described in Section 3.4.

Devices were then investigated under stereomicroscope for more subtle observations of tissue infiltrate. On the gear devices, the gearbox cover was removed by applying force between it and the baseplate. Additional pictures were taken to document observations of tissue around and inside the devices. This tissue was removed and fixed for histology when possible.

To clean devices after use, parts were sonicated in PBS and then 70% ethanol to remove tissue and sterilize the device. Any remaining tissue was removed manually. Devices were soaked in dichloromethane (Sigma Aldrich, St. Louis, MO) in 1-hour intervals or in an overnight bath to loosen the epoxy residues from the device. After manual removal of softened epoxy, the devices were stored until needed for reuse. In the event that a part was reused in another implant, surfaces were freshly grit blasted and polished before repeating the cleaning steps leading to assembly as listed above. Reused gear boxes were tracked and evenly distributed throughout the groups so as not to bias the results.

5.6 Results

5.6.1 Gross Observations

Animals tolerated the devices very well. Within one week after implant, any redness and swelling around the eye had decreased significantly, and it was not apparent to a casual observer that any change had been made to the animal. No infections were reported in any rabbit, and they continued feeding and moving normally in their cages. Only one animal did not survive to the intended time point of the study, due to its failure to acclimate to the cage feeding system. Devices from that animal were removed for mechanical testing within 18 hours upon finding it deceased, 10 days after implantation. Results from those devices were grouped with similar ones implanted for 2 weeks, as shown in Table 5.1.

From one of the ball bearing devices, one set of sutures had come loose at the time of removal, causing the device to dangle in front of the rabbit's cornea. This displacement occurred during the three days before the end of its 10 week implant time. The cornea in the region beneath the device was more opaque than surrounding tissue. The device was otherwise evaluated in the same manner as the rest of the group.

Upon pulling the lid back from each eye, observations could be made about the conjunctiva on top of the device (Figure 5.6). In the case of the gear devices, in general the tissue was significantly thicker than normal at both 2 and 10 weeks, as compared to that of Figure 5.5f. Vasculature was usually apparent in this tissue, and it was often tough and somewhat gelatinous in texture. Three of four titanium gear devices and two of eight 10-week stainless steel devices showed a slightly thinner conjunctiva, with the ability to observe the device through the tissue. Similarly, all three ball bearing devices were associated with a relatively thinner conjunctiva.

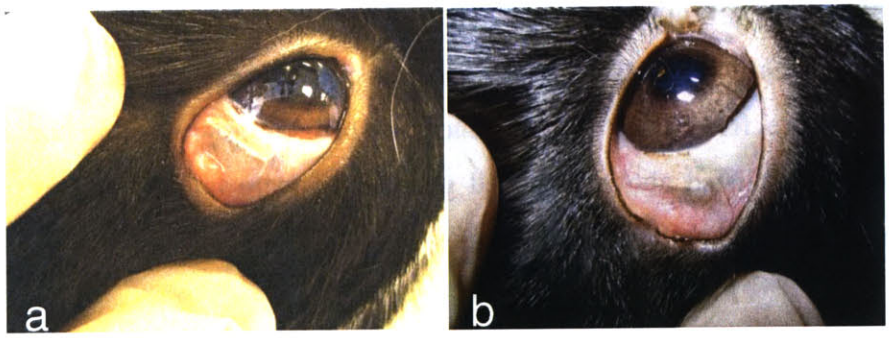

Figure 5.6 Photographs of gear devices on the rabbit eye immediately before removal: (a) Ti-l device showing thinner conjunctiva, (b) SS-s device showing thicker conjunctiva.

After cutting through the sutures, it was observed that all devices were in fact held in place on the sclera by tissue attached between the bottom of the device and the eye wall. It was necessary to cut away this tissue in order to remove the devices from the eye. In the majority of cases, this tissue connected to midsection of the base of the device. One SS-l and one SSM-l device were attached around the edges of the base only. Four 10-week gear devices were so tightly held to the sclera that some scleral tissue may have been removed when cutting away the device. The two ball bearing devices that remained in place were surrounded entirely by a thin, distinct, relatively transparent tissue. To remove the implant, it was necessary to cut this membrane away from the sclera. It pulled away from the eye wall as an intact sheet.

When removing the device covers, it was apparent that the tissue did not adhere directly to the metal. Thickened conjunctiva pulled away from the devices cleanly, except where it had grown through the suture holes and attached to suture material. On the gear devices, any difficulty removing the conjunctiva from the cover came from its connection to tissues residing inside the device. Gear device covers slid off of the gearboxes easily, though often with some encouragement by pushing on the gear shafts. The inside pocket of the covers were clean from any tissue. Gross inspection of implant interiors revealed that gear devices were filled with tissue to some degree. This tissue appeared to have been continuous with the conjunctiva and sclera. While one ball bearing device appeared free from any interior tissue, the other two bearing devices also showed some tissue in the drug ports.

Investigating the devices under stereomicroscope after mechanical testing revealed information about tissue formation inside and around the devices. Comparing gear devices at the two time points, much less tissue was found inside the 2-week devices (5 implants) as compared to the 10-week devices (12 implants), shown in Figure 5.7. All gearboxes in the latter group were encased in a thin, smooth, translucent layer of tissue (Figure 5.7e,f), and the interior space was filled with a tougher, less organized tissue (Figure 5.7g,h). Gearboxes at two weeks showed the early stages of a thin tissue forming on the top and sides of the devices (Figure 5.7a,b). In some cases, areas of the tougher internal tissue were also found. It was also apparent that webs of tissue were beginning to form between the gear teeth at short time points (Figure 5.7d).

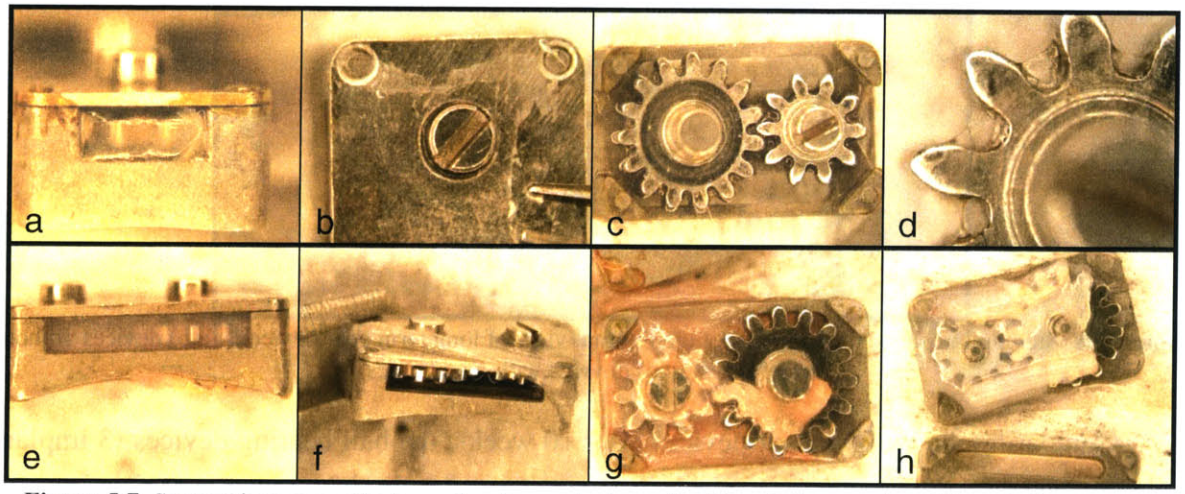

Figure 5.7 Stereomicroscope photographs of gear devices after 2 week (top row) or 10 week (bottom row implantation times: (a,b,e,f) translucent layer around gearboxes, (c,d,g,h) tissue around gears.

Within the gear device group, a comparison was made between gearboxes with (7 devices) and without (6 devices) a porous membrane covering the drug ports (Figure 5.8). At short time points, there was some evidence that the membrane decreased the amount of tissue in the gear space, including one such device that showed almost no tissue in this area. Long-term membrane covered implants, however, had similar amounts of tissue inside and surrounding the gearbox as the uncovered implants, and the gear space was similarly filled with tissue. However, there was no communication of tissue through the membrane covered drug ports, as there was clearly in the uncovered devices. Any tissue that grew into the drug ports from the inside of the device was not attached to the membrane. Additionally, tissue in the gear space of membrane devices tended to encase one or both gears into a single sac (Figure 5.8c,d), while in uncovered devices, tissue tended to fill any open space (Figure 5.8a,b). Finally, at both short and long time points, the outer surface of the membranes was clearly glossy with tissue and in some long-term cases, showed evidence of tissue tightly adhering to the filter.

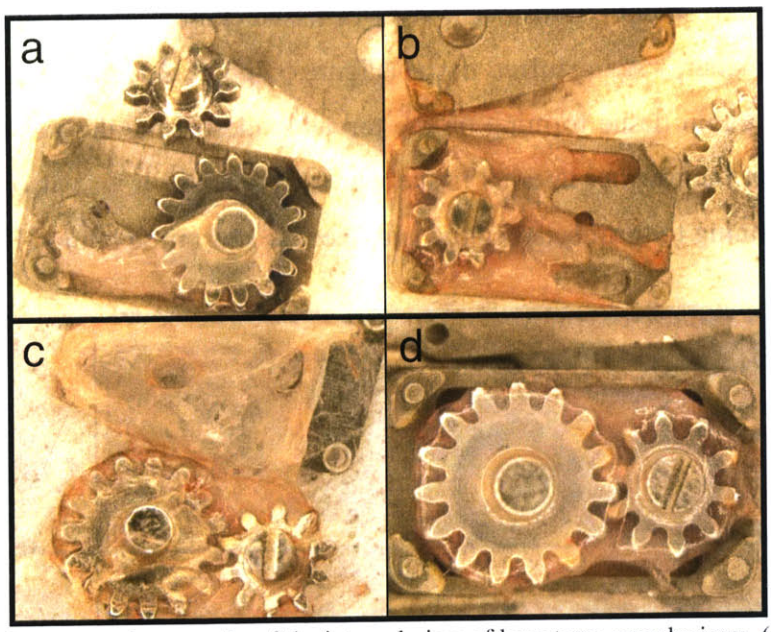

Figure 5.8 Stereomicroscope photographs of the internal view of long term gear devices: (a,b) devices without membranes, (c,d) devices with membranes.

Comparing the two types of devices after 10 weeks, the ball bearing devices (3 implants) were less likely to have any tissue infiltration than the gear devices (10 implants). The ball bearing devices had a thin, distinct layer of tissue surrounding the entire device (partially shown in Figure 5.9b_1), while the gear devices had a slightly thicker layer that penetrated under the

cover and through the entire gearbox. Ball bearing device photographs are shown in Figure 5.9. Device 3 had fallen out of place by the end of the implant period.

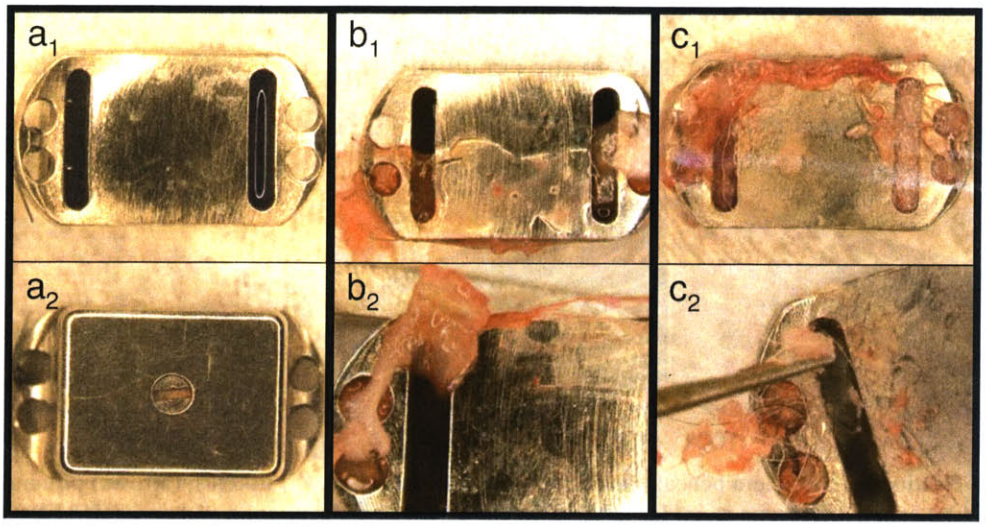

Figure 5.9 Stereomicroscope photographs of the three BB-l devices after implant: (a_1,a_2) device 1, (b_1,b_2) device 2, (c_1,c_2) device 3.

In the long-term gear group, comparing the titanium devices (4 implants) to the stainless steel devices (8 implants) revealed a similar type of tissue encasing and infiltrating gearboxes of both materials. Generally, titanium devices were associated with less reaction in the conjunctiva than their stainless steel counterparts. However, titanium gear devices were implanted in animals of a different age, potentially complicating the evaluation of this variable.

5.6.2 Histology Results

Histology sections of the sclera beneath the device and the conjunctiva above the device were available from the SSM-s, SS-l, SSM-l and BB-l groups. Sections of tissue from the insides of devices were available from all 10-week groups. Sections through only the PTFE membranes were made for devices in the SSM-l group.

Eye wall sections showed no erosion to the sclera itself. On the contrary, all devices encouraged a layer of new growth, continuous with the sclera in the area between the device and the eye. In the short term devices, this tissue was highly cellular and included many inflammatory granulocytes (Figure 5.10). With the long term devices, however, this tissue was more densely fibrous and included mostly fibroblasts, with occasional inflammatory cells (Figure 5.11). This tissue disrupted the architecture of nearby muscles. Some neovascularization was apparent in this tissue, as noted in the BB-l group (Figure 5.11a,b). No consistent differences

were identified between the scleral surfaces of long-term experimental groups. While there were differences in thickness of the fibrosis between samples, it was not conclusively correlated to any particular device type. For example, one SS-l device displayed a frayed layer of fibrous tissue and one SSM-l device had a thin layer in the center of the section, with much thicker areas near the edges of the device (Figure 5.11c,d).

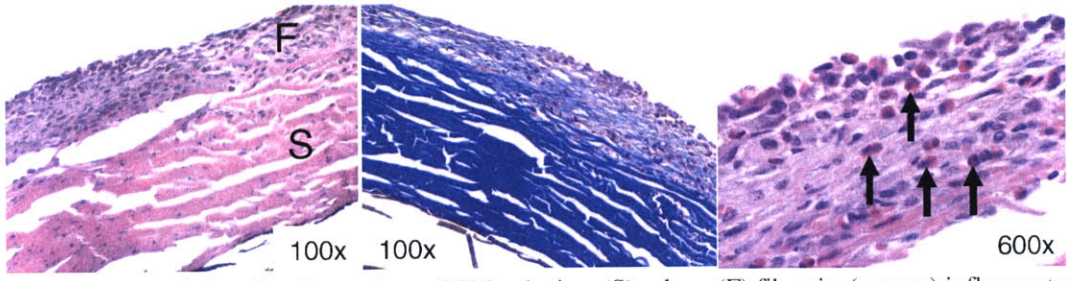

Figure 5.10 Sections of the sclera beneath one SSM-s device: (S) sclera, (F) fibrosis, (arrows) inflammatory cells. Middle panel: tricrhome stain, far left and far right panels: haematoxylin and eosin (H&E) stain.

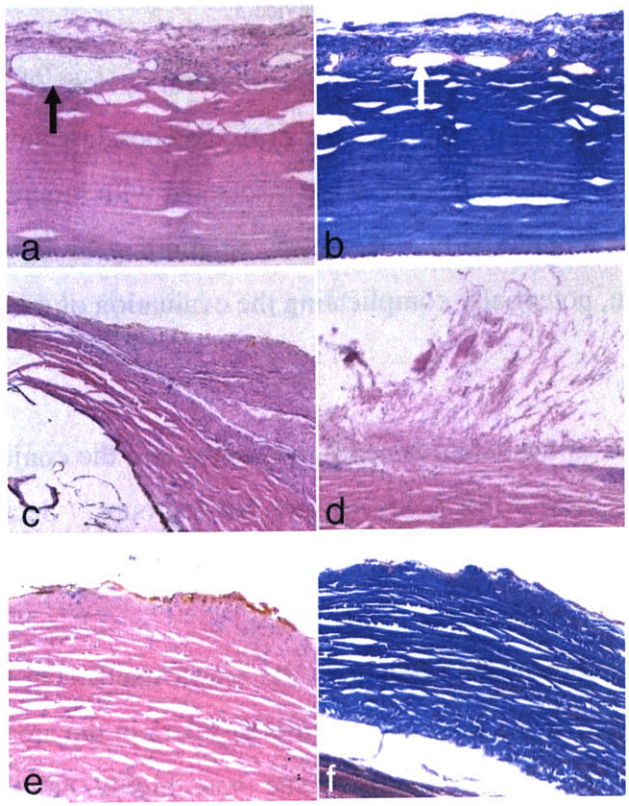

Figure 5.11 Sections of the sclera beneath long-term devices: (a,b) one BB-l device, (c,d) two SS-l devices, (e,f) one SSM-l device. (a,c,d,e) H&E, (b,f) trichrome, all 100x magnification.

The conjunctiva was notably filled with new fibrous tissue in the stromal layer for all devices (Figure 5.12). For most devices, there were small focal areas within this tissue showing

inflammatory granulocytes. One SSM-l device had a particularly large amount of inflammation present in the conjunctiva (Figure 5.12b), though that result was not apparent for the entire group. Neovascularization in the newly formed fibrous tissue was shown in several samples. The BB-l devices encouraged notably less fibrosis than its SS-l counterparts. This fibrous tissue disrupted the entire architecture of the conjunctiva in the SS-l case, as compared to the BB-l group, where the fibrosis grew as an extra layer inside the stroma (Figure 5.12c,e).

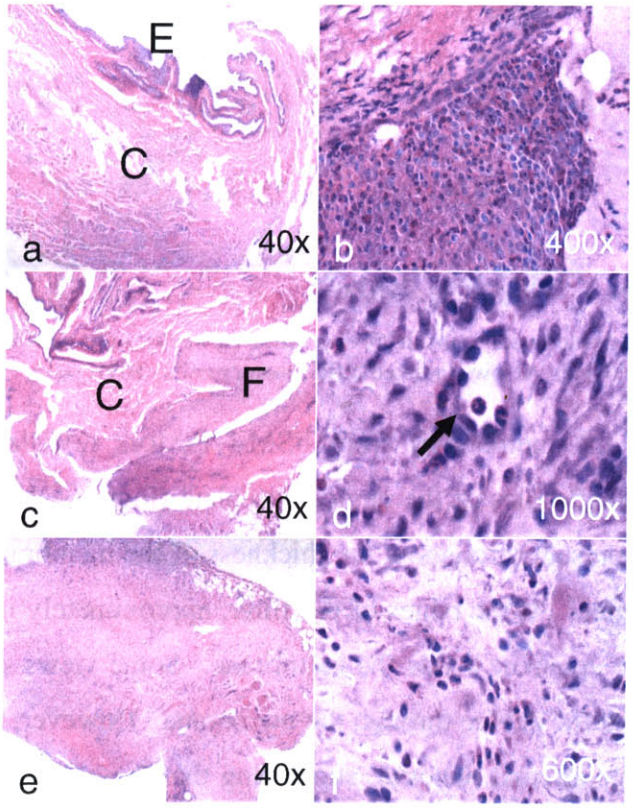

Figure 5.12 Sections of the conjunctiva above devices: (a) control animal with no device showing epithelial layer (E) and connective tissue (C), (b) one SSM-l device, (c,d) one BB-l device showing fibrosis (F) and neovascularization (arrows), (e,f) one SS-l device. H&E stain.

Inside the devices, tissue was mostly fibrous with varying amounts of focal inflammation (Figure 5.13). This type of tissue was evident in all long-term experimental groups. There were no apparent differences in the tissue between groups, with the exception of the BB-l device that had come out of position during the study. Inside that device, tissue was highly cellular and contained a large amount of necrotic material.

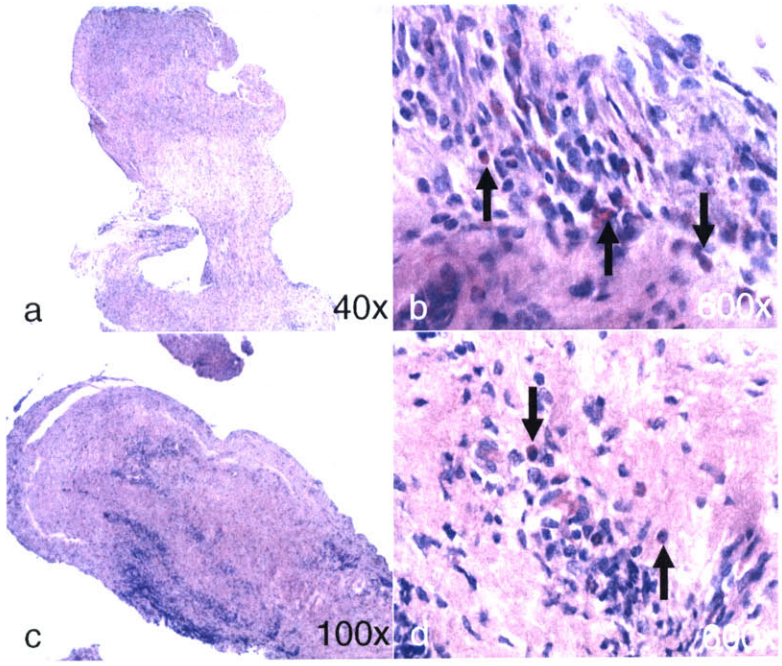

Figure 5.13 Sections from tissue residing inside devices after 10 weeks: (a,b) one BB-1 device, (c,d) one SS-1 device. Arrows indicate inflammatory cells. H&E stain.

Sections through the membranes from SSM-1 devices revealed two bulbs of tissue protruding into the gear shaft holes of the device baseplate (Figure 5.14, left). Stemming from those regions, cells were present throughout the thickness of the membrane in the mid-section of the filter (Figure 5.14, right). At the edges of the filter, approximately in the area where epoxy was placed, no cells were apparent inside the membrane. Some views suggested that cells had migrated from the inside of the device through the membrane. However, the bulbs of tissue were not connected to any other internal material, suggesting that the cells had migrated through the membrane from the scleral side.

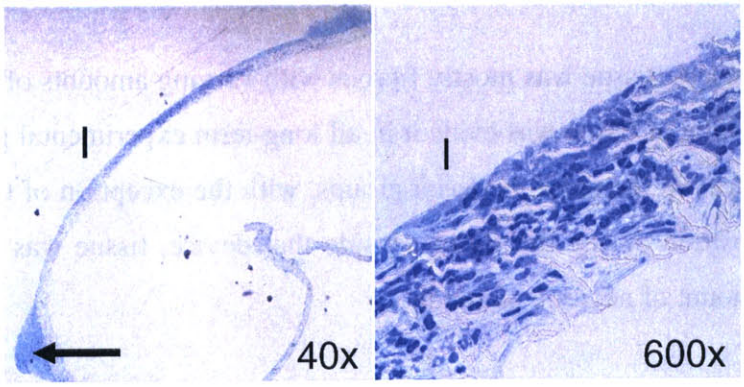

Figure 5.14 Sections of the PTFE membrane from the base of one SSM-1 device. Arrow indicates bulb of tissue. Toluidine blue stain.

5.6.3 *Torque Evaluation*

Torque values for both pre- and post-testing were recorded over ten turns of the moving elements. An average, steady state value was calculated from this data for each test on each device and was used for all statistical comparisons. Both gear and ball bearing devices required low torque to turn the moving elements before implantation, often less than 10dynecm. On every device, pre-implant torque requirements were recorded at three different motor speeds (4, 7 and 13rpm). Student's t-tests were performed to compare the effects of speed within device groups in this data (Figure 5.15). Within each of the Ti-l, SS-l and BB-l groups, comparisons were performed between the 4 and 7rpm, the 4 and 13rpm, and the 7 and 13rpm data sets. No statistical significance was found between any of these groups ($p>0.707$ for Ti-l, $p>0.584$ for SS-l and $p>0.504$ for BB-l). It was therefore assumed that in all groups, every device was effectively tested three times at the same speed before implantation. Pre-test torque data was grouped across motor speeds for the remainder of the analysis.

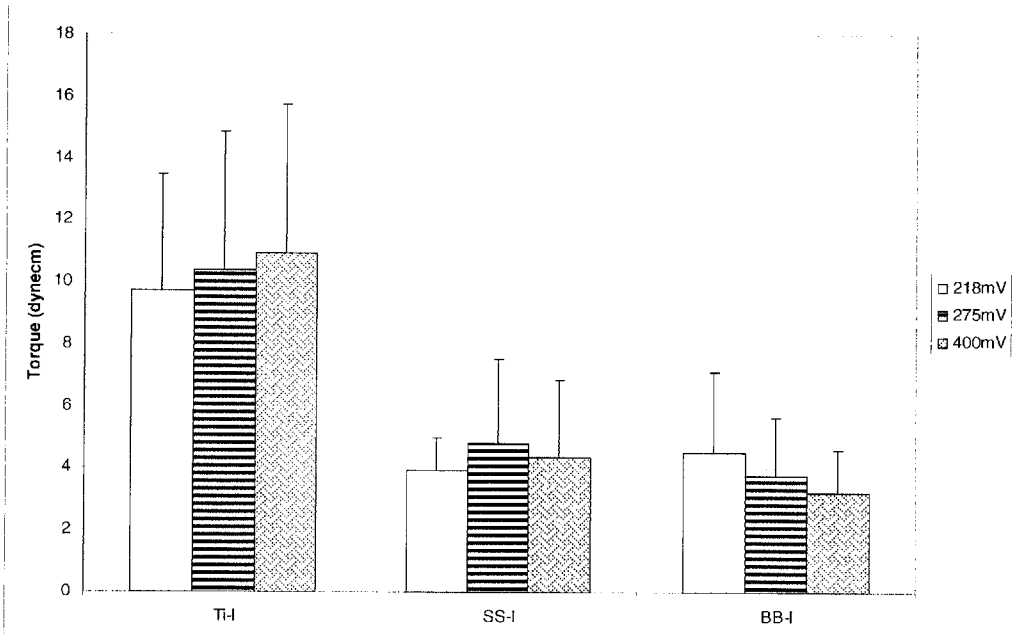

Figure 5.15 Speed effects during pre-testing for three long-term groups.

Post-implant devices often required more torque than was available from the dynamometer system, especially after 10 weeks of residence in the animal. Ball bearing devices were only tested at certain speeds, and all post-testing for the 10-week gear devices was performed on the manual torque watch system as described in Section 3.4. Comparisons

between post-test values recorded at different speeds were therefore not possible. All post-test data used for the following analysis was taken at 13rpm for the SS-s, SSM-s and BB-l groups.

Table 5.2 shows the average pre- and post-test torque values for each device type and p-values generated by comparing the two sets by one-tailed Student's t-tests. Implantation caused a significant torque increase ($p<0.05$) in all 10-week gear devices by approximately 3 orders of magnitude for devices without membranes and 2 for those with a membrane. The BB-l devices experienced a similar increase by 2 orders of magnitude, though high variance contributed to less statistical significance in this data ($p<0.10$). Short-term gear devices also showed increases in torque required after implant, though no statistical significance could be attributed to these groups ($p>0.20$).

Device Group	Pre Test (dynecm ± SD)	Post Test (dynecm ± SD)	P-Value from t-Test
Ti - l	10.3 ± 4.0	11500 ± 3316	0.003
SS - l	4.4 ± 2.0	4550.0 ± 3637.3	0.029
SSM - l	11.2 ± 12.9	700 ± 0	0.000
BB - l	3.8 ± 4.1	419.7 ± 704.8	0.096
SS - s	8.2 ± 12.6	328.6 ± 290.5	0.244
SSM - s	15.6 ± 1.8	149.2 ± 191.7	0.213

Table 5.2 Comparison of pre- and post-test average torque required to turn the moving elements for each experimental group.

To investigate differences between experimental groups, a magnitude (or fold) increase in torque requirements was calculated for each device. Pre-test data was averaged across speeds for each device. The post-test torque value recorded for the same device was divided by this average pre-test value. The data was organized by experimental group and applied to one-tailed Student's t-tests. This method was intended to eliminate inherent differences between devices of the same group.

Figure 5.16 shows the average (plus standard deviation) and the median of this data for each type of device and time point. The trend in the medians shows much larger increases in torque in the Ti-l and SS-l gear devices as compared to any other groups. No statistical differences were shown between these two 10-week gear device groups. The attachment of a

membrane to the gear devices contributed to a significantly smaller torque increase, when comparing the SS-l and SSM-l groups. Between the parallel short-term implants (SS-s and SSM-s), however, no differences were observed. Next comparing across time points, there were significant torque increases after long-term implant as shown between the SSM-l and SSM-s groups ($p<0.05$). Similarly, a low p-value was obtained when comparing the SS-l and SS-s groups ($p<0.07$). Investigating the effects of device type, the Ti-l devices showed a significantly larger increase in torque requirements compared to the BB-l devices ($p<0.05$).

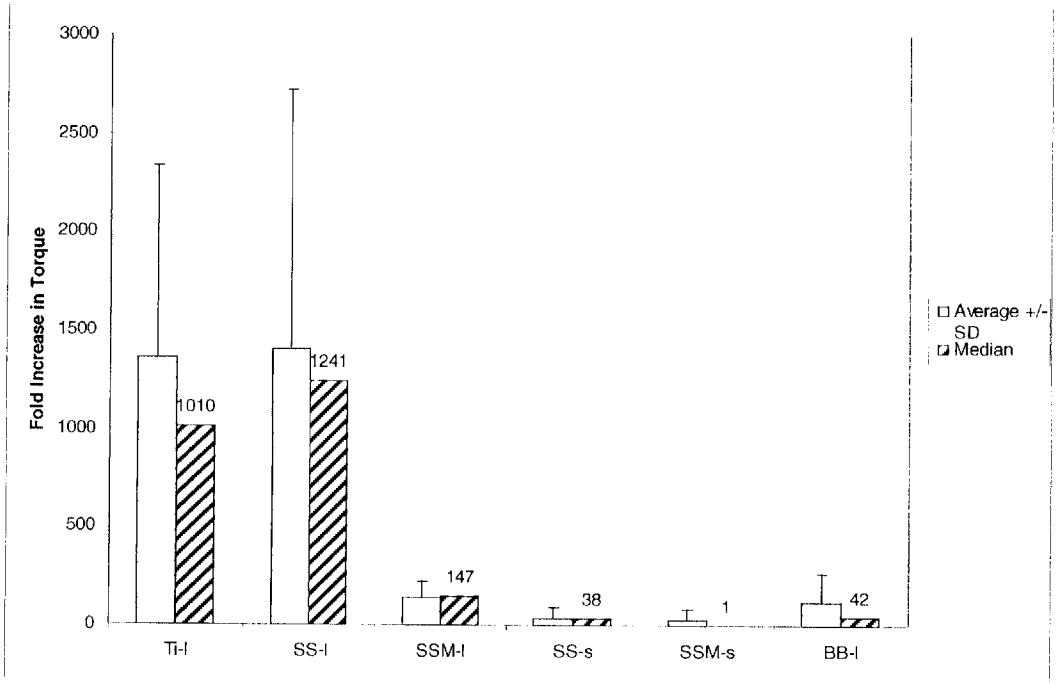

Figure 5.16 Average and median torque increase for each experimental group.

Chapter 6: Discussion and Conclusions

Delivery of drug to the posterior eye presents significant clinical challenges. The region is not only physically inaccessible from the exterior, but systemic delivery is also often blocked by the selective blood-ocular barrier. Clinicians now use intraocular injection for local placement of drug in the back of the eye. In the case of therapeutics to treat age-related macular degeneration, this procedure is repeated monthly, increasing the risk of infections, disruption to intraocular pressure and other side effects with each injection. Alternatively, devices have been designed for residence either inside or immediately outside the eye for the sustained release of drug over days or weeks. Often these devices are drug-loaded molds of passively biodegradable polymers. Actively controlled devices have not to date been applied to a long-term implantable solution for delivery to the posterior eye.

In this vein, Draper Laboratory and Massachusetts Eye and Ear Infirmary (MEEI) have proposed an implantable, fully programmable, active release device for long-term attachment to the eyeball. This device would be sutured to the sclera and covered by the conjunctiva. It would allow for the drug to travel to the eye surface and then diffuse through the eye wall for delivery. While metallic devices have been implanted often, the effects of such a device on the eye environment were unknown. Similarly, while a foreign body reaction was expected around the device, it was uncertain the degree to which an attack would disrupt the function of miniature scale moving parts. The report presented here investigated the feasibility of implanting this device with respect to its biocompatibility, both its effects on the body and the body's effects on its function.

Two metallic devices were designed to mimic several elements of the Draper/MEEI device. These included materials, moving elements (gears or ball bearings) and the presence of an open drug port at the eye surface. Their biocompatibility was evaluated via in vivo rabbit model. Two and ten-week implantation periods served to show the progression of any foreign body response from initial to steady state. Test devices were designed to be static while implanted, thus representing the limiting case of potential tissue growth on the devices. Both qualitative investigation of effects in the surrounding tissues and quantitative analysis of device function served to elucidate the feasibility of this device.

Routine observations of the animals revealed that the implantation surgery was well tolerated. The procedure was minimally invasive and did not create large wounds around the area. Rabbit sclera is thin compared to that of the human eye, which did lead to some difficulty in securing the devices with suture. This complication is likely the cause for one ball bearing device to have fallen out of place on one side. All other devices maintained their position. The rabbits moved around their cages normally throughout the study. No inflammation or scar tissue formation was evident from routine observations of the animals, and no difference was seen in rabbits with one or two total implants.

Investigation of the tissue surrounding each device revealed some level of inflammation or fibrous tissue formation in the conjunctiva above all devices at both long and short time points. This effect is not surprising, since in both humans and rabbits, the conjunctiva is known to produce dense areas of inflammation during an immune response [83]. Additional inflammatory and scar tissue growth was found between the sclera and the device. However, no other tissue damage was observed. No erosion of the sclera was evident, and other areas of the conjunctiva appeared healthy. Both titanium and stainless steel are commonly known to be non-toxic implant materials, and results showed no differences between test devices of the two metals.

The degree of scarring evident in the conjunctiva was greater around the gear device than the ball bearing. Visual assessment of the thicker tissue correlated with greater fibrosis and disruption of the tissue architecture when investigated under microscope. Geometry of device casing most likely had the greatest impact on this result. Due to space and functional constraints, the gear device was designed with greater height and narrower width than the ball bearing device. Gear devices therefore disrupted natural movement of the conjunctiva to a greater degree. They also created a greater "dead-space" between the eye and conjunctiva, which may have increased the body's response. These differences suggest that the shorter and wider the device cover, the less response and damage may be seen in the conjunctiva.

The conjunctiva contains several glands as well as cells responsible for lubricating the area. It is unclear from this study the degree to which the inflammatory response, fibrous tissue formation and disruption of the conjunctival architecture shown here change the function and health of this mucous membrane. Animals in this study proceeded normally even after the buildup of scar tissue around eyes with the devices. While it is assumed that less fibrous tissue

formation causes less damage to the tissue function, future study is necessary to identify the upper limit to any tissue infiltration to maintain acceptable function.

Fibrosis on the scleral surface did not seem to disrupt the eye wall itself significantly, and it is assumed that this level of tissue formation would not affect the function or structural integrity of the eye wall. However, the added tissue thickness could alter the ability of a drug to diffuse through it. Transscleral drug diffusion studies have previously been performed with normal sclera, which contains minimal vasculature. Any neovascularization in new fibrous tissue may also complicate local delivery by removing the drug to the blood stream. Since all devices in this report elicited some level of fibrosis on the sclera, future permeability studies should be performed to determine the efficacy for drug delivery in this case.

While some level of fibrous tissue encapsulation was expected, results suggest that a detrimental amount of tissue infiltration may invade the interior of some implants. Gear devices especially showed fibrous tissue almost completely filling their interior at 10 week time points. Devices implanted for short term study showed signs of this tissue beginning to form in and around the gearbox. The volume of scar tissue observed inside the devices correlates with the amount of torque increase in most cases. Tests of function revealed that the torque required to turn device elements jumped approximately 1000 fold in the basic gear devices in the presence of this tissue. Ball bearing devices implanted for the same period, however, showed minimal, if any, penetration of tissue into the device. Torque increased approximately 100 fold after in vivo residence of these devices. Since minimal fibrosis was present inside, tissue trapped around other bearing surfaces may have contributed largely to the increased turning resistance.

In addition to the differences in cover shape, the gear and ball bearing devices also differed in baseplate geometry. Gear devices were designed as a gearbox that allowed for visualization of the device interior through windows on its sides. There were therefore 6 unsealed openings on each gearbox – two facing the sclera to mimic drug ports and 4 windows on the sides. This gearbox unit slipped loosely into the device cover. The cover was sutured to the sclera, holding the gearbox in place. However, some amount of micro motion was still allowed between the gearbox and the cover while implanted. Conversely, the ball bearing device was designed as one integral unit. The internal elements and the device cover were bonded directly to the baseplate, which was in turn sutured to the sclera. While this device allowed no

micro motion within itself on the eye surface with this design, minimal investigation of the device interior was possible after implant.

Results suggest that the dissimilarity in geometry contributed to differences in tissue infiltration and effects on device function. Around each ball bearing device, a distinct, thin fibrous sheet formed, and little, if any, tissue penetrated inside. On the other hand, gear devices without any protection over the drug ports showed tissue communication through both these openings and the gap between the gearbox and the cover. Gearboxes implanted for ten weeks were covered by a thin tissue layer that entirely filled this gap and was often connected to fibrous tissue inside the device. These results suggest that this extra space, the additional openings into the gear area and the added micro motion of the gear device design may have contributed to significantly greater amounts of tissue infiltrate. Additionally, it was observed that tighter spaces are greater encouragement for formation of a continuous tissue network.

Due to the geometry contributions, direct comparisons between the moving elements themselves were more challenging. The articulating surfaces of the gears are by nature more exposed to invading cells and tissues. As shown, the winding surface of the teeth also present pockets for tissue attachment even at the early stages of the foreign body response. Articulating elements of the ball bearing, however, are encased on several sides by the smooth, metallic races. In the configuration presented here, especially, invading fibrous cells from the scleral surface could not affect the balls until migrating over the races into the ball space. It was not evident from these devices that any tissue grew past the height of the outer races.

A porous polytetrafluoroethylene filter was attached to the base of some gearboxes with the intention of preventing the migration of tissue into the gear space while still allowing for potential drug diffusion. The membrane itself was tested in vitro for its permeability to fibroblasts and showed that few cells could penetrate from one side to the other over three days. These in vitro tests revealed that cells will, however, readily adhere to the near side of the filter. When used to augment gear devices in vivo, fibrosis on the sclera clearly attached to the midsection of the membrane on the device. Additionally, no communication of tissue through the drug ports was evident.

In these devices, a large amount of fibrous tissue was observed inside the gear space, along with a fibrous capsule around the gearbox. The capsule tended to be well connected through the gearbox windows to any tissue inside the device. Interior tissue typically encased

the gears into one sac, as compared to the more sprawling fibrosis inside gear devices without a membrane. The organization of this tissue around the gears likely contributed to the lower torque requirements after implantation as compared to non-membrane devices.

Histology sections of the polytetrafluoroethylene membranes after implantation showed cells present throughout the thickness of the material. Bulbs of fibrous tissue penetrated from here into the lower gear shaft holes, though not into the drug ports. This tissue was not connected to other similar fibrosis inside the device, suggesting that these cells migrated inward from the sclera area but did not travel farther than the baseplate.

Accuracy of results presented here is limited by the small sample sizes available. For the gear devices, group size was 3 or 4 for long-term implant and 2 or 3 for short term implant. Three ball bearing devices were tested, though one did not remain in place for the entire implant period. One set of gears grouped with the short term data came from devices removed only ten days after surgery. Any statistical significance and histological observations were made based on these sample sizes. Similarities between experimental groups did allow for effectively greater numbers of replicates, which led to various observations and recommendations.

The mechanical testing apparatus also limited accuracy of results and may have contributed to some variance within experimental groups. Alignment of the motor adaptor shaft on the devices was performed visually. While several measures guided correct placement, an offset from vertical still produced oscillations in the recorded torque data. Random motion in the motor shaft created some variations in torque. In some instances, adhesive or residue on the end of the shaft caused torque spikes throughout the data. The use of a manual testing apparatus also introduced large amounts of error. However, the requirement for the latter system alone indicated torque requirements orders of magnitude greater than before implantation. With these large differences in addition to qualitative observations, several conclusions could be made. To make conclusions regarding smaller differences in torque, it may be necessary to add a precision tool to align and place the motor shaft reliably on every device.

This thesis investigated the feasibility of implanting a metallic device on the sclera that depends on internal moving parts to function in the milieu of the body. Based on a rabbit model, it can be concluded that these metal implants are relatively well tolerated when implanted, especially with a low, wide profile contacting the conjunctiva. As expected with any foreign body, fibrous tissue encapsulation occurs around these devices, requiring a future test of drug

permeability through any extra tissue layers. Micro motion within such a device and multiple openings were shown to encourage mass tissue infiltration. A porous polytetrafluoroethylene membrane prevents some of this cell invasion. For future devices of this type, it is recommended first to create an integral design, thereby decreasing micro motion and second to cover any ports, thereby decreasing the opportunity for tissue growth inside the device. These design characteristics reduce the volume of tissue inside the implant, therefore minimizing the power necessary to operate the device.

Appendix: Engineering Drawings

Notes:
1 These holes line up with 1 on gearboxcover and cover.
Shafts from GearA and GearB fit in these holes.
*for Baseplate-2: 2x 0.0175 +0.0003, -0.000

2 These holes line up with 2 on gearboxcover

3 Gear shafts should not extend farther than the bottom of baseplate at this location.

Baseplate and gearboxcover loosely slip fit into cover.

No sharp outer edges.

Baseplate-1, Baseplate-2
Page 1 of 2

S. Cohen 4/26/06
All dimensions in inches
Tolerances: +/- 0.001 unless otherwise noted
Scale 15:1
Third Angle Projections
Material: 316L Stainless Steel or Grade 5 Titanium

Baseplate-1, Baseplate-2
Page 2 of 2

S. Cohen 4/26/06
All dimensions in inches
Tolerances: +/- 0.001 unless otherwise noted
Scale 15:1
Third Angle Projections
Material: 316L Stainless Steel or Grade 5 Titanium

Gear Specifications
AGMA 10
Backlash Class C (0.0013in tooth thinning)
120 Diametral Pitch
20 Degree Pressure Angle
15 Teeth
0.1270in enlarged pitch diameter
(Addendum modification coefficient 0.240)

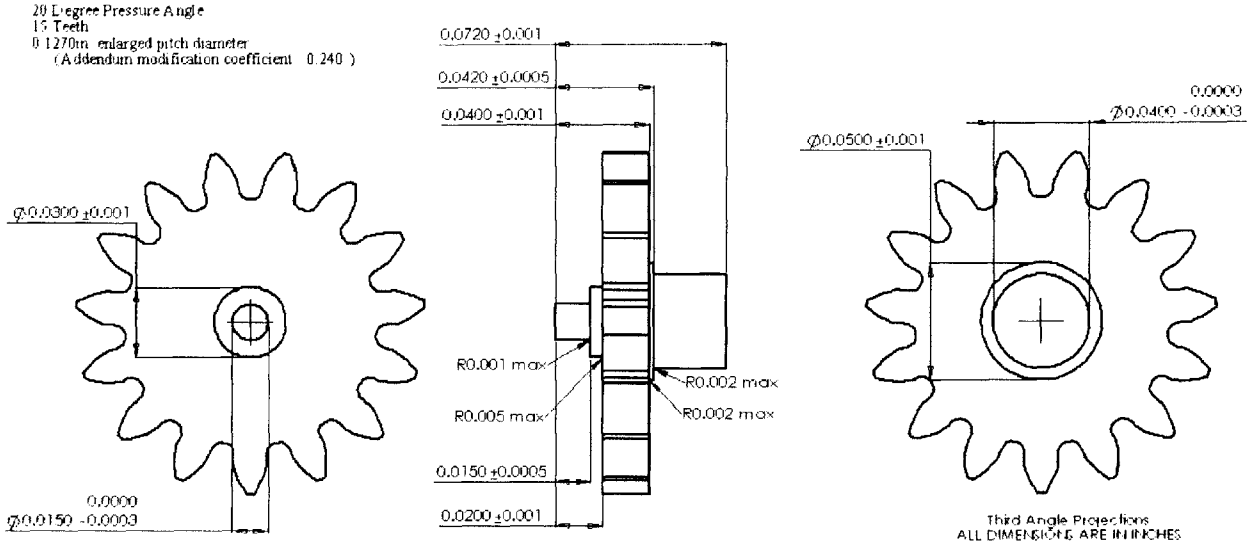

Gear Specifications
AGMA 10
Backlash Class C (0.0013in tooth thinning)
120 Diametral Pitch
20 Degree Pressure Angle
10 Teeth
0.0902in. enlarged pitch diameter
(Addendum modification coefficient 0.432)

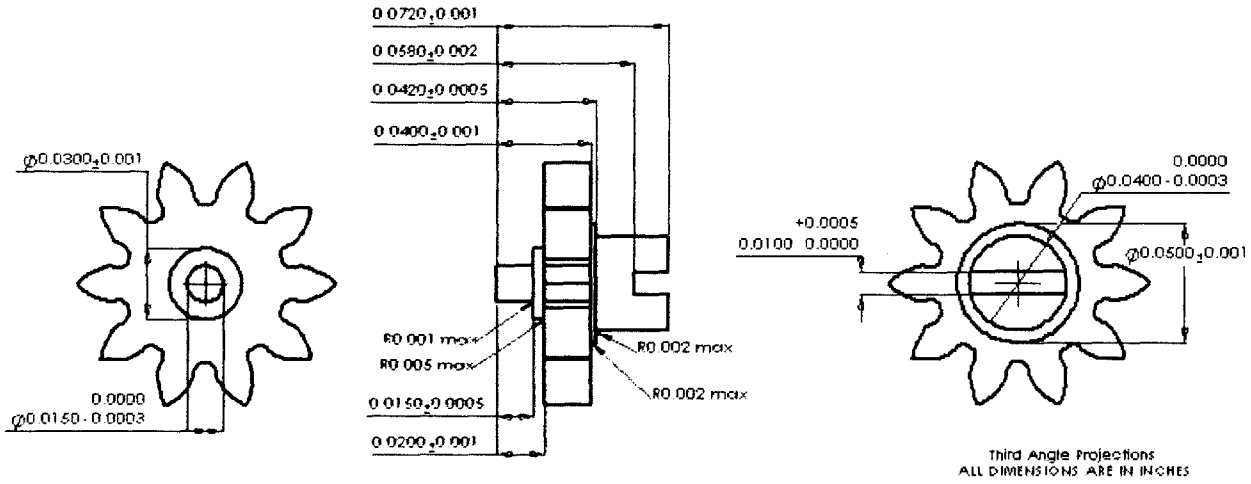

Notes:
1. These holes lines up with 1 on gearboxcover and baseplate.
   Shafts from GearA and GearB slip tl through these holes.
   *for Cover-2: Ø0.0425 +0.0000, -0.0000

Baseplate and gearboxcover loosely slip tl into cover.

No sharp outer edges.

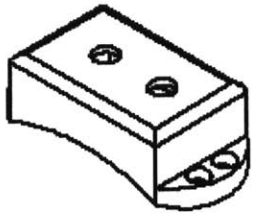

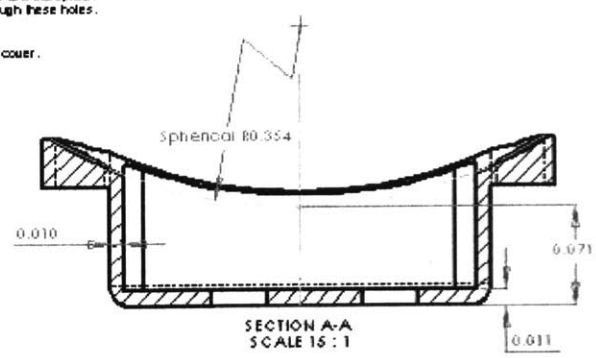

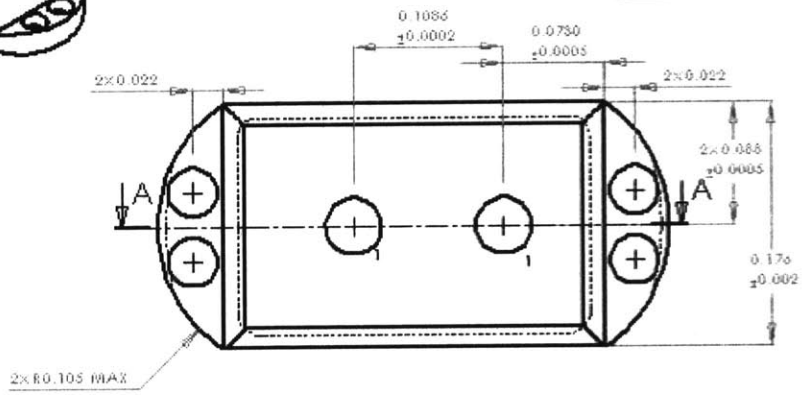

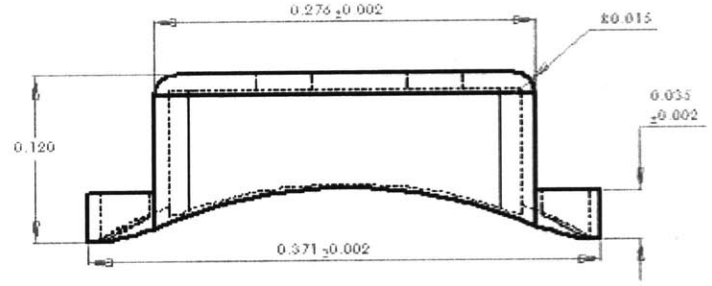

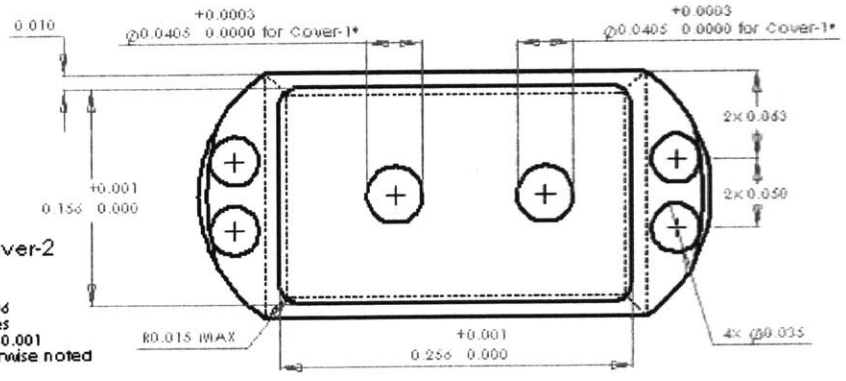

Cover-1, Cover-2
Rev. 1

S. Cohen 5/30/06
All units in inches
Tolerances: +/- 0.001
unless otherwise noted
Scale 15:1
Third Angle Projections
Material: 316L Stainless Steel or Grade 5 Titanium

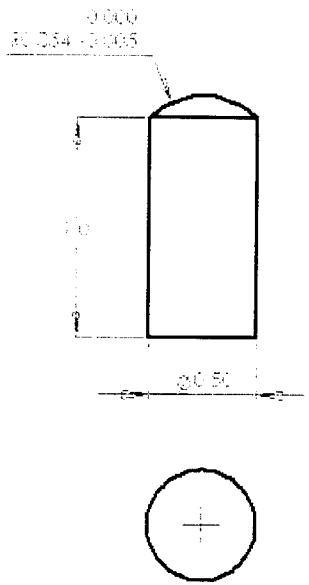

Membrane tool
Page 1 of 1

S. Cohen 10/25/06
All dimensions in inches
Tolerances: .xx +/- 0.01
.x +/- 0.1
Unless otherwise noted.
Scale 2:1
Third Angle Projections
Material: Teflon

Notes:
1 These holes line up with 1 on baseplate and cover.
GearA and GearB shafts slip fit into these holes
*for Gearboxcover-2: 0.0425 +0.0003, -0.0000
**for Gearboxcover-2: 0.0175 +0.0005, -0.0000

2 These holes line up with 2 on baseplate.
The posts slip fit over the posts on the baseplate

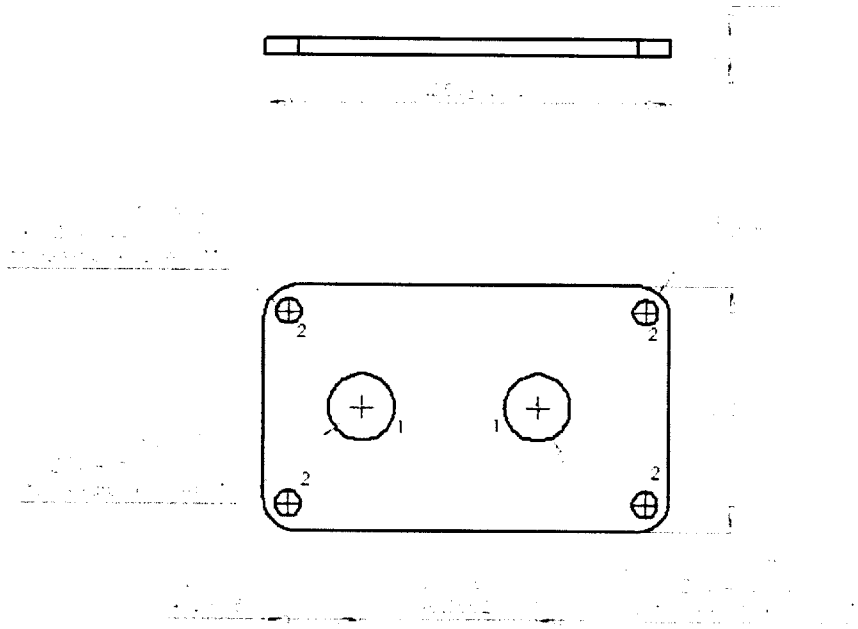

Gearboxcover-1, Gearboxcover-2

S. Cohen 5/30/06
All units in inches
Tolerances: +/- 0.001unless otherwise noted
Scale 1.5:1
Third Angle Projections
Material: 316L Stainless Steel or Grade 5 Titanium

Notes:

Polish curved side of part;
grit blast all other surfaces.

No sharp outer edges on sides
or bottom of part.

⚠ The inner surfaces of Cover-Ball Bearing slip fit over these edges.

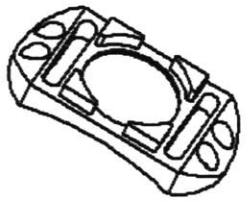

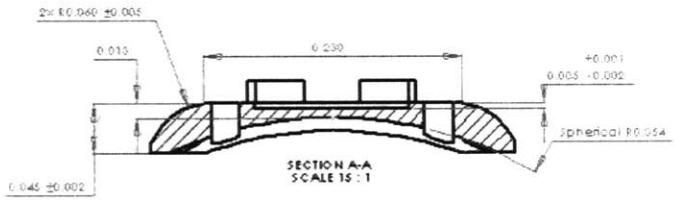

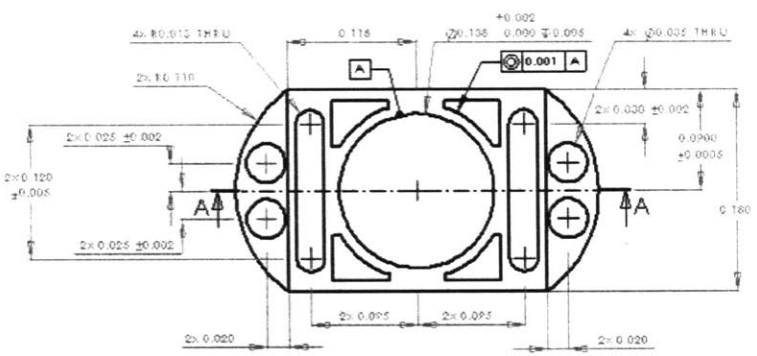

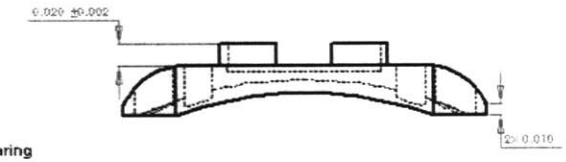

Baseplate-Ball Bearing
Page 1 of 2

S. Cohen 7/12/06
All dimensions in inches
Tolerances: +/- 0.001 unless otherwise noted
Scale 15:1
Third Angle Projections
Material: Grade 5 Titanium

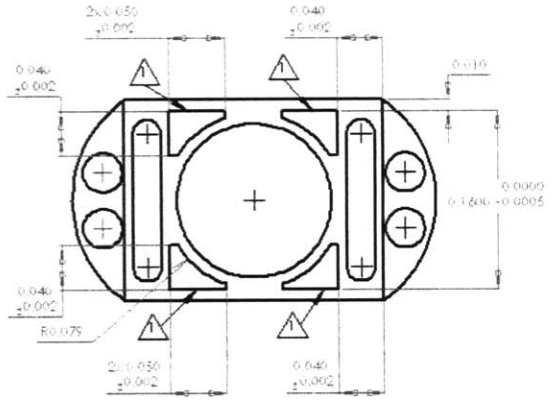

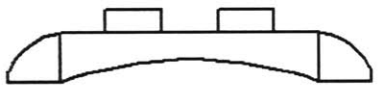

Baseplate-Ball Bearing
Page 2 of 2

S. Cohen 7/12/06
All dimensions in inches
Tolerances: +/- 0.001 unless otherwise noted
Scale 15:1
Third Angle Projections
Material: Grade 5 Titanium

Notes:

Grit blast interior surfaces only.

No sharp outer edges.

These surfaces slip fit over (1) on Baseplate-Ball Bearing.

(2) The Shaft-Ball Bearing fits into this hole.

(3) This edge slip fits over the ball bearing race outer diameter,
this edge is concentric with (2)

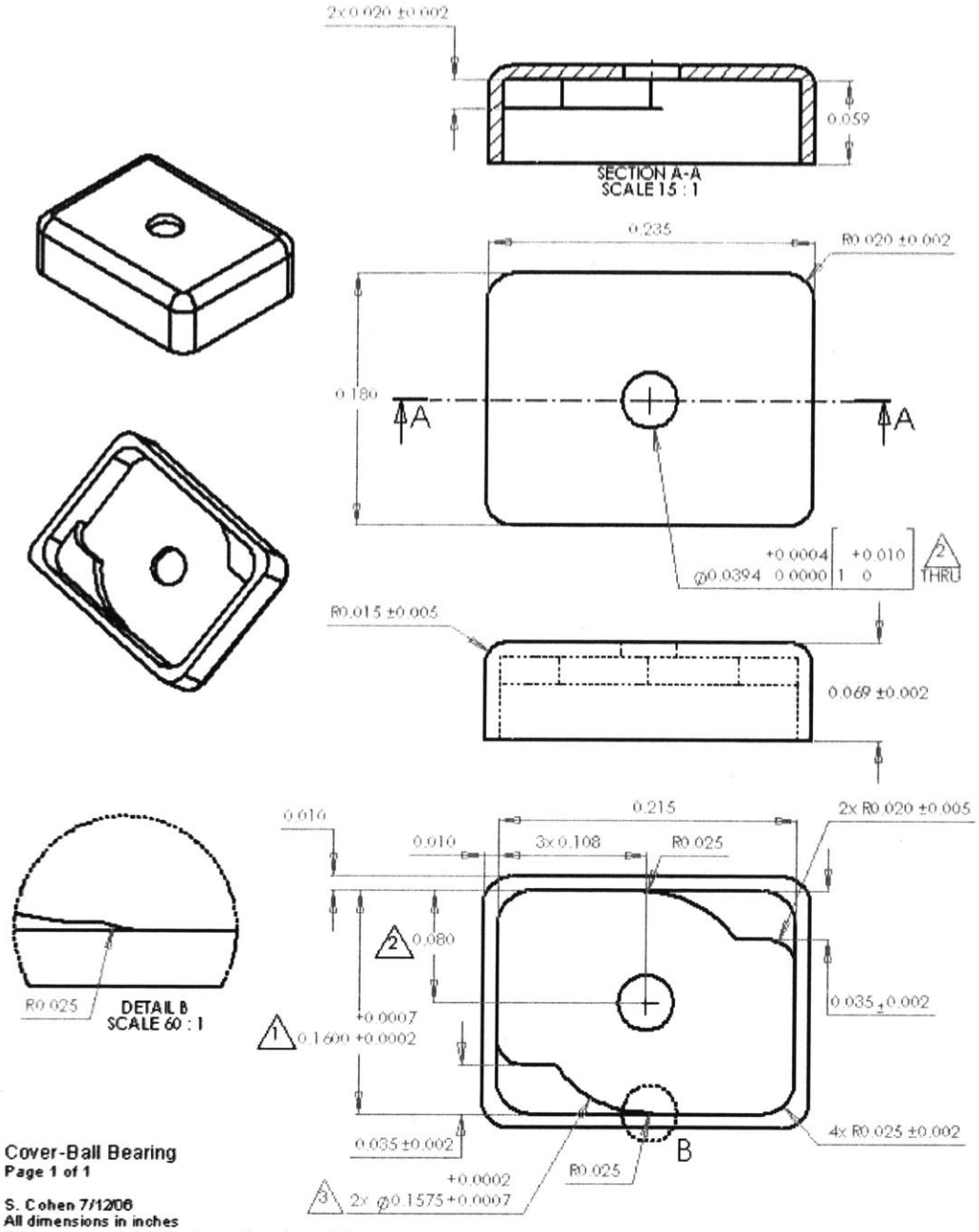

Cover-Ball Bearing
Page 1 of 1

S. Cohen 7/12/06
All dimensions in inches
Tolerances: +/- 0.001 unless otherwise noted
Scale 15:1
Third Angle Projections
Material: Grade 5 Titanium (TI6AI4V)

Notes:

2 The top of this shaft slip fits through the hole in Cover-Ball Bearing. The bottom of this shaft slip fits into the center of the ball bearing race.

4 The end of the Motor Adaptor-Tool slip fits into this notch.

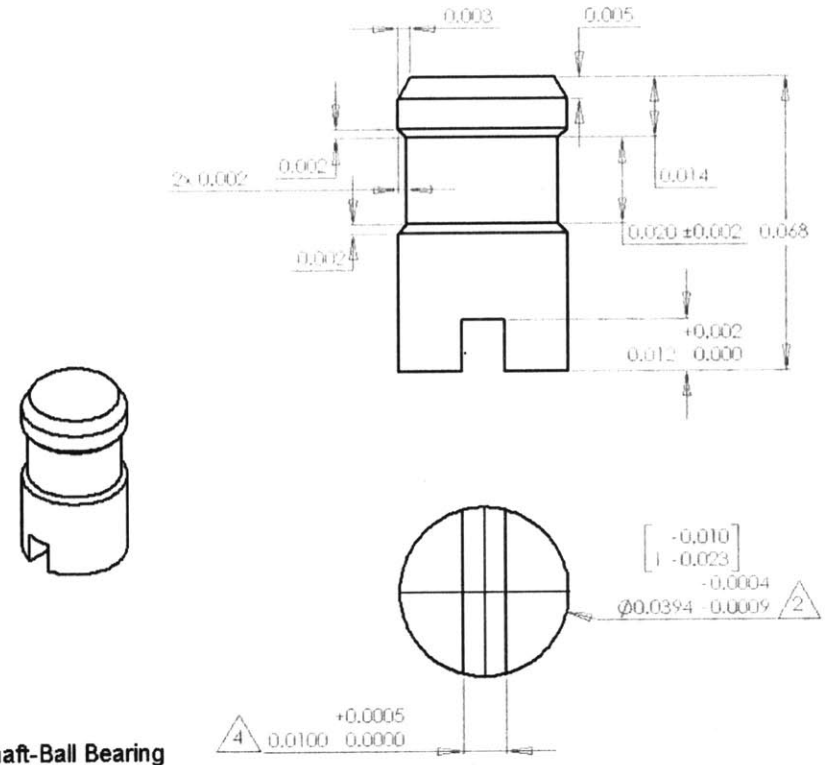

Shaft-Ball Bearing
Page 1 of 1

S. Cohen 7/12/06
All dimensions in inches
Tolerances: +/- 0.001 unless otherwise noted
Scale 40:1
Third Angle Projections
Material: Grade 5 Titanium (Ti6Al4V)

Mechanical Testing Apparatus

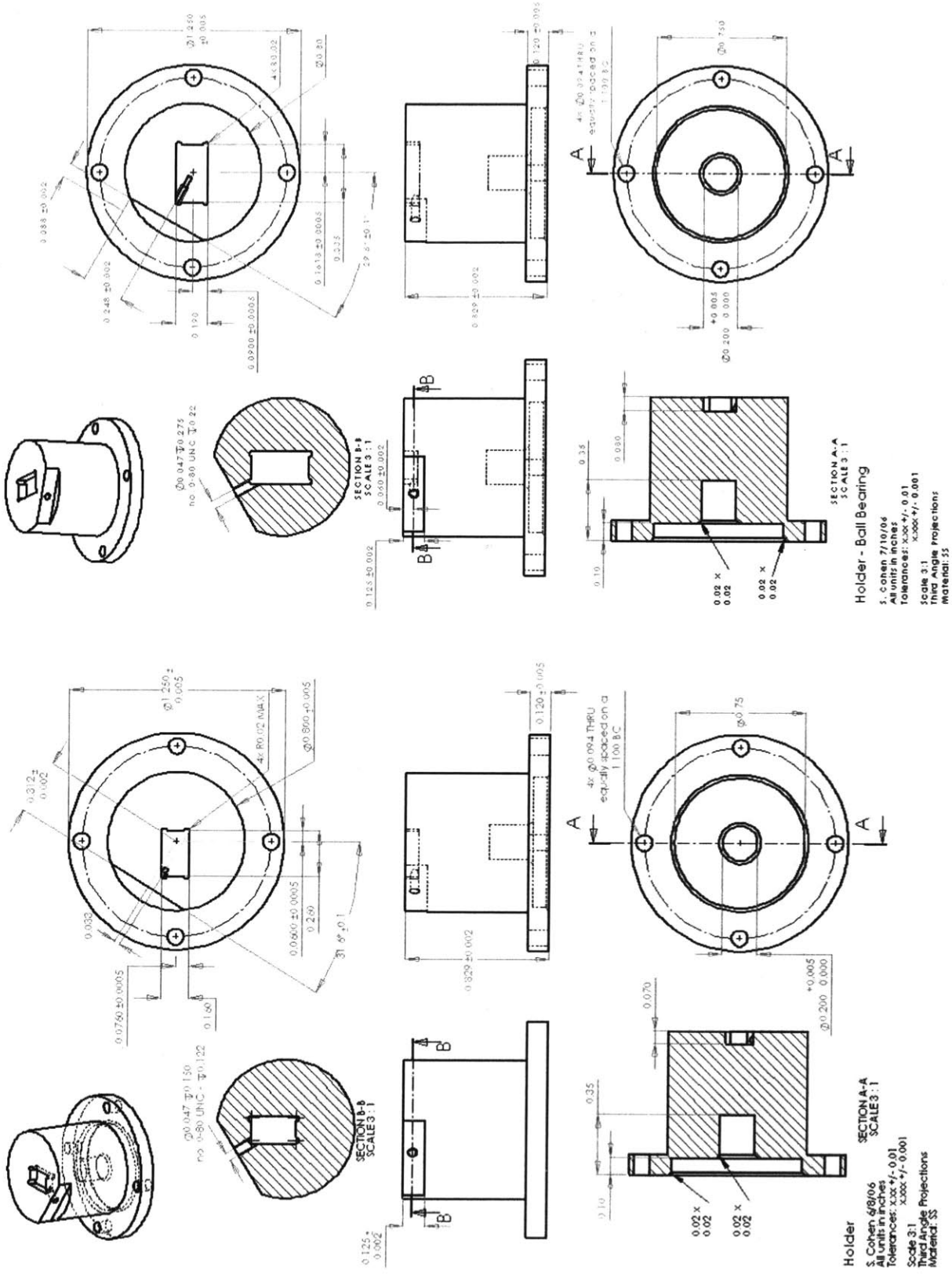

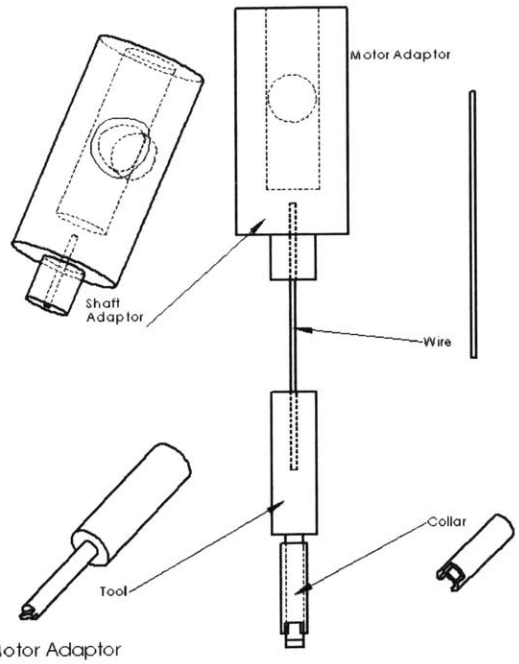

Motor Adaptor

S. Cohen 5/30/06
All units in inches
Tolerances: x.xx +/- 0.01
x.xxx +/- 0.001
Scale 3:1
Third Angle Projections
Material: SS

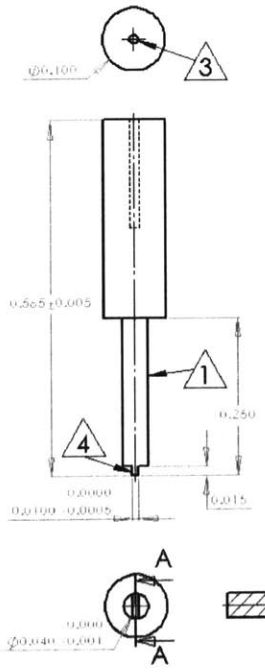

Motor Adaptor: Tool

S. Cohen 5/30/06
All units in inches
Tolerances: x.xx +/- 0.01
x.xxx +/- 0.001
Scale 8:1
Third Angle Projections
Material: SS

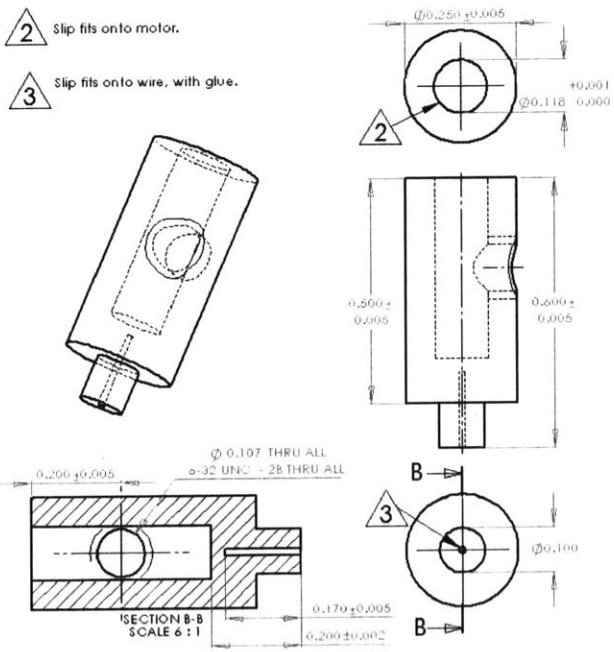

Motor Adaptor: Shaft Adaptor

S. Cohen 5/30/06
All units in inches
Tolerances: x.xx +/- 0.01
x.xxx +/- 0.001
Scale 6:1
Third Angle Projections
Material: SS

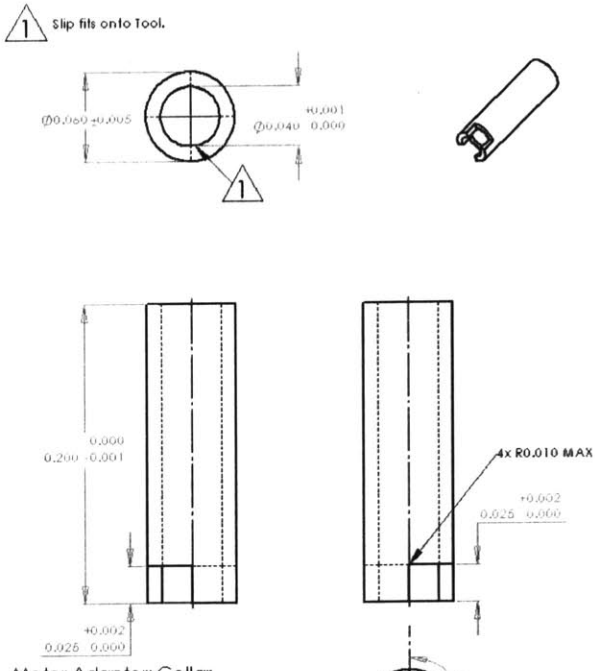

Motor Adaptor: Collar

S. Cohen 5/30/06
All units in inches
Tolerances: x.xx +/- 0.01
x.xxx +/- 0.001
Scale 20:1
Third Angle Projections
Material: SS

Biographic Note

Sarah J. Cohen was born and raised outside of Atlanta, GA where she acquired her southern charm, learned to play the viola and practiced her engineering skills in her father's workshop. A 1998 graduate of North Springs High School, Sarah received her B.S. in biomedical engineering at Tulane University in New Orleans, LA in 2002. At Tulane, she worked in the orthopedic biomechanics laboratory of Dr. Francis Suh on her undergraduate thesis titled, "Periosteum use in tendon-bone tunnel healing: an in vitro study." After college, Sarah was a research assistant in the hematology/oncology research laboratory of Dr. Gary Gilliland at Brigham and Women's Hospital in Boston. Her work included research presented in the 2004 article, "Conditional expression of oncogenic K-ras from its endogenous promoter is sufficient to induce a myeloproliverative disease," *Journal of Clinical Investigation*. Sarah later worked in biochemical sensor development as a member of the bioengineering group at Draper Laboratory before returning to graduate school as a Draper Laboratory Fellow.

References

1. Nowak, J.Z., "Age-related macular degeneration (AMD): pathogenesis and therapy," *Pharmacological Reports : PR,* Vol. 58, No. 3, 2006, pp. 353-363.
2. Fatt, I., "Physiology of the Eye: An Introduction to the Vegetative Functions," The Butterworth Group, Woburn, MA, 1978.
3. Shier, D., Butler, J., and Lewis, R., "Sense of Sight," *Hole's Human Anatomy and Physiology,* WCB McGraw-Hill, Boston, MA, 1999, pp. 457-474.
4. Robinson, J.R. ed., "Ophthalmic Drug Delivery Systems," American Pharmaceutical Association, Washington, D.C., 1980.
5. Davidson, H. ed., "The Eye," Vol. 1b: Vegetative Physiology and Biochemistry, Academic Press, Inc., Orlando, FL, 1984.
6. Berger, J.W., Fine, S.L., and Maguire, M.G. eds., "Age-Related Macular Degeneration," Mosby, Inc., St. Louis, MO, 1999.
7. Oyster, C.W., "The Human Eye, Structure and Function," Sinauer Associates, Inc., Sunderland, MA, 1999.
8. Fine, B.S., and Yanoff, M., "Conjunctiva and Muller's Muscle," *Ocular Histology, A Text and Atlas,* Harper and Row Publishers, Inc., Hagerstown, MD, 1979, pp. 307-310.
9. Peyman, G.A., "Vitreoretinal Diseases: Pathological Aspects and Therapeutic Strategies," *Ocular Therapeutics and Drug Delivery: A Multi-disciplinary Approach,* I.K. Reddy, ed., Technomic Publishing Company, Inc., Lancaster, PA, 1996, pp. 265-273.
10. Joseph, J., and Grierson, I., "Anterior Segment Changes in Glaucoma," *Pathobiology of Ocular Disease,* edited by A. Garner and G.K. Klintworth, Vol. Part A, Marcel Dekker, Inc., New York, NY, 1994, pp. 433-468.
11. Ayyala, R.S., Duarte, J.L., and Sahiner, N., "Glaucoma drainage devices: state of the art," *Expert Review of Medical Devices,* Vol. 3, No. 4, 2006, pp. 509-521.
12. Klintworth, G.K., and Garner, A., "The Causes, Types and Morphology of Cataracts," *Pathobiology of Ocular Disease,* edited by A. Garner and G.K. Klintworth, Vol. Part A, Marcel Dekker, Inc., New York, NY, 1994, pp. 481-532.
13. Lloyd, A.W., Faragher, R.G., and Denyer, S.P., "Ocular biomaterials and implants," *Biomaterials,* Vol. 22, No. 8, 2001, pp. 769-785.
14. Hartong, D.T., Berson, E.L., and Dryja, T.P., "Retinitis pigmentosa," *Lancet,* Vol. 368, No. 9549, 2006, pp. 1795-1809.
15. Holtz, F.G., and Spaide, R.F. eds., "Medical Retina," *Essentials in Ophthalmology,* Krieglestein, G.K. and Weinreb, R.N. eds., Springer, Netherlands, 2005, pp. 185.
16. Hardy, R.A., and Crawford, J.B., "Retina," *General Ophthalmology,* edited by D. Vaughan T. Asbury and P. Riordan-Eva, McGraw-Hill, New York, NY, 1999, pp. 178-199.
17. Colthurst, M.J., Williams, R.L., Hiscott, P.S., "Biomaterials used in the posterior segment of the eye," *Biomaterials,* Vol. 21, No. 7, 2000, pp. 649-665.
18. Congdon, N., O'Colmain, B., Klaver, C.C., "Causes and prevalence of visual impairment among adults in the United States," *Archives of Ophthalmology,* Vol. 122, No. 4, 2004, pp. 477-485.
19. Kulkarni, A.D., and Kuppermann, B.D., "Wet age-related macular degeneration," *Advanced Drug Delivery Reviews,* Vol. 57, No. 14, 2005, pp. 1994-2009.

20. Ferris, F.L.,3rd, Fine, S.L., and Hyman, L., "Age-related macular degeneration and blindness due to neovascular maculopathy," *Archives of Ophthalmology,* Vol. 102, No. 11, 1984, pp. 1640-1642.
21. Binder, S., Stolba, U., Krebs, I., "Transplantation of autologous retinal pigment epithelium in eyes with foveal neovascularization resulting from age-related macular degeneration: a pilot study," *American Journal of Ophthalmology,* Vol. 133, No. 2, 2002, pp. 215-225.
22. Mruthyunjaya, P., Stinnett, S.S., and Toth, C.A., "Impact of fluorescein angiographic characteristics of macular lesions on outcomes after macular translocation 360 degree surgery in eyes with age-related macular degeneration," *Retina,* Vol. 25, No. 5, 2005, pp. 597-607.
23. Gragoudas, E.S., Adamis, A.P., Cunningham, E.T.,Jr, "Pegaptanib for neovascular age-related macular degeneration," *The New England Journal of Medicine,* Vol. 351, No. 27, 2004, pp. 2805-2816.
24. Ferrara, N., "Vascular endothelial growth factor: basic science and clinical progress," *Endocrine Reviews,* Vol. 25, No. 4, 2004, pp. 581-611.
25. Rosenfeld, P.J., Rich, R.M., and Lalwani, G.A., "Ranibizumab: Phase III clinical trial results," *Ophthalmology Clinics of North America,* Vol. 19, No. 3, 2006, pp. 361-372.
26. "FDA Approves New Biologic Treatment for Wet Age-Related Macular Degeneration," FDA, 2006. [http://www.fda.gov/bbs/topics/NEWS/2006/NEW01405.html. Accessed 2007.]
27. Dee, K.C., Puleo, D.A., and Bizios, R., "An Introduction to Tissue-Biomaterial Interactions," John Wiley & Sons, Inc., Hoboken, NJ, 2002.
28. Black, J., "Biological Performance of Materials: Fundamentals of Biocompatibility, 3rd edition, Revised and Expanded," Marcel Dekker, Inc., New York, NY, 1999.
29. Spector, M., and Lalor, P.A., "Testing biomaterials: In vivo assessment of tissue compatibility," pp. 220-228.
30. Sanders, J.E., and Rochefort, J.R., "Fibrous encapsulation of single polymer microfibers depends on their vertical dimension in subcutaneous tissue," *Journal of Biomedical Materials Research. Part A,* Vol. 67, No. 4, 2003, pp. 1181-1187.
31. Davis, J.R ed., "Handbook of Materials in Medical Devices," ASM International, Materials Park, OH, 2003.
32. "Required Biocompatibility Training and Toxicology Profiles for Evaluation of Medical Devices," 1995. [http://www.fda.gov/cdrh/g951.html. Accessed 2007.]
33. Black, J., and Hastings, G. eds., "Handbook of Biomaterial Properties," Chapman & Hall, London, England, 1998.
34. Hin, T.S. ed., "Engineering Materials for Biomedical Applications," World Scientific Publishing Co., 2004.
35. Anderson, J.M., and Langone, J.J., "Issues and perspectives on the biocompatibility and immunotoxicity evaluation of implanted controlled release systems," *Journal of Controlled Release: Official Journal of the Controlled Release Society,* Vol. 57, No. 2, 1999, pp. 107-113.
36. Yang, C., Zhao, C., Wold, L., "Biocompatibility of a physiological pressure sensor," *Biosensors & Bioelectronics,* Vol. 19, No. 1, 2003, pp. 51-58.

37. Voskerician, G., Shawgo, R.S., Hiltner, P.A., "In vivo inflammatory and wound healing effects of gold electrode voltammetry for MEMS micro-reservoir drug delivery device," *IEEE Transactions on Bio-Medical Engineering,* Vol. 51, No. 4, 2004, pp. 627-635.
38. Voskerician, G., Shive, M.S., Shawgo, R.S., "Biocompatibility and biofouling of MEMS drug delivery devices," *Biomaterials,* Vol. 24, No. 11, 2003, pp. 1959-1967.
39. Le Rouic, J.F., Bettembourg, O., D'Hermies, F., "Late swelling and removal of Miragel buckles: a comparison with silicone indentations," *Retina,* Vol. 23, No. 5, 2003, pp. 641-646.
40. Giordano, G.G., and Refojo, M.F., "Biomaterials in Ophthalmology," *Human Biomaterials Applications,* edited by D.L. Wise D.J. Trantolo D.E. Altobelli, Humana Press, Inc., Totowa, NJ, 1996, pp. 301-302-317.
41. Scribbick, F.W., and Scribbick, A.T., "Ophthalmic implants and explants," *Emergency Medicine Clinics of North America,* Vol. 12, No. 3, 1994, pp. 793-800.
42. Ayyala, R.S., Harman, L.E., Michelini-Norris, B., "Comparison of different biomaterials for glaucoma drainage devices," *Archives of Ophthalmology,* Vol. 117, No. 2, 1999, pp. 233-236.
43. Boswell, C.A., Noecker, R.J., Mac, M., "Evaluation of an aqueous drainage glaucoma device constructed of ePTFE," *Journal of Biomedical Materials Research,* Vol. 48, No. 5, 1999, pp. 591-595.
44. Langer, R., "Where a Pill Won't Reach: How to get drugs where they need to go," *Scientific American,* Vol. 288, No. 4, 2003.
45. Langer, R., "Drug delivery. Drugs on target," *Science,* Vol. 293, No. 5527, 2001, pp. 58-59.
46. Xie, Y., Xu, B., and Gao, Y., "Controlled transdermal delivery of model drug compounds by MEMS microneedle array," *Nanomedicine : The Official Journal of the American Academy of Nanomedicine,* Vol. 1, No. 2, 2005, pp. 184-190.
47. Park, J.H., Allen, M.G., and Prausnitz, M.R., "Biodegradable polymer microneedles: fabrication, mechanics and transdermal drug delivery," *Journal of Controlled Release : Official Journal of the Controlled Release Society,* Vol. 104, No. 1, 2005, pp. 51-66.
48. Medtronic, Inc. [www.medtronic.com. Accessed 2007.]
49. Moses, M.A., Brem, H., and Langer, R., *Cancer Cell,* Vol. 4, 2003, pp. 337-341.
50. Yasukawa, T., Ogura, Y., Sakurai, E., "Intraocular sustained drug delivery using implantable polymeric devices," *Advanced Drug Delivery Reviews,* Vol. 57, No. 14, 2005, pp. 2033-2046.
51. Shawgo, R.S., Richards Grayson, A.C., Li, Y., "BioMEMS for drug delivery," *Current Opinion in Solid State and Materials Science,* Vol. 6, 2002, pp. 329-334.
52. Prescott, J.H., Lipka, S., Baldwin, S., "Chronic, programmed polypeptide delivery from an implanted, multireservoir microchip device," *Nature Biotechnology,* Vol. 24, No. 4, 2006, pp. 437-438.
53. Mitra, A.K. ed., "Ophthalmic Drug Delivery Systems," *Drugs and the Pharmaceutical Sciences,* Vol. 130, Marcel Dekker, New York, NY, 2003, pp. 727.
54. Moshfeghi, A.A., and Peyman, G.A., "Micro- and nanoparticulates," *Advanced Drug Delivery Reviews,* Vol. 57, No. 14, 2005, pp. 2047-2052.
55. Ozkiris, A., and Erkilic, K., "Complications of intravitreal injection of triamcinolone acetonide," *Canadian Journal of Ophthalmology,* Vol. 40, No. 1, 2005, pp. 63-68.

56. Martidis, A., Duker, J.S., Greenberg, P.B., "Intravitreal triamcinolone for refractory diabetic macular edema," *Ophthalmology,* Vol. 109, No. 5, 2002, pp. 920-927.
57. Scott, I.U., and Flynn, H.W.,Jr, "Reducing the risk of endophthalmitis following intravitreal injections," *Retina,* Vol. 27, No. 1, 2007, pp. 10-12.
58. Geroski, D.H., and Edelhauser, H.F., "Drug delivery for posterior segment eye disease," *Investigative Ophthalmology & Visual Science,* Vol. 41, No. 5, 2000, pp. 961-964.
59. Kimura, H., and Ogura, Y., "Biodegradable polymers for ocular drug delivery," *Ophthalmologica.,* Vol. 215, No. 3, 2001, pp. 143-155.
60. Beeley, N.R., Stewart, J.M., Tano, R., "Development, implantation, in vivo elution, and retrieval of a biocompatible, sustained release subretinal drug delivery system," *Journal of Biomedical Materials Research Part A,* Vol. 76, No. 4, 2006, pp. 690-698.
61. Alikacem, N., Yoshizawa, T., Nelson, K.D., "Quantitative MR imaging study of intravitreal sustained release of VEGF in rabbits," *Investigative Ophthalmology & Visual Science,* Vol. 41, No. 6, 2000, pp. 1561-1569.
62. Beeley, N.R., Rossi, J.V., Mello-Filho, P.A., "Fabrication, implantation, elution, and retrieval of a steroid-loaded polycaprolactone subretinal implant," *Journal of Biomedical Materials Research Part A.,* Vol. 73, No. 4, 2005, pp. 437-444.
63. Haesslein, A., Ueda, H., Hacker, M.C., "Long-term release of fluocinolone acetonide using biodegradable fumarate-based polymers," *Journal of Controlled Release : Official Journal of the Controlled Release Society,* Vol. 114, No. 2, 2006, pp. 251-260.
64. Heller, J., "Ocular delivery using poly(ortho esters)," *Advanced Drug Delivery Reviews,* Vol. 57, No. 14, 2005, pp. 2053-2062.
65. Andrieu-Soler, C., Aubert-Pouessel, A., Doat, M., "Intravitreous injection of PLGA microspheres encapsulating GDNF promotes the survival of photoreceptors in the rd1/rd1 mouse," *Molecular Vision,* Vol. 11, 2005, pp. 1002-1011.
66. Ambati, J., Canakis, C.S., Miller, J.W., "Diffusion of high molecular weight compounds through sclera," *Investigative Ophthalmology & Visual Science,* Vol. 41, No. 5, 2000, pp. 1181-1185.
67. Ambati, J., Gragoudas, E.S., Miller, J.W., "Transscleral delivery of bioactive protein to the choroid and retina," *Investigative Ophthalmology & Visual Science,* Vol. 41, No. 5, 2000, pp. 1186-1191.
68. Kim, J.W., Lindsey, J.D., Wang, N., "Increased human scleral permeability with prostaglandin exposure," *Investigative Ophthalmology & Visual Science,* Vol. 42, No. 7, 2001, pp. 1514-1521.
69. Okabe, J., Kimura, H., Kunou, N., "Biodegradable intrascleral implant for sustained intraocular delivery of betamethasone phosphate," *Investigative Ophthalmology & Visual Science,* Vol. 44, No. 2, 2003, pp. 740-744.
70. Carrasquillo, K.G., Ricker, J.A., Rigas, I.K., "Controlled delivery of the anti-VEGF aptamer EYE001 with poly(lactic-co-glycolic)acid microspheres," *Investigative Ophthalmology & Visual Science,* Vol. 44, No. 1, 2003, pp. 290-299.
71. Eljarrat-Binstock, E., and Domb, A.J., "Iontophoresis: A non-invasive ocular drug delivery," *Journal of Controlled Release: Official Journal of the Controlled Release Society,* Vol. 110, No. 3, 2006, pp. 479-489.
72. Davies, J.B., Ciavatta, V.T., Boatright, J.H., "Delivery of several forms of DNA, DNA-RNA hybrids, and dyes across human sclera by electrical fields," *Molecular Vision,* Vol. 9, 2003, pp. 569-578.

73. Myles, M.E., Neumann, D.M., and Hill, J.M., "Recent progress in ocular drug delivery for posterior segment disease: emphasis on transscleral iontophoresis," *Advanced Drug Delivery Reviews,* Vol. 57, No. 14, 2005, pp. 2063-2079.
74. Adamis, A.P., Miller, J.W., Gragoudas, E.S., "Implantable drug delivery device and use thereof," U.S. Patent App. No. 20030069560, 2003.
75. Mescher, M.J., Dube, C.E., Fiering, J.O., "A Programmable Device for Long-Term Transscleral Drug Delivery," *Transactions of the 31st Annual Meeting of the Society for Biomaterials,* Vol. 29, Pittsburgh, PA, 2006.
76. Roberts, C.J., Williams, P.M., Davies, J., "Real-Space Differentiation of IgG and IgM Antibodies Deposited on Microtiter Wells by Scanning Force Microscopy," *Langmuir: The ACS Journal of Surfaces and Colloids,* Vol. 11, 1995, pp. 1822-1826.
77. Kumar, G., Meng, J.J., Ip, W., "Cell motility assays on tissue culture dishes via non-invasive confinement and release of cells," *Langmuir: The ACS Journal of Surfaces and Colloids,* Vol. 21, No. 20, 2005, pp. 9267-9273.
78. Lallier, T.E., Miner, Q.W., Jr, Sonnier, J., "A simple cell motility assay demonstrates differential motility of human periodontal ligament fibroblasts, gingival fibroblasts, and pre-osteoblasts," *Cell and Tissue Research,* 2007, pp. 339-354.
79. Thampatty, B.P., and Wang, J.H., "A new approach to study fibroblast migration," *Cell Motility and the Cytoskeleton,* Vol. 64, No. 1, 2007, pp. 1-5.
80. Zaman, M.H., Trapani, L.M., Sieminski, A.L., "Migration of tumor cells in 3D matrices is governed by matrix stiffness along with cell-matrix adhesion and proteolysis," *Proceedings of the National Academy of Sciences of the United States of America,* Vol. 103, No. 29, 2006, pp. 10889-10894.
81. Chen, F., Lu, Y., Castranova, V., "Loss of Ikkβ promotes migration and proliferation of mouse embryo fibroblast cells," *The Journal of Biological Chemistry,* Vol. 281, No. 48, 2006, pp. 37142-37149.
82. Pritt, S., and LaMadeleine, F.R., "Test Result Certificate, Project Number 03-3037-N1," Toxikon, 2003.
83. Manning, P.J., Ringler, D.H., and Newcomer, C.E. eds., "The Biology of the Laboratory Rabbit," Academic Press, San Diego, CA, 1974, pp. 483.